Mechanism of Acquired Temozolomide Resistance in Glioblastoma

by

José L. McFaline-Figueroa

B.S. Chemistry
University of Puerto Rico at Mayagüez, 2006

SUBMITTED TO THE DEPARTMENT OF BIOLOGY IN PARTIAL FULFILLMENT OF THE REQUIREMENTS FOR THE DEGREE OF

DOCTORATE OF PHILOSOPHY
AT THE
MASSACHUSETTS INSTITUTE OF TECHNOLOGY

JUNE 2014

Signature redacted

Signature of Author_____
Department of Biology
April 16th, 2014

Signature redacted

Certified by_____
Leona D. Samson
Professor of Biological Engineering and Biology
Thesis Supervisor

Signature redacted

Certified by_____
Forest. M. White
Professor of Biological Engineering and Biology
Thesis Supervisor

Signature redacted

Accepted by_____
Amy E. Keating
Associate Professor of Biology
Co-Chair, Biology Graduate Committee

Mechanism of Acquired Temozolomide Resistance in Glioblastoma

by

José L. McFaline-Figueroa

Abstract

Glioblastoma (GBM) is the most common and malignant form of brain cancer. After aggressive treatment, therapy resistant tumors inevitably recur. However, the molecular mechanisms underlying such resistance remain unclear. We isolated GBM cells resistant to temozolomide (TMZ), the frontline chemotherapy agent for GBM, and observed modest decreases in the mismatch repair (MMR) components MSH2 and MSH6. The modest decrease in MSH2, and relatively modest decrease in MSH6, did not seem sufficient to account for the very large increase in TMZ resistance. However, shRNA-mediated modulation of MSH2 and MSH6 levels *in vitro* confirmed that such decreases in MSH2 and MSH6 provide a potent mechanism for TMZ resistance. We demonstrate in an *in vivo* GBM mouse model that minor changes in MSH2 suppress TMZ-induced tumor regression, and moreover, show that even minor decreases in *MSH2* transcript levels correlate with decreased survival in TMZ treated GBM patients. These modest changes in MMR are unlikely to alter classical markers of MMR deficiency, namely microsatellite instability and a mutator phenotype. Our results suggest that the involvement of MMR deregulation in mediating TMZ resistance is likely to be much more prevalent than previously appreciated.

Additionally, we have employed phosphoproteomic network analysis to identify changes at the signaling network level that accompany the acquisition of TMZ resistance. Through mathematical and computational approaches, we identified changes that suggest increased PDGFR and integrin/FAK1 signaling in response to repeated TMZ exposure. Additionally, kinase motif analysis identified widespread alterations in phosphorylation of peptides containing motifs associated with the CDK/MAPK kinase family. Currently, we are applying molecular biology techniques to investigate the effects of these altered cellular signals on MMR activity and the sensitivity of GBM cells to TMZ.

Thesis Supervisor: Leona D. Samson
Title: Professor of Biological Engineering and Biology

Thesis Supervisor: Forest M. White
Title: Professor of Biological Engineering

Acknowledgements

I begin by expressing my deepest gratitude to my advisors Leona D. Samson and Forest M. White for their support, motivation and guidance throughout my graduate career, which has allowed me to grow as a scientist and a teacher. I would like to thank the members of my committee Jackie Lees and Mike Hemann for their counsel and contributions to my project.

I am grateful for all of my friends and colleagues from the Samson and White laboratories for their endless advice, encouragement and fun times. Additionally, I would like to thank all of my friends from the Biology, Biological Engineering and Koch Institute communities for making my time as a graduate student both educational and extremely entertaining.

I would like to thank my family. To my beautiful wife Nelly, thank you for all of your support through out the years. Thanks to Ana, José Enrique, Cristina and José Guilllermo for taking me into their family. To my uncles Agnelis, Dahri, Manolo, Lizette and cousins Raul, Mariela and Daniel thank you for your encouragement and friendship. Thanks to my brother Ricky and my sister Jennifer for an absolute fantastic time growing up and continued support. To my little brother Luis Manuel for letting me be a kid again. To my parents, Magaly and Berto for innumerable things, especially for always pushing me to go forward and achieve my dreams. Thanks to my gradparents Casilda, Octavio, Natividad and Luis, for their inspiration and for being the best cheerleaders for my siblings and myself. All of you have allowed me to be where I am today and I find myself truly blessed and grateful.

Table of Contents

List of Figures

List of Tables

List of Abbreviations

Abbreviation	Definition
AAG/MPG	Alkyladenine DNA glycosylase
AKT	Protein Kinase B
ANOVA	Analysis of variance
ATM	Ataxia Telangiectasia mutated
ATR	Ataxia Telangiectasia and Rad3 related
AURKC	Aurora kinase C
BCNU	1,3-Bis(2-chloroethyl)-1-nitrosourea
BER	Base excision repair
CAK	CDK activating complex
CD133	Prominin 1
CDC2	Cyclin dependent protein kinase 1 (CDK1)
CDK	Cyclin dependent protein kinase
CDK2	Cyclin dependent protein kinase 2
CHK1	Checkpoint kinase 1
CHK2	Checkpoint kinase 2
CSC	Cancer stem cell
CSF	Cerebrospinal fluid
CSNK1E	Casein kinase 1
DMEM	Dulbecco's modificed eagle media
DNA-PK	DNA protein kinase
DSB	Double strand break
DTIC	Dacarbazine
EGFR	Epidermal growth factor receptor
EGFRvIII	Epidermal growth factor receptor varaint III
EXO1	Exonuclease 1
FAK1	Focal adhesion kinase 1
FBS	Fetal bovine serum
FER	Fer tyrosine kinase
FIP1L1	factor interacting with PAPOLA and CPSF1
GBM	Glioblastoma multiforme
GFAP	Glia fibrillary acidic protein
GFP	Green fluorescent protein
GSC	Glioblastoma cancer stem cell
GSK3A	Glycogen synthase kinase α
GSK3B	Glycogen synthase kinase β
GTF2F1	General transcription factor 2F 1
HCR	Host cell reactivation
HPLC	High pressure liquid chromatography
HR	Homologous recombination
IDH1	Isocitrate dehydrogenase 1

IDH2	Isocitrate dehydrogenase 2
IMAC	Immobilized metal affinity chromatography
IR	Ionizing radiation
ITGA3	Integrin α3
iTRAQ	Isobaric tag for relative and absolute quantitation
JNK	c-Jun N-terminal kinase
KEA	Kinase enrichment analysis
LC-MS/MS	Liquid chromatography tandem mass spectrometry
MAPK	Mitogen activated protein kinase
MAPK10	Mitogen activated protein kinase 10/c-Jun N-terminal kinase 3 (JNK3)
MAPK13	Mitogen activated protein kinase 13/Stress activated protein kinase (SAPK4)
MAPK14	Mitogen activated protein kinase 14/p38 mitogen activated protein kinase α (p38MAPKα)
MAPK8	Mitogen activated protein kinase 1/c-Jun N-terminal kinase 1 (JNK1)
MDM2	Mouse double minute homolog 2
MERTK	c-mer proto oncogene tyrosine kinase
MGMT	O^6-methylguanine methyltransferase
MLH1	MutL homolog 1
MMR	Mismatch repair
MNNG	*N*-Methyl-*N'*-nitro-*N*-nitrosoguanidine
MRE11	Meiotic recombination 11
MRI	Magnetic resonance imaging
MRN	Mre11-Rad50-Nbs1 complex
MSH2	MutS homolog 2
MSH3	MutS homolog 3
MSH6	MutS homolog 6
MSI	Microsatellite instability
MTZ	Mitozolomide
N3-meA	N3-methyladenine
N7-meG	N7-methylguanine
nbs1	Nijmegen syndrome 1 protein
NER	Nucleotide excision repair
NF1	Neurofibromin 1
NHEJ	Non-homologous end joining
NTRK3	Neurotrophic tyrosine kinase type 3
O^4-meT	O^4-methylthymine
O^6-meG	O^6-methylguanine
p38MAPK	p38 mitogen activated protein kinase
PCNA	Proliferating cell nuclear antigen
PDGF	Platelet derived growth factor
PDGFRα	Platelet derived growth factor receptor α
PDGFRβ	Platelet derived growth factor receptor β

PI3K	Phosphoinositol-3-kinase
PMS2	Postmeiotic segregation increased 2
PRKCB1	Protein kinase C, β1
pS	phosphoserine
pT	phosphothreonine
PTEN	Phosphatase and tensin homolog
pY	phosphotyrosine
RPS6KA3	ribosomal protein S6 kinase, 90kDa, polypeptide 3
RT	Radiotherapy
SGK	serum/glucocorticoid regulated kinase
SGK3	serum/glucocorticoid regulated kinase 3
SNRK	SNF related kinase
SP	Side population
ssDNA	singl- stranded DNA
SVZ	Subventricular zone
TCGA	The Cancer Genome Atlas
TK	Thymidine kinase
TLS	Translesion
TMZ	Temozolomide
TRIM33	tripartite motif containing 33

Chapters

Chapter I: Introduction

Chapter 1: Introduction

WHO grade IV glioma or Glioblastoma Multiforme

Glioblastoma (GBM) is the most common and most malignant neoplasm of the brain. Rudolf Virchow, a noted German pathologist, first described brain glioma in 1865 with the first modern pathologic description of GBM, known at the time as spongioblastoma multiforme, conducted by Dr. Harvey Cushing and Dr. Percival Bailey in 1926 (DeAngelis and Mellinghoff, 2011). GBM is classified as the highest grade astrocytoma due to the proposed astrocyte cell of origin (Ray-Chaudhury, 2010). GBM is most common in patients over 45 years of age and can arise as a tumor in either or both cerebral lobes (termed butterfly GBM when encompassing both lobes), with patients usually presenting with headaches, nausea, epileptic episodes and/or changes in mood or personality (Ray-Chaudhury, 2010). At the macroscopic level, GBM was termed multiforme due to the wide variety of cell types and cell sizes apparent during histologic examination, with the more extreme cases including giant cell GBM and GBM with oligodendroglial features. Microscopically, GBM is characterized by invasive tumor cells infiltrating far into normal brain, hyperchromatic nuclei, vascular proliferation and high levels of necrosis, including pseudopalisading necrosis (Newcomb and Zagzag, 2009; Ray-Chaudhury, 2010). Seminal work by Hans Joachim in the 1940s established the first subtype classification of GBM through the identification of its primary (most prevalent) and secondary forms, that is, GBMs that arose *de novo* versus those that progressed from lower grade glioma, respectively (Scherer, 1940). More recent work led to the identification of a molecular signature that distinguishes primary and secondary GBM, namely EGFR overactivation and p53 mutations, respectively (DeAngelis and

Mellinghoff, 2011). Current work by The Cancer Genome Atlas (TCGA) has changed our view on these molecular signatures through the identification of DNA sequence, copy number, epigenetic changes and gross chromosomal re-arrangements in GBM tumors. Looking mostly at primary GBM, The Cancer Genome Atlas (TCGA) found that up to 35% of primary GBMs harbor somatic p53 mutations making it one of the most commonly mutated tumor suppressor genes in all of GBM and not just limited to secondary GBM (The Cancer Genome Atlas Research Network, 2008). Currently, all GBM tumors are characterized by mutations in diverse cellular components that lead to the overactivation of receptor tyrosine kinase signaling and decreased activation of the p53 and RB pathways (Chen et al., 2012b). With the advent of global gene expression and microRNA profiling through microarrays distinct molecular subtypes of GBM have been identified with mutations of specific targets in the afore mentioned pathways. The molecular characteristics of these subtypes and the clinical differences between them are explored in a later section.

Classification of GBM subtypes

GBM subtypes as defined by gene expression profiling. As described previously, GBM subtypes have been identified on the basis of histologic variation and whether they arose *de novo* or from a lower grade neoplasm. These observations define GBM as primary or secondary and as GBM or GBM with oligodendroglial features (DeAngelis and Mellinghoff, 2011; Scherer, 1940; Vitucci et al., 2011). Gene expression profiling combined with clustering analysis has allowed for unbiased assignment of tumor specimens to various categories allowing for the determination of tumor subtypes with a resolution not found in classical histologic analysis. Initial studies investigating

differences in gene expression profiling of high-grade glioma samples (grade III/anaplastic astrocytoma and grade IV/GBM) identified three classes of malignancy, namely proliferative, mesenchymal and proneural glioma; proliferative and mesenchymal display decreased survival compared to the proneural subtype (Phillips et al., 2006). Subtypes in GBM have now been identified based on gene expression, genetic mutations, expression of lineage markers, stage of differentiation and microRNA expression profile (Kim et al., 2011; Verhaak et al., 2010). Verhaak and colleagues performed clustering analysis of gene expression data for GBM tumors collected by the TCGA network and identified four major subtypes; classical, mesenchymal, neural and proneural GBM (The Cancer Genome Atlas Research Network, 2008; Verhaak et al., 2010). These subtypes are characterized as follows:

- *Classical GBM subtype.* Displays increased EGFR activity, frequent chromosome 7 amplification, chromosome 10 loss, *CDKN2A* deletion (which encodes a shared exon between the p14Arf/p16INK4A tumor suppressors) and an absence of p53 mutations (Verhaak et al., 2010).
- *Mesenchymal GBM subtype*. Displays increased Met tyrosine kinase expression, NF1 heterozygous deletion, increased expression tumor necrosis factor and NF-κB signaling components. These inflammatory signals are consistent with the increased necrosis and inflammation observed in this subtype. The presence of the mesenchymal and astrocytic markers CD44 and METRK, respectively suggest a type of EMT-like transition (Chen et al., 2012b; Verhaak et al., 2010). In gliomas in general, the mesenchymal signature displays the worst prognosis with the lowest overall survival (Chen et al., 2012b; Phillips et al., 2006) however it has not been demonstrated that the mesenchymal subtype leads to lower survival in GBM patients.

- *Neural GBM subtype*. Characterized primarily by expression of neural markers and enrichment of gene ontology terms associated with neural projection and axon synaptic transmission. Importantly, this classification was shown to not to be a result of contamination from normal brain cells (Verhaak et al., 2010).
- *Proneural GBM subtype*. Display PDGFRα mutations (mostly by gene amplification), inactivating IDH1 and p53 mutations, activating PI3K mutations and expression of oligodendrocytic markers and proneural developmental genes (Verhaak et al., 2010). Compared to the other three subtypes, proneural GBM patients display increased overall survival. However, in terms of therapeutic response, both the classical and mesenchymal GBM subtypes were found to have a significant increase in survival upon aggressive treatment, the neural subtype had marginal response whereas the proneural subtype displayed no advantage to standard therapy (radiation and temozolomide; the standard of care for GBM is discussed in the following section) indicating that the increase in overall survival was independent of therapy (Figure 1.1) (Verhaak et al., 2010).

GBM subtypes as defined by miRNA expression profiling. Using miRNA profiling of TCGA GBM samples, Kim *et al.* identified 5 distinct GBM subtypes each of which was enriched for miRNAs specific for progenitors of various cell types found in the brain, namely the neural, oligoneural and astrocytic subtypes; other subtypes were characterized by expression of miRNAs associated with multipotent neural precursors (later termed radial glial), the expression of miRNAs involved in the differentiation of both neural and mesenchymal tissues (Kim et al., 2011). Comparing the classification of GBM samples by miRNA to the previously obtained mRNA expression there was concordance between the oligoneural miRNA subtype and the proneural mRNA subtype, the astrocytic miRNA subtype and the mesenchymal mRNA subtype, and the radial glia

miRNA subtype and classical mRNA subtype (Kim et al., 2011). Consistent with mRNA classification, therapeutic intervention with standard therapy did not significantly alter survival in the oligoneural miRNA subtype (which corresponds to the proneural mRNA subtype) (Figure 1.2).

Current standard of care for patients with initial GBM presentation

Surgical resection. Therapy for patients with newly diagnosed GBM usually begins with surgical resection of the main tumor mass (Stupp et al., 2010). In the case of patients with increased cranial pressure or epileptic seizures a course of anti-edema or anti-epileptic medication, respectively, is administered prior to surgery (Stupp et al., 2010). The extent of tumor resection correlates with increased survival in GBM with even partial resection leading to a significant survival advantage (Wolbers, 2014). The area of resection is defined by magnetic resonance imaging (MRI) prior to surgery and the extent of tumor resection analyzed by MRI post-surgery. Recently, the use of intraoperative MRI to maximize tumor resection has been shown to increase progression free survival by allowing surgeons to continuously analyze tumor boundaries (Senft et al., 2011; Wolbers, 2014). Moreover, intraoperative awake mapping allows surgeons to confidently remove tumors from areas where resection of normal tissue would be detrimental thus giving confidence that cognitive damage will not result from tumor removal (Wolbers, 2014). Currently, intraoperative MRI and awake mapping are not part of the standard of care in GBM treatment. At the time of surgical resection, carmustine, also know as BCNU, laden wafers (Gliadel)) may be implanted at the tumor site to eradicate any remaining tumor cells. However this treatment approach is still in its early phases (McGirt et al., 2009; Stupp et al., 2010).

Concurrent radio- and chemotherapy and chemotherapy maintenance phase. After resection, standard of care for GBM treatment entails concurrent radiotherapy (RT) and temozolomide (TMZ) treatment followed by a maintenance phase of various cycles of TMZ alone. For the concurrent treatment phase, 75 mg/m^2 of TMZ, an oral S_N1 monoalkylating agent, is administered a few hours prior to RT (usually 2Gy) this treatment is repeated for 40-49-days, for a total of 60 Gy. After completion of this initial phase, TMZ is administered for six cycles. The first cycle consists of treatment with a 150 mg/m^2 dose for the first 5 days of a 28-day cycle. Each subsequent cycle is identical to the first with the exception that a higher, 200 mg/m^2 dose of TMZ is administered (Stupp et al., 2005; Stupp et al., 2010). This combination of RT and TMZ results in an increase in the median survival of GBM patients of 2.5 months compared to patients treated with RT alone (Stupp et al., 2005).

Temozolomide, the main chemotherapeutic agent in the treatment of GBM

Identification and chemical properties. The chemotherapeutic agent TMZ was derived in the 1990s to overcome the shortcomings of the prior alkylating agents dacarbazine (DTIC) and mitozolomide (MTZ). Both of these where shown to have potent anti-tumorigenic effects in rodent cancer models yet their efficacy was found to be low in humans due to poor metabolic activation and high myelosupression, respectively (Newlands et al., 1997). At physiological pH, TMZ is non-enzymatically metabolized to MTIC (the intermediate also produced from enzymatic DTIC metabolism) and, after several steps, to the reactive methyldiazonium ion. Various moieties in the cell, including DNA bases, become methylated due to nucleophillic attack of the methyl group of the methyldiazonium (Figure 1.3) (Kaina et al., 2007; Newlands et al., 1997).

TMZ induced DNA damage. TMZ produces a variety of lesions in the DNA with the major product being methylation at the N^7 position of guanine followed by the N^3 position of adenine and the O^6 position of guanine. N7-methylguanine (N7-meG) is not considered a toxic or mutagenic lesion however it does lead to increased guanine depurination leading to formation of abasic sites, which in turn display mutagenic and toxic properties and can act as a block to replication. N3-methyladenine (N3-meA) is a toxic and mutagenic lesion that induces a potent replication block and A:T to T:A transversions. The base excision repair (BER) pathway efficiently repairs both N7-meG and N3-meA. The BER pathway is initiated by substrate specific glycosylases that recognize damaged bases. Both N7-meG and N3-meA are substrates for the alkyladenine DNA glycosylase (known as AAG or MPG). Additionally, N3-meA can also be a substrate for the nucleotide excision repair pathway especially when the glycosylase is limiting (Fu et al., 2012).

Mechanism of action. The efficacy of TMZ as a DNA damaging agent results primarily from the formation of O^6-methylguanine (O^6-meG) lesions in the DNA and toxicity of O^6-meG is dependent on a functional mismatch repair (MMR) pathway (Cejka et al., 2003; Fu et al., 2012). During DNA replication, replicative DNA polymerases insert a thymine opposite the O^6-meG, creating a O^6-meG:T mismatch that is recognized by MMR machinery. Currently, there are two models for how MMR-dependent processing of the O^6-meG:T mismatch leads to toxicity. The direct signaling model posits that recognition of the mismatch by the MMR machinery directly leads to ATM and ATR activation and, ultimately, to cell cycle arrest and/or cell death. In support of this model, *in vitro* incubation of an O^6-meG:T containing plasmid with MMR components and the ATR-ATRIP kinase complex led to activation of ATR, measured by phosphorylation of Chk1. This ATR activation was demonstrated to be specific for O^6-meG:T as no activation was observed with a G:T mismatch containing plasmid. In addition, this activation was

dependent on both the mismatch recognition and processing complexes MutSα (composed of MSH2 and MSH6) and MutLα (composed of PMS2 and MLH1), respectively (Yoshioka et al., 2006). A second model, termed the futile cycling model, posits that toxicity from O^6-meG lesions is dependent on repeated cycles of MMR processing. After recognition of O^6-meG:T mispairs by MutSα, recruitment of MutLα and EXO1 leads to excision of a stretch of single-stranded DNA containing the thymine opposite O^6-meG, creating a single stranded gap in the DNA. To finalize mismatch repair DNA polymerase fills the gap, only to once again incorporate a thymine opposite O^6-meG, stimulating another round of MMR. This futile cycling leads to accumulation of ssDNA gaps that generate double strand breaks at collapsed replication forks during a second round of replication, that in turn stimulate cell cycle arrest or cell death (Figure 1.4) (Cejka et al., 2003; Fu et al., 2012; Li, 2008; Mojas et al., 2007; Quiros et al., 2010). Consistent with this model, the toxic effects of TMZ do not appear to elicit a significant response at the cellular level until two cell cycle times post-treatment consistent with the time where MMR induced double strand breaks are generated (Mojas et al., 2007). In reality it is likely a mixture of both of direct signaling and futile cycling processes are at play, however, it is still unknown why direct activation of ATR during the initial recognition of the mispair does not elicit a cellular response during the first cell cycle time post treatment.

Pharmacokinetics. TMZ's stability at acidic pH makes it an ideal drug for oral consumption. TMZ displays wide biodistribution after administration including efficiently crossing the blood-brain barrier. Moreover, it has been suggested that the slightly basic pH of the brain enhances its breakdown to its active form upon crossing the barrier (Newlands et al., 1997). Detailed kinetic characterization has shown that bioavailability of TMZ varies linearly with dose with drug concentration in the cerebrospinal fluid being approximately $1/5^{th}$ of the plasma concentration, with peak plasma (14 μg/mL) and CSF

(2 μg/mL) levels being reached approximately 1.5 hr after taking the drug (Ostermann et al., 2004).

DNA repair pathways that alter sensitivity to TMZ

MGMT. Deficiencies and levels of various DNA repair components have been shown to alter the sensitivity of GBM tumors to TMZ. Of these, expression of O^6-methylguanine-DNA-methyltransferase (MGMT) levels is inarguably the best studied. MGMT is a direct reversal protein that is able to efficiently transfer the alkyl groups from the O^6 position of guanine (O^6-meG) and, to a lesser extent, the O^4 position of thymine (O^4-meT) that is induced by TMZ at extremely low levels, to a cysteine residue on its active site (Figure 1.4) (Kaina et al., 2007). In *E. coli*, the direct reversal protein Ada removes methyl groups from methyl phosphodiesters formed on the DNA backbone in addition to O^6-meG and O^4-meT, MGMT appears to only remove methyl groups from extracyclical oxygen atoms of DNA bases (Wyatt and Pittman, 2006). As expected due to its ability to reverse toxic O^6-meG lesions, MGMT expression has a profound effect on the survival of TMZ treated GBM patients because of its influence on the ability of TMZ to kill GBM tumor cells. A lack of MGMT expression due to epigenetic silencing of the *MGMT* locus is a frequent event in GBM and *MGMT* methylation has been shown to strongly correlate with increased survival of TMZ treated GBM patients with *MGMT* promoter methylation that correlates with a 6 month increase in the median survival of GBM patients treated with TMZ and radiotherapy (Hegi et al., 2005).

AAG. Recently, the expression level of AAG has been implicated in altering the response of GBM to TMZ. Agnihotri and colleagues demonstrated that increased expression of AAG decreased the sensitivity of GBM cells *in vitro* and to GBM tumors *in*

vivo in a GBM xenograft model. Bisulfite sequencing of the *AAG* promoter in GBM tumors revealed that many tumors displayed a range of methylation at the *AAG* locus where increased methylation correlated with decreased AAG protein expression. Lastly, high AAG protein expression was significantly correlated with decreased survival of TMZ treated GBM patients (Agnihotri et al., 2012). Additionally, a separate study found that increased AAG expression strongly correlated to increased glioma tumor grade (Liu et al., 2012). Currently, the mechanism by which AAG may alter malignant transformation has not been explored.

MMR. The mismatch repair pathway proceeds from mismatch repair recognition followed by removal of the daughter strand past the mismatch and the re-synthesis of the daughter strand to the appropriate Watson-Crick base pair and finally DNA ligation. Mismatch recognition is performed by heterodimers composed of the *E. coli* MutS homologs (MSH) MSH2/MSH6 (MutSα) and MSH2/MSH3 (MutSβ). The MutSα heterodimer has affinity for single base pair mismatches and small DNA loops formed by 1-2 base pair insertion/deletions while the MutSβ recognizes large loops made by insertion/deletions of more than 2 base pairs (Jiricny, 2006). Following substrate recognition, recruitment of the MutL heterodimer and the EXO1 exonuclease, excision of mismatched DNA is directed towards the newly synthesized daughter strand. In *E. coli*, daughter strand repair is mediated by directing MMR processing towards the newly synthesized unmethylated strand. The mechanism of identification of the daughter strand in eukaryotic systems is still debated. Nicks such as those found on the lagging strand due to Okazaki fragments are thought to direct MMR to the daughter strand where EXO1 (a 5' to 3' exonuclease) function removes the new strand past the mismatch. For the leading strand the MutL heterodimer possesses PCNA dependent endonuclease activity, which allows formation of a nick for EXO1 to excise the daughter strand (Li, 2008); however, MutL would still need to identify the new strand. Exciting

work has recently demonstrated that DNA polymerase occasionally inserts ribonucleotides instead of deoxyribonucleotides into newly synthesized DNA and ribonucleotides mediate strand gaps, due cleavage by RNase H2, can serve as strand discrimination signals for MMR (Ghodgaonkar et al., 2013; Nick McElhinny et al., 2010). MMR deficiency leads to instability of short repeat sequences throughout the genome, a phenotype termed microsatellite instability (MSI) (Jiricny, 2006). MSI is infrequently found in high grade glioma suggesting that, unlike certain other cancers, decreased MMR activity is not a driver in GBM (Lundin et al., 1998; Martinez et al., 2005). Numerous studies have found that MMR deficiency leads to resistance of cells to TMZ treatment *in vitro*. Mutations in MMR components have been identified almost exclusively in recurrent GBM suggesting a selective pressure due to TMZ treatment (Cahill et al., 2007; The Cancer Genome Atlas Research Network, 2008; Yip et al., 2009).

Genetic changes and signaling network nodes proposed to alter the sensitivity of GBM cells to TMZ

p53. The p53 tumor suppressor is one of the major nodes in the response of cells to oncogenic stress and DNA damage. In terms of the response to TMZ and other damaging agents *in vitro*, p53 has been proposed to have a protective role upon drug exposure (Hirose et al., 2001; Wang et al., 2004). Although both p53 proficient and deficient cells demonstrate an accumulation at G2/M and polyploidy, in response to treatment p53 deficient cells progress to cell death whereas p53 proficient cells appear to maintain checkpoint activation and arrest. It should be noted, however, that p53 status does not appear to alter the survival of GBM patients suggesting that this effect may not

occur *in vivo* (Kyritsis et al., 1995; Newcomb et al., 1998; Shiraishi et al., 2002; Weller et al., 2009).

p38 and JNK MAPK. The stress activated p38 mitogen activated protein kinases (p38MAPK) and c-Jun N-terminal kinases (JNK) are members of the MAPK superfamily that regulate a diverse set of responses to numerous stimuli. In contrast to the Erk family of MAPKs, which regulate cell growth and proliferation in response to growth factor stimulation, p38MAPK and JNK are stress responsive kinases activated by oxidative stress, DNA damage, inflammatory cytokines and other damaging stimuli (Cargnello and Roux, 2011). Inhibition of both of these kinases has been shown to decrease G2/M accumulation and increase the sensitivity of GBM cells to TMZ *in vitro* (Hirose et al., 2003; Ohba et al., 2009).

PTEN/AKT. Deletion of the Phospatase and Tensin Homolog (PTEN) is a frequent even in glioblastoma (Wang et al., 1997). PTEN is the negative regulator of protein kinase B (AKT) which display increased activity in up to 70% of GBM (Koul, 2008). *In vitro*, AKT activation has been shown to lead to an abrogation of the G2/M arrest following TMZ exposure,. In contrast to arrest abrogation by p38MAPK or JNK inhibition, decreased checkpoint activation after TMZ exposure due to increased AKT activity correlates with decreased TMZ sensitivity (Hirose et al., 2005). In patients, PTEN status does not appear to alter the response of GBM patients to TMZ treatment (Carico et al., 2012). However, the results of this study should not be taken to imply that AKT activity does not alter TMZ response *in vivo* as increased AKT activity is observed even in the absence of PTEN loss.

IDH1. Mutations in isocitrate dehydrogenase 1 (IDH1), and to a lesser extent in IDH2, are a frequent event in glioma. *IDH1* mutations are found in more than 70% of low grade gliomas and secondary GBM suggesting it may be a driver for gliomagenesis (DeAngelis and Mellinghoff, 2011). Further, *IDH1* mutation strongly correlates to increased patient

survival regardless of treatment (Labussiere et al., 2010; Nobusawa et al., 2009; Yan et al., 2009). Regarding TMZ sensitivity, secondary GBM patients with *IDH1* mutations display a marked increased in survival after TMZ treatment (SongTao et al., 2012). In primary GBM, *IDH1* mutations occur at a much lower rate suggesting it is not a driver for *de novo* GBM (Labussiere et al., 2010). In primary GBM, *IDH1* mutations characterize the proneural GBM subtype (Verhaak et al., 2010). This is consistent with the observation that proneural GBM patients display the longest overall survival amongst the recognized GBM subtypes. In contrast, proneural GBM is regarded as non-responsive to therapy therefore it appears *IDH1* mutation does not confer a TMZ or RT sensitivity phenotype to primary GBM (Verhaak et al., 2010).

Glioblastoma cancer stem cells and response of GBM to therapy

CSCs. The first concept of a cancer stem cell (CSC)-like hypothesis was proposed as the embryonal rest theory, and stated that cancer cells display properties similar to cells in embryonic tissues. Later work investigating the origin of malignant teratomas identified a subset of undifferentiated cells with high mitotic activity and proposed to be stem cells capable of giving rise to the more differentiated tumor. Currently, CSCs are proposed to be a subset of cells within a tumor that are responsible for tumor maintenance (Nguyen et al., 2012).

Identification of glioma cancer stem cells and associated markers. Glioma was one of the first solid tumors in which stem cells were identified (Singh et al., 2004). The glioma stem cells (GSCs) were identified on the basis of expression of the cell surface antigen CD133 (Prominin I), a marker of hematopoietic and neural stem cells, and expression of Nestin, a neural progenitor marker (Kania et al., 2005). Sorting cells from patient glioma

tumors based on CD133 status, Singh *et al.* demonstrated that as little as 100 $CD133^+$ cells are able to recapitulate a brain tumor in immunodeficient mice while up to 1 million $CD133^-$ cells could not (Singh et al., 2004). Recent studies have questioned the validity of CD133 as a GSC marker. Beier and colleagues recently demonstrated that both $CD133^+$ and $CD133^-$ cells isolated from glioblastoma tumors could recapitulate brain tumors in NOD/SCID immunodeficient mice (Beier et al., 2007). Currently, it is becoming apparent that CD133 is a marker for a subset of GSCs and the heterogeneous nature of GBM tumors can be explained by having multiple GSCs with distinct stem cell niches in a given GBM tumor (Stopschinski et al., 2013).

GSC niche. The stem cell niche is also controversial in GBM; endothelial cells found in the vasculature increase proliferation of GSCs *in vitro* and increase tumorigenicity when co-implanted *in vivo* (Calabrese et al., 2007; Zhu et al., 2011). However, in the tumor setting, GSCs are frequently found in white matter tracts, away from vasculature suggesting another niche promotes pluripotency (Chen et al., 2012b). Recent studies have found that hypoxic conditions are a second niche for GSCs; further, GSCs were found to differentiate into the vasculature necessary to increase proliferation (Pistollato et al., 2010). The cell of origin for GSCs is also under debate; studies have been able to induce glioma tumor formation by inducing oncogenic changes in both neural stem cells (NSCs) that reside in the subventricular zone (SVZ), and by dedifferentiation of mature astrocytes and neurons (Alcantara Llaguno et al., 2009; Friedmann-Morvinski et al., 2012). In reality, both of these mechanisms may be at work as the location of GBM varies greatly as tumors can with, or lacking, contact to the NSC containing SVZ (Lim et al., 2007).

GSCs and resistance to therapy. A frequent area of study in GBM chemotherapy considers the sensitivity of GSCs to treatment. As these cells are proposed to be responsible for tumor maintenance in GBM, their sensitivity to treatment may dictate

recurrence and therefore progression free survival and overall survival of GBM patients. Multiple studies have suggested that cells displaying GSC markers are better able to withstand TMZ exposure. In a murine model of GBM driven by loss of the neurofibromin 1 (NF1), p53 and PTEN tumor suppressors specifically in cells expressing Nestin, a marker of NSCs, or glial fibrillary acidic protein (GFAP), a marker for both NSCs and mature astrocytes, Alcantara-Llaguno and colleagues found that proliferating cells that gave rise to tumors originated from the SVZ, the niche for adult NSCs (Alcantara Llaguno et al., 2009). In the same model, Chen at al. demonstrated that when tumor bearing mice where treated with TMZ, only non-GFAP expressing tumor cells appeared depleted by exposure suggesting that GFAP expressing cells were inherently chemoresistant. Further, when this model was crossed to mice expressing a thymidine kinase (TK) allele under the control of the Nestin promoter, a marker specific to adult NSCs, administration of ganciclovir (a compound that is toxic to TK expressing cells) led to ablation of this chemoresistant GFAP expressing population suggesting these TMZ resistant cells are GSCs with inherent chemoresistant properties (Chen et al., 2012a).

The side population (SP) phenotype is a commonly used as a marker for CSCs based on the low Hoechst staining of cells as observed by flow cytometry. This phenotype is due to expression of the ABCG2 transporter, a membrane pump frequently expressed specifically in stem cells that exports Hoechst from cells (Goodell et al., 1996). An SP has been identified in GBM mouse models and has been shown to have a higher tumorigenicity compared to non-SP GBM cells (Bleau et al., 2009). Further, TMZ treatment was shown to increase the proportion SP GBM cells suggesting decreased sensitivity compared to their non-SP counterparts. Importantly, this effect was not due to ABCG2 expression itself, but presumably to a function of the cell's stemness; cells made to express ABCG2 did not become TMZ resistant suggesting the effect is not due to TMZ being a substrate for ABCG2 (Bleau et al., 2009).

In contrast, a recent study has demonstrated that $CD133^+$ and $CD133^-$ GSCs lose proliferative and tumorigenic potential after TMZ treatment with the bulk of the tumor population appearing resistant compared to GSCs. Moreover, this effect was independent of MGMT (Beier et al., 2008).

Temozolomide resistance in recurrent GBM

Despite aggressive treatment, GBM recurrence is considered inevitable with recurrent disease most frequently occurring 2 to 3 cm from the border of the previously resected tumor (Hou et al., 2006). In terms of surgical resection of recurrent tumors, no prospective studies have been done to investigate the effectiveness of this intervention (Hou et al., 2006; Walbert and Mikkelsen, 2011). Radiation therapy of recurrent disease is also not a routinely used option due to the small time frame between initial radiotherapy and recurrence and the fear of damaging normal brain tissue (Walbert and Mikkelsen, 2011). A recent study looking into the effect of TMZ rechallenge in recurrent GBM found that TMZ sensitivity upon rechallenge was inversely correlated with the extent of TMZ therapy upon initial disease presentation (Perry et al., 2010). Similarly, Norden, *et al.* found that treatment of recurrent GBM with a dose-intense TMZ regimen (TMZ treatment for 21 days out of a 28 day cycle), while safe, had only minor efficacy in patients initially treated with standard therapy (RT and TMZ) (Norden et al., 2013).

Increased MGMT expression is amongst the factors believed to decrease TMZ sensitivity in recurrent GBM (Brandes et al., 2010; Kitange et al., 2012). However, recurrent GBM patients that have failed TMZ therapy are not sensitized to TMZ treatment by MGMT inhibition (Quinn et al., 2009). Moreover, a study by the German Glioma Network comparing 80 matched primary and recurrent GBM, one of the largest

studies of its kind, found that *MGMT* promoter methylation as well as transcript and protein levels were maintained at recurrence (Felsberg et al., 2011). Therefore, although MGMT status is a factor in the initial response of GBM to TMZ there does not appear to be a selective pressure to increase MGMT activity in response to chronic TMZ exposure. Deficiencies in MMR have also been postulated to lead to the TMZ resistant phenotype of recurrent GBM. MSI analysis, the most prevalent marker for complete MMR deficiency, is infrequently altered in recurrent GBM, most of which have encountered TMZ therapy, and this has been taken to mean that MMR deficiency is not a frequent driver of resistance to TMZ (Maxwell et al., 2008). Recent studies, however, have shown that MMR protein levels are frequently decreased in recurrent GBM tumors compared to their primary counterparts (Felsberg et al., 2011). Moreover, this effect has been replicated in TMZ resistant GBM cells generated *in vitro* and shown to occur in the absence of inactivating MMR mutations (Happold et al., 2012). These studies suggest MMR deregulation is much more prevalent than what has been identified based on MSI status or mutation in MMR components.

Overview of the current study

In the work presented here, we show that minor decreases in the MutSα mismatch-recognition component MSH2 can drastically alter the TMZ sensitivity of cultured GBM cells, and of GBM tumors in an *in vivo* syngeneic mouse model. Further, we demonstrate that even minor decreases in *MSH2* transcript levels correlate with decreased survival in TMZ treated GBM patients. These modest changes in MMR are unlikely to alter classical markers of MMR deficiency, namely microsatellite instability and a hypermutative phenotype. Our results suggest that the involvement of MMR

deregulation in mediating TMZ resistance is likely to be much higher than previously appreciated. In addition, phosphoproteomic analysis identified changes at the cellular signaling network level that accompany the acquisition of TMZ resistance *in vitro*. This analysis identified major changes in phosphorylation sites associated with receptor tyrosine kinase activity, integrin signaling and CDK/MAPK activity.

Figures

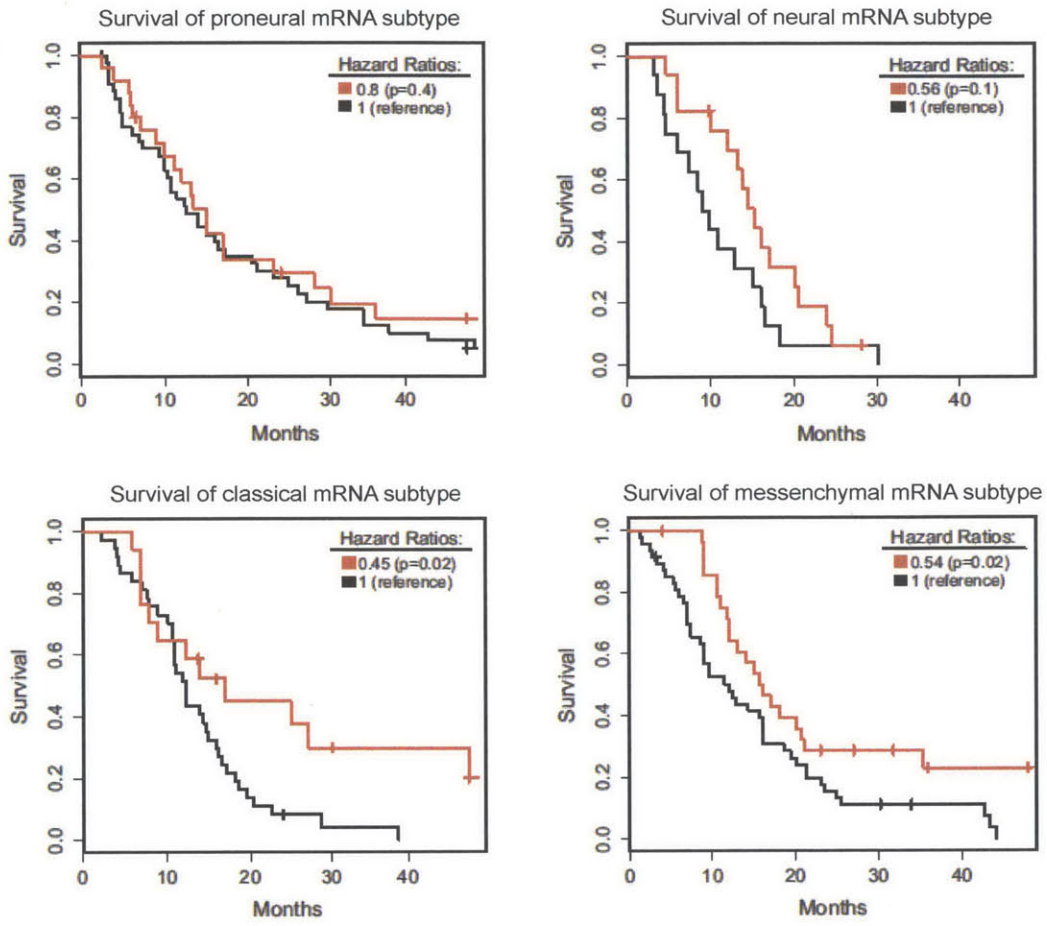

Figure 1.1 Survival differences amongst GBM subtypes as classified by mRNA expression.

Survival of GBM patients according to GBM subtype as measured by mRNA expression after more (red lines) or less (black lines) intensive therapy. More intensive therapy is defined as concurrent chemotherapy and radiation and/or > 3 cycles of chemotherapy while less intensive therapy is defined as non-concurrent chemotherapy and radiation and/or < 4 cycles of chemotherapy. Figure adapted from (Verhaak et al., 2010).

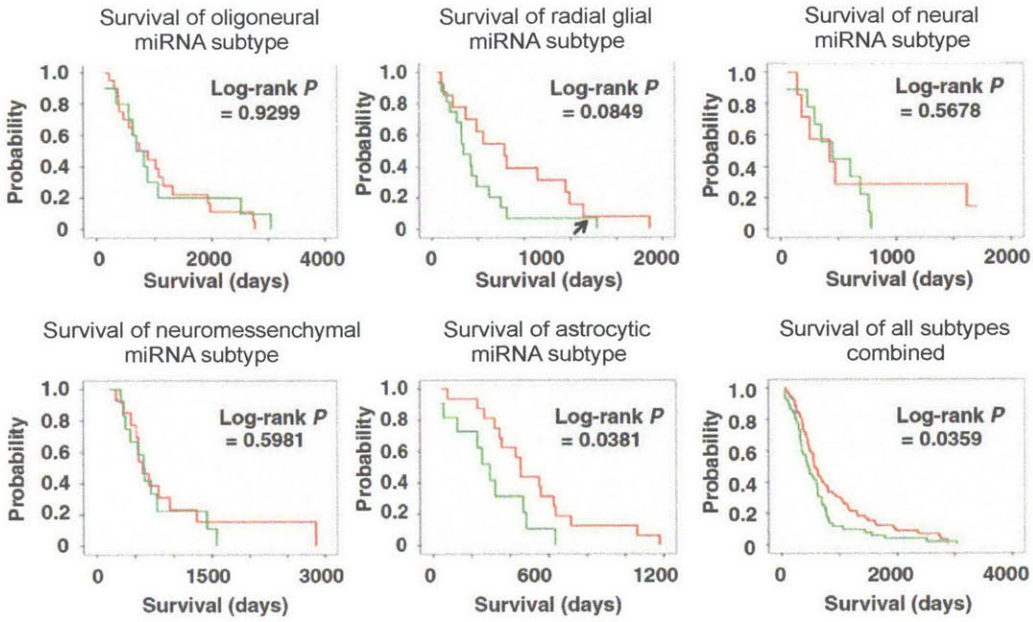

Figure 1.2 Survival differences amongst GBM subtypes as classified by miRNA expression.

Survival of GBM patients according to GBM subtype as measured by mRNA expression after radiation and 2 or more cycles of TMZ (red lines) and all other treatments (green lines). Figure adapted from (Kim et al., 2011).

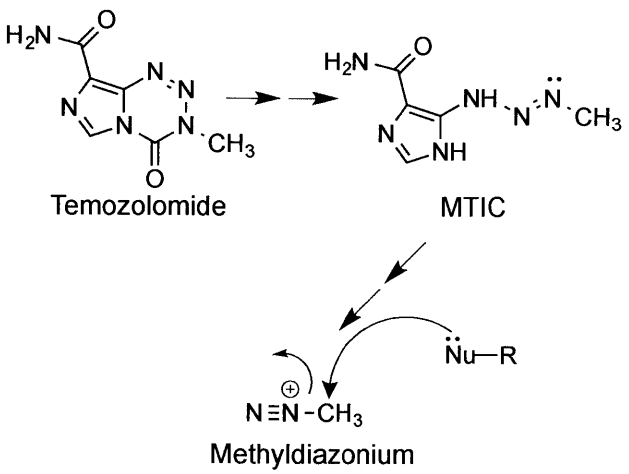

Figure 1.3 TMZ is non-enzymatically metabolized to the reactive methyldiazonium ion.

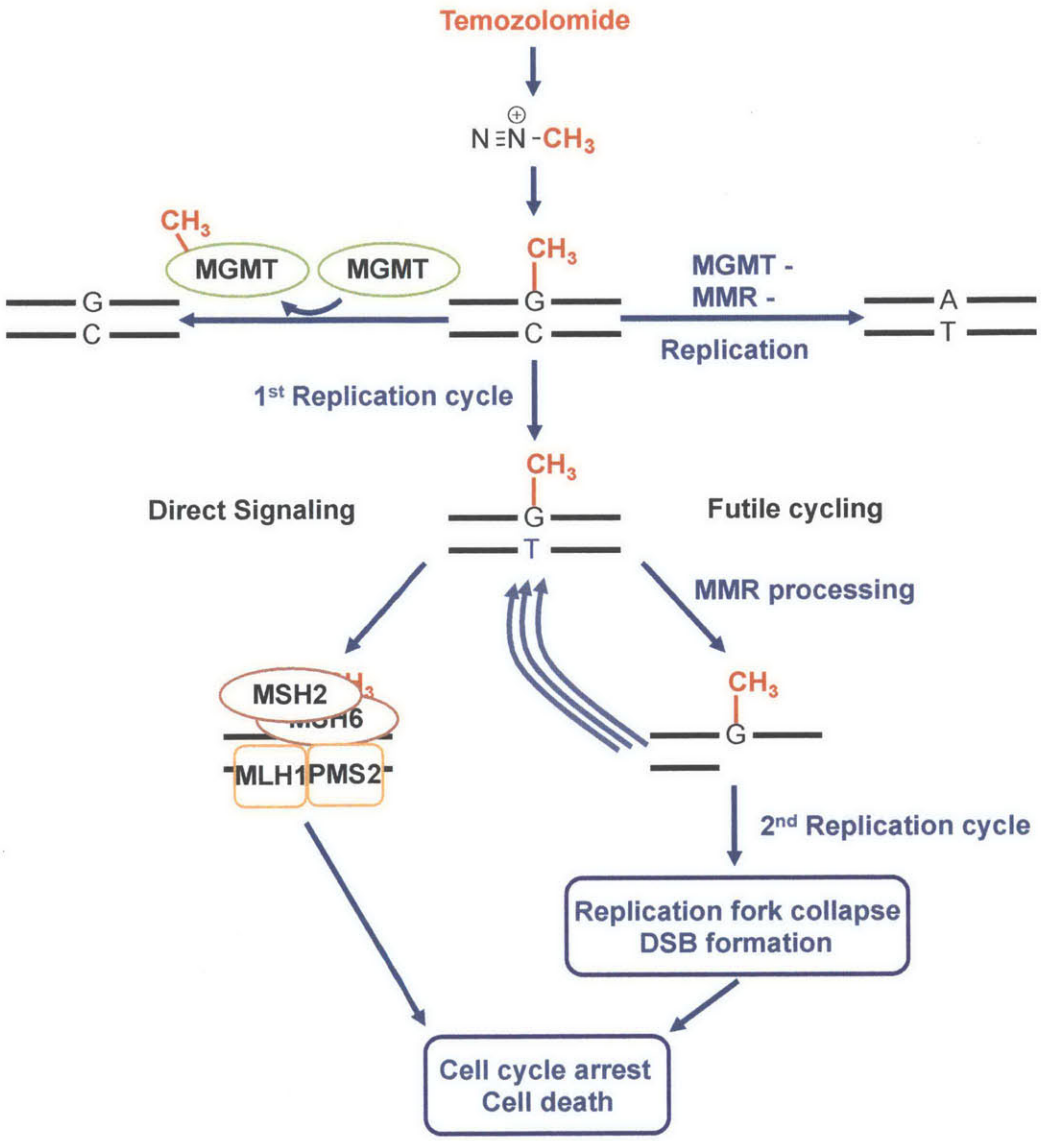

Figure 1.4 Fate of TMZ induced O^6-meG lesions.

Methyldiazonium-induced O^6-meG lesions can be repaired by MGMT to restore the normal G:C base pair. In the absence of MGMT, MMR potentiates O^6-meG toxicity by direct signaling to activate the DNA damage response or futile MMR processing to induce cell cycle arrest and cell death. Finally, in the absence of MGMT expression and deficient MMR, O^6-meG gives rise to G:C to A:T transitions.

References

Agnihotri, S., Gajadhar, A. S., Ternamian, C., Gorlia, T., Diefes, K. L., Mischel, P. S., Kelly, J., McGown, G., Thorncroft, M., Carlson, B. L., *et al.* (2012). Alkylpurine-DNA-N-glycosylase confers resistance to temozolomide in xenograft models of glioblastoma multiforme and is associated with poor survival in patients. J Clin Invest *122*, 253-266.

Alcantara Llaguno, S., Chen, J., Kwon, C. H., Jackson, E. L., Li, Y., Burns, D. K., Alvarez-Buylla, A., and Parada, L. F. (2009). Malignant astrocytomas originate from neural stem/progenitor cells in a somatic tumor suppressor mouse model. Cancer cell *15*, 45-56.

Beier, D., Hau, P., Proescholdt, M., Lohmeier, A., Wischhusen, J., Oefner, P. J., Aigner, L., Brawanski, A., Bogdahn, U., and Beier, C. P. (2007). CD133(+) and CD133(-) glioblastoma-derived cancer stem cells show differential growth characteristics and molecular profiles. Cancer research *67*, 4010-4015.

Beier, D., Rohrl, S., Pillai, D. R., Schwarz, S., Kunz-Schughart, L. A., Leukel, P., Proescholdt, M., Brawanski, A., Bogdahn, U., Trampe-Kieslich, A., *et al.* (2008). Temozolomide preferentially depletes cancer stem cells in glioblastoma. Cancer research *68*, 5706-5715.

Bleau, A. M., Hambardzumyan, D., Ozawa, T., Fomchenko, E. I., Huse, J. T., Brennan, C. W., and Holland, E. C. (2009). PTEN/PI3K/Akt pathway regulates the side population phenotype and ABCG2 activity in glioma tumor stem-like cells. Cell stem cell *4*, 226-235.

Brandes, A. A., Franceschi, E., Tosoni, A., Bartolini, S., Bacci, A., Agati, R., Ghimenton, C., Turazzi, S., Talacchi, A., Skrap, M., *et al.* (2010). O(6)-methylguanine DNA-methyltransferase methylation status can change between first surgery for newly

diagnosed glioblastoma and second surgery for recurrence: clinical implications. Neuro-oncology *12*, 283-288.

Cahill, D. P., Levine, K. K., Betensky, R. A., Codd, P. J., Romany, C. A., Reavie, L. B., Batchelor, T. T., Futreal, P. A., Stratton, M. R., Curry, W. T., *et al.* (2007). Loss of the mismatch repair protein MSH6 in human glioblastomas is associated with tumor progression during temozolomide treatment. Clinical cancer research : an official journal of the American Association for Cancer Research *13*, 2038-2045.

Calabrese, C., Poppleton, H., Kocak, M., Hogg, T. L., Fuller, C., Hamner, B., Oh, E. Y., Gaber, M. W., Finklestein, D., Allen, M., *et al.* (2007). A perivascular niche for brain tumor stem cells. Cancer cell *11*, 69-82.

Cargnello, M., and Roux, P. P. (2011). Activation and function of the MAPKs and their substrates, the MAPK-activated protein kinases. Microbiology and molecular biology reviews : MMBR *75*, 50-83.

Carico, C., Nuno, M., Mukherjee, D., Elramsisy, A., Dantis, J., Hu, J., Rudnick, J., Yu, J. S., Black, K. L., Bannykh, S. I., and Patil, C. G. (2012). Loss of PTEN is not associated with poor survival in newly diagnosed glioblastoma patients of the temozolomide era. PloS one *7*, e33684.

Cejka, P., Stojic, L., Mojas, N., Russell, A. M., Heinimann, K., Cannavo, E., di Pietro, M., Marra, G., and Jiricny, J. (2003). Methylation-induced G(2)/M arrest requires a full complement of the mismatch repair protein hMLH1. The EMBO journal *22*, 2245-2254.

Chen, J., Li, Y., Yu, T. S., McKay, R. M., Burns, D. K., Kernie, S. G., and Parada, L. F. (2012a). A restricted cell population propagates glioblastoma growth after chemotherapy. Nature *488*, 522-526.

Chen, J., McKay, R. M., and Parada, L. F. (2012b). Malignant glioma: lessons from genomics, mouse models, and stem cells. Cell *149*, 36-47.

DeAngelis, L. M., and Mellinghoff, I. K. (2011). Virchow 2011 or how to ID(H) human glioblastoma. Journal of clinical oncology : official journal of the American Society of Clinical Oncology *29*, 4473-4474.

Felsberg, J., Thon, N., Eigenbrod, S., Hentschel, B., Sabel, M. C., Westphal, M., Schackert, G., Kreth, F. W., Pietsch, T., Loffler, M., *et al.* (2011). Promoter methylation and expression of MGMT and the DNA mismatch repair genes MLH1, MSH2, MSH6 and PMS2 in paired primary and recurrent glioblastomas. Int J Cancer *129*, 659-670.

Friedmann-Morvinski, D., Bushong, E. A., Ke, E., Soda, Y., Marumoto, T., Singer, O., Ellisman, M. H., and Verma, I. M. (2012). Dedifferentiation of neurons and astrocytes by oncogenes can induce gliomas in mice. Science *338*, 1080-1084.

Fu, D., Calvo, J. A., and Samson, L. D. (2012). Balancing repair and tolerance of DNA damage caused by alkylating agents. Nature reviews Cancer *12*, 104-120.

Ghodgaonkar, M. M., Lazzaro, F., Olivera-Pimentel, M., Artola-Boran, M., Cejka, P., Reijns, M. A., Jackson, A. P., Plevani, P., Muzi-Falconi, M., and Jiricny, J. (2013). Ribonucleotides misincorporated into DNA act as strand-discrimination signals in eukaryotic mismatch repair. Molecular cell *50*, 323-332.

Goodell, M. A., Brose, K., Paradis, G., Conner, A. S., and Mulligan, R. C. (1996). Isolation and functional properties of murine hematopoietic stem cells that are replicating in vivo. The Journal of experimental medicine *183*, 1797-1806.

Happold, C., Roth, P., Wick, W., Schmidt, N., Florea, A. M., Silginer, M., Reifenberger, G., and Weller, M. (2012). Distinct molecular mechanisms of acquired resistance to temozolomide in glioblastoma cells. Journal of neurochemistry *122*, 444-455.

Hegi, M. E., Diserens, A. C., Gorlia, T., Hamou, M. F., de Tribolet, N., Weller, M., Kros, J. M., Hainfellner, J. A., Mason, W., Mariani, L., *et al.* (2005). MGMT gene

silencing and benefit from temozolomide in glioblastoma. The New England journal of medicine *352*, 997-1003.

Hirose, Y., Berger, M. S., and Pieper, R. O. (2001). p53 effects both the duration of G2/M arrest and the fate of temozolomide-treated human glioblastoma cells. Cancer research *61*, 1957-1963.

Hirose, Y., Katayama, M., Mirzoeva, O. K., Berger, M. S., and Pieper, R. O. (2005). Akt activation suppresses Chk2-mediated, methylating agent-induced G2 arrest and protects from temozolomide-induced mitotic catastrophe and cellular senescence. Cancer research *65*, 4861-4869.

Hirose, Y., Katayama, M., Stokoe, D., Haas-Kogan, D. A., Berger, M. S., and Pieper, R. O. (2003). The p38 mitogen-activated protein kinase pathway links the DNA mismatch repair system to the G2 checkpoint and to resistance to chemotherapeutic DNA-methylating agents. Molecular and cellular biology *23*, 8306-8315.

Hou, L. C., Veeravagu, A., Hsu, A. R., and Tse, V. C. (2006). Recurrent glioblastoma multiforme: a review of natural history and management options. Neurosurgical focus *20*, E5.

Jiricny, J. (2006). The multifaceted mismatch-repair system. Nature reviews Molecular cell biology *7*, 335-346.

Kaina, B., Christmann, M., Naumann, S., and Roos, W. P. (2007). MGMT: key node in the battle against genotoxicity, carcinogenicity and apoptosis induced by alkylating agents. DNA repair *6*, 1079-1099.

Kania, G., Corbeil, D., Fuchs, J., Tarasov, K. V., Blyszczuk, P., Huttner, W. B., Boheler, K. R., and Wobus, A. M. (2005). Somatic stem cell marker prominin-1/CD133 is expressed in embryonic stem cell-derived progenitors. Stem cells *23*, 791-804.

Kim, T. M., Huang, W., Park, R., Park, P. J., and Johnson, M. D. (2011). A developmental taxonomy of glioblastoma defined and maintained by MicroRNAs. Cancer research *71*, 3387-3399.

Kitange, G. J., Mladek, A. C., Carlson, B. L., Schroeder, M. A., Pokorny, J. L., Cen, L., Decker, P. A., Wu, W. T., Lomberk, G. A., Gupta, S. K., *et al.* (2012). Inhibition of Histone Deacetylation Potentiates the Evolution of Acquired Temozolomide Resistance Linked to MGMT Upregulation in Glioblastoma Xenografts. Clinical Cancer Research *18*, 4070-4079.

Koul, D. (2008). PTEN signaling pathways in glioblastoma. Cancer biology & therapy *7*, 1321-1325.

Kyritsis, A. P., Bondy, M. L., Hess, K. R., Cunningham, J. E., Zhu, D., Amos, C. J., Yung, W. K., Levin, V. A., and Bruner, J. M. (1995). Prognostic significance of p53 immunoreactivity in patients with glioma. Clinical cancer research : an official journal of the American Association for Cancer Research *1*, 1617-1622.

Labussiere, M., Sanson, M., Idbaih, A., and Delattre, J. Y. (2010). IDH1 gene mutations: a new paradigm in glioma prognosis and therapy? The oncologist *15*, 196-199.

Li, G. M. (2008). Mechanisms and functions of DNA mismatch repair. Cell research *18*, 85-98.

Lim, D. A., Cha, S., Mayo, M. C., Chen, M. H., Keles, E., VandenBerg, S., and Berger, M. S. (2007). Relationship of glioblastoma multiforme to neural stem cell regions predicts invasive and multifocal tumor phenotype. Neuro-oncology *9*, 424-429.

Liu, C., Tu, Y., Yuan, J., Mao, X., He, S., Wang, L., Fu, G., Zong, J., and Zhang, Y. (2012). Aberrant expression of N-methylpurine-DNA glycosylase influences patient survival in malignant gliomas. Journal of biomedicine & biotechnology *2012*, 760679.

Lundin, D. A., Blank, A., Berger, M. S., and Silber, J. R. (1998). Microsatellite instability is infrequent in sporadic adult gliomas. Oncology research *10*, 421-428.

Martinez, R., Schackert, H. K., Appelt, H., Plaschke, J., Baretton, G., and Schackert, G. (2005). Low-level microsatellite instability phenotype in sporadic glioblastoma multiforme. Journal of cancer research and clinical oncology *131*, 87-93.

Maxwell, J. A., Johnson, S. P., McLendon, R. E., Lister, D. W., Horne, K. S., Rasheed, A., Quinn, J. A., Ali-Osman, F., Friedman, A. H., Modrich, P. L., *et al.* (2008). Mismatch repair deficiency does not mediate clinical resistance to temozolomide in malignant glioma. Clinical cancer research : an official journal of the American Association for Cancer Research *14*, 4859-4868.

McGirt, M. J., Than, K. D., Weingart, J. D., Chaichana, K. L., Attenello, F. J., Olivi, A., Laterra, J., Kleinberg, L. R., Grossman, S. A., Brem, H., and Quinones-Hinojosa, A. (2009). Gliadel (BCNU) wafer plus concomitant temozolomide therapy after primary resection of glioblastoma multiforme. Journal of neurosurgery *110*, 583-588.

Mojas, N., Lopes, M., and Jiricny, J. (2007). Mismatch repair-dependent processing of methylation damage gives rise to persistent single-stranded gaps in newly replicated DNA. Genes & development *21*, 3342-3355.

Newcomb, E. W., Cohen, H., Lee, S. R., Bhalla, S. K., Bloom, J., Hayes, R. L., and Miller, D. C. (1998). Survival of patients with glioblastoma multiforme is not influenced by altered expression of p16, p53, EGFR, MDM2 or Bcl-2 genes. Brain pathology *8*, 655-667.

Newcomb, E. W., and Zagzag, D. (2009). The murine Gl261 glioma experimental model to assess novel brain tumor treatments. In CNS Cancer: Models, Markers, Prognostic Factors, Targets, and Therapeutic Approaches, E.G. Van Meir, ed. (Humana Press), pp. 227-241.

Newlands, E. S., Stevens, M. F., Wedge, S. R., Wheelhouse, R. T., and Brock, C. (1997). Temozolomide: a review of its discovery, chemical properties, pre-clinical development and clinical trials. Cancer treatment reviews *23*, 35-61.

Nguyen, L. V., Vanner, R., Dirks, P., and Eaves, C. J. (2012). Cancer stem cells: an evolving concept. Nature reviews Cancer *12*, 133-143.

Nick McElhinny, S. A., Kumar, D., Clark, A. B., Watt, D. L., Watts, B. E., Lundstrom, E. B., Johansson, E., Chabes, A., and Kunkel, T. A. (2010). Genome instability due to ribonucleotide incorporation into DNA. Nature chemical biology *6*, 774-781.

Nobusawa, S., Watanabe, T., Kleihues, P., and Ohgaki, H. (2009). IDH1 mutations as molecular signature and predictive factor of secondary glioblastomas. Clinical cancer research : an official journal of the American Association for Cancer Research *15*, 6002-6007.

Norden, A. D., Lesser, G. J., Drappatz, J., Ligon, K. L., Hammond, S. N., Lee, E. Q., Reardon, D. R., Fadul, C. E., Plotkin, S. R., Batchelor, T. T., *et al.* (2013). Phase 2 study of dose-intense temozolomide in recurrent glioblastoma. Neuro-oncology *15*, 930-935.

Ohba, S., Hirose, Y., Kawase, T., and Sano, H. (2009). Inhibition of c-Jun N-terminal kinase enhances temozolomide-induced cytotoxicity in human glioma cells. Journal of neuro-oncology *95*, 307-316.

Ostermann, S., Csajka, C., Buclin, T., Leyvraz, S., Lejeune, F., Decosterd, L. A., and Stupp, R. (2004). Plasma and cerebrospinal fluid population pharmacokinetics of temozolomide in malignant glioma patients. Clinical Cancer Research *10*, 3728-3736.

Perry, J. R., Belanger, K., Mason, W. P., Fulton, D., Kavan, P., Easaw, J., Shields, C., Kirby, S., Macdonald, D. R., Eisenstat, D. D., *et al.* (2010). Phase II trial of continuous dose-intense temozolomide in recurrent malignant glioma: RESCUE study.

Journal of clinical oncology : official journal of the American Society of Clinical Oncology *28*, 2051-2057.

Phillips, H. S., Kharbanda, S., Chen, R., Forrest, W. F., Soriano, R. H., Wu, T. D., Misra, A., Nigro, J. M., Colman, H., Soroceanu, L., *et al.* (2006). Molecular subclasses of high-grade glioma predict prognosis, delineate a pattern of disease progression, and resemble stages in neurogenesis. Cancer cell *9*, 157-173.

Pistollato, F., Abbadi, S., Rampazzo, E., Persano, L., Della Puppa, A., Frasson, C., Sarto, E., Scienza, R., D'Avella, D., and Basso, G. (2010). Intratumoral hypoxic gradient drives stem cells distribution and MGMT expression in glioblastoma. Stem cells *28*, 851-862.

Quinn, J. A., Jiang, S. X., Reardon, D. A., Desjardins, A., Vredenburgh, J. J., Rich, J. N., Gururangan, S., Friedman, A. H., Bigner, D. D., Sampson, J. H., *et al.* (2009). Phase II trial of temozolomide plus o6-benzylguanine in adults with recurrent, temozolomide-resistant malignant glioma. Journal of clinical oncology : official journal of the American Society of Clinical Oncology *27*, 1262-1267.

Quiros, S., Roos, W. P., and Kaina, B. (2010). Processing of O6-methylguanine into DNA double-strand breaks requires two rounds of replication whereas apoptosis is also induced in subsequent cell cycles. Cell cycle *9*, 168-178.

Ray-Chaudhury, A. (2010). Pathology of Glioblastoma Multiforme. In Glioblastoma: Molecular mechanisms of pathogenesis and current therapeutic strategies, S.K. Ray, ed., pp. 77-84.

Scherer, H. J. (1940). A critical review: The pathology of cerebral gliomas. Journal of Neurology and Psychiatry *3*, 147-177.

Senft, C., Bink, A., Franz, K., Vatter, H., Gasser, T., and Seifert, V. (2011). Intraoperative MRI guidance and extent of resection in glioma surgery: a randomised, controlled trial. The lancet oncology *12*, 997-1003.

Shiraishi, S., Tada, K., Nakamura, H., Makino, K., Kochi, M., Saya, H., Kuratsu, J., and Ushio, Y. (2002). Influence of p53 mutations on prognosis of patients with glioblastoma. Cancer *95*, 249-257.

Singh, S. K., Hawkins, C., Clarke, I. D., Squire, J. A., Bayani, J., Hide, T., Henkelman, R. M., Cusimano, M. D., and Dirks, P. B. (2004). Identification of human brain tumour initiating cells. Nature *432*, 396-401.

SongTao, Q., Lei, Y., Si, G., YanQing, D., HuiXia, H., XueLin, Z., LanXiao, W., and Fei, Y. (2012). IDH mutations predict longer survival and response to temozolomide in secondary glioblastoma. Cancer science *103*, 269-273.

Stopschinski, B. E., Beier, C. P., and Beier, D. (2013). Glioblastoma cancer stem cells--from concept to clinical application. Cancer letters *338*, 32-40.

Stupp, R., Mason, W. P., van den Bent, M. J., Weller, M., Fisher, B., Taphoorn, M. J., Belanger, K., Brandes, A. A., Marosi, C., Bogdahn, U., *et al.* (2005). Radiotherapy plus concomitant and adjuvant temozolomide for glioblastoma. The New England journal of medicine *352*, 987-996.

Stupp, R., Tonn, J. C., Brada, M., Pentheroudakis, G., and Group, E. G. W. (2010). High-grade malignant glioma: ESMO Clinical Practice Guidelines for diagnosis, treatment and follow-up. Annals of oncology : official journal of the European Society for Medical Oncology / ESMO *21 Suppl 5*, v190-193.

The Cancer Genome Atlas Research Network, T. (2008). Comprehensive genomic characterization defines human glioblastoma genes and core pathways. Nature *455*, 1061-1068.

Verhaak, R. G., Hoadley, K. A., Purdom, E., Wang, V., Qi, Y., Wilkerson, M. D., Miller, C. R., Ding, L., Golub, T., Mesirov, J. P., *et al.* (2010). Integrated genomic analysis identifies clinically relevant subtypes of glioblastoma characterized by abnormalities in PDGFRA, IDH1, EGFR, and NF1. Cancer cell *17*, 98-110.

Vitucci, M., Hayes, D. N., and Miller, C. R. (2011). Gene expression profiling of gliomas: merging genomic and histopathological classification for personalised therapy. British journal of cancer *104*, 545-553.

Walbert, T., and Mikkelsen, T. (2011). Recurrent high-grade glioma: a diagnostic and therapeutic challenge. Expert review of neurotherapeutics *11*, 509-518.

Wang, S. I., Puc, J., Li, J., Bruce, J. N., Cairns, P., Sidransky, D., and Parsons, R. (1997). Somatic mutations of PTEN in glioblastoma multiforme. Cancer research *57*, 4183-4186.

Wang, Y., Zhu, S., Cloughesy, T. F., Liau, L. M., and Mischel, P. S. (2004). p53 disruption profoundly alters the response of human glioblastoma cells to DNA topoisomerase I inhibition. Oncogene *23*, 1283-1290.

Weller, M., Felsberg, J., Hartmann, C., Berger, H., Steinbach, J. P., Schramm, J., Westphal, M., Schackert, G., Simon, M., Tonn, J. C., *et al.* (2009). Molecular predictors of progression-free and overall survival in patients with newly diagnosed glioblastoma: a prospective translational study of the German Glioma Network. Journal of clinical oncology : official journal of the American Society of Clinical Oncology *27*, 5743-5750.

Wolbers, J. G. (2014). Novel strategies in glioblastoma surgery aim at safe, supra-maximum resection in conjunction with local therapies. Chinese journal of cancer *33*, 8-15.

Wyatt, M. D., and Pittman, D. L. (2006). Methylating agents and DNA repair responses: Methylated bases and sources of strand breaks. Chemical research in toxicology *19*, 1580-1594.

Yan, H., Parsons, D. W., Jin, G., McLendon, R., Rasheed, B. A., Yuan, W., Kos, I., Batinic-Haberle, I., Jones, S., Riggins, G. J., *et al.* (2009). IDH1 and IDH2 mutations in gliomas. The New England journal of medicine *360*, 765-773.

Yip, S., Miao, J., Cahill, D. P., Iafrate, A. J., Aldape, K., Nutt, C. L., and Louis, D. N. (2009). MSH6 mutations arise in glioblastomas during temozolomide therapy and mediate temozolomide resistance. Clinical cancer research : an official journal of the American Association for Cancer Research *15*, 4622-4629.

Yoshioka, K., Yoshioka, Y., and Hsieh, P. (2006). ATR kinase activation mediated by MutSalpha and MutLalpha in response to cytotoxic O6-methylguanine adducts. Molecular cell *22*, 501-510.

Zhu, T. S., Costello, M. A., Talsma, C. E., Flack, C. G., Crowley, J. G., Hamm, L. L., He, X., Hervey-Jumper, S. L., Heth, J. A., Muraszko, K. M., *et al.* (2011). Endothelial cells create a stem cell niche in glioblastoma by providing NOTCH ligands that nurture self-renewal of cancer stem-like cells. Cancer research *71*, 6061-6072.

Chapter II: Response of glioblastoma cells to acute and periodic temozolomide exposure

José L. McFaline, Zachary Nagel, Patrizia Mazzucato, Dewakar Sangaraju, Yimin Chen, Amanda Vargas, Natalia Tretyakova, Forest M. White and Leona D. Samson

Experimental contributions: Z.N. and P.M. performed the Host Cell reactivation experiments on Figures 2.13 and 2.15. D.S. performed the quantitation for O^6-meG levels in TMZ treated GBM cells in Table 2.1.

Chapter II: Response of glioblastoma cells to acute and periodic temozolomide exposure

Introduction

Even with aggressive treatment, GBM is considered incurable, with recurrent tumors displaying a chemo- and radio-resistant phenotype. Frontline chemotherapy in the treatment of GBM consists of temozolomide (TMZ), an oral S_N1 mono-alkylating agent shown to increase overall survival when administered with radiotherapy (Stupp et al., 2005). Although considered a success, on average TMZ extends survival by only one to two months, with recurrent GBM showing a strong chemoresistant phenotype.

While TMZ induces a variety of DNA base lesions its toxicity is mediated primarily by mismatch repair (MMR) dependent processing of O^6-methylguanine (O^6-meG) DNA base lesions produced by TMZ (Li, 2008) that can be prevented by O^6-methylguanine methyltransferase (MGMT) mediated repair. MGMT is a direct reversal DNA repair protein able to efficiently remove the methyl group from the O^6 position of guanine (van Nifterik et al., 2010). In approximately half of all GBM, MGMT is epigenetically silenced at the *MGMT* locus by promoter methylation. MGMT levels are inversely correlated to the response of GBM patients to TMZ (Hegi et al., 2005); in other words, tumors with low MGMT respond better to TMZ therapy. To date, *MGMT* promoter methylation status remains the most widely used prognostic indicator for initial therapeutic response to TMZ. In the absence of MGMT mediated O^6-meG repair, the MMR machinery potentiates the toxicity of O^6-meG lesions in the following way: during replication, DNA polymerases insert thymidine opposite O^6-meG and the MutSα recognition complex, a heterodimer composed of MSH2 and MSH6, binds to the O^6-meG:T mismatch before recruiting the MutLα heterodimer, composed of MLH1 and

PMS2, and Exo1; together these proteins excise a stretch of single-stranded DNA containing the thymine opposite O^6-meG creating a gap in the DNA. To complete mismatch repair DNA polymerases fill the gap prior to DNA ligation, only to once again incorporate a thymine opposite O^6-meG, stimulating another round of MMR. This futile cycling leads to accumulation of ssDNA gaps that generate double strand breaks at collapsed replication forks during a second round of replication. The double strand breaks lead to DNA damage response activation to signal for cell cycle arrest or cell death (Cejka et al., 2003; Li, 2008).

In this study, we characterize the response of p53 proficient and p53 deficient glioblastoma cells to both acute and periodic temozolomide exposure. We find that a single, high dose of TMZ leads to a robust accumulation of cells in the G2/M phase of the cell cycle. This arrest is cell cycle dependent with cells accumulating two cell doublings post-treatment consistent with the timing for the formation of O^6-meG induced double strand breaks. Consistent with double strand break formation a robust activation of Chk2 accompanies cell cycle arrest two doublings post-treatment. In contrast to previous reports, p53 status does not appear to alter the sensitivity of GBM cells to TMZ. However, p53 does appear to alter the magnitude and persistent of the cell cycle arrest following TMZ exposure.

Materials and methods

Reagents

TMZ, 1,3-Bis(2-chloroethyl)-1-nitrosourea (BCNU), *N*-Methyl-*N'*-nitro-*N*-nitrosoguanidine (MNNG), Hoechst, and propidium iodide were purchased from Sigma-Aldrich. TMZ was

dissolved in DMSO, BCNU was dissolved in ethanol and MNNG was dissolved in 0.1M sodium acetate pH 5. Aliquots of stock solutions were stored at -80°C.

Antibodies

Antibodies to MGMT (ab7045), MSH2 (ab9146), MSH6 (ab92471), PMS2 (ab110638) and MLH1 (ab9144) were purchased from Abcam. Anti-MSH2 (2850), anti-phospho T68 Chk2 (2661) and anti-Chk2 (2662) were purchased from Cell Signaling Technologies. Anti-phospho S139 H2AX (05-636) and anti-H2AX (07-627) were purchased from Millipore. Anti-p53 (sc-253) was purchased from Santa Cruz Biotechnologies. Alexa Fluor 647 anti-BrdU (560209) was purchased from BD Biosciences.

Cell culture

Human U87MG GBM cells were purchased from ATCC. All cell lines were cultured in DMEM medium supplemented with 10% fetal bovine serum (FBS) and 1% penicillin/streptomycin (pen-strep). Cells were maintained under standard incubation conditions.

shRNA constructs

For knockdown experiments in the human U87MG cell line, pGIPZ lentiviral vectors expressing a scrambled hairpin control (RHS4346) or hairpins targeting human p53 transcripts (RHS4430-98486236 ID: V2LHS_217) were purchased from Open Biosystems (Table 2.2).

Generation of p53 knockdown cells

Lentiviral shRNA constructs and packaging plasmids (psPAX2 and pMD2.G) were co-transfected into 293T cells to produce lentiviral particles. Subsequently, U87MG cells

were infected with lentivirus and shRNA expressing cells selected by puromycin treatment.

Acute drug treatments

U87MG GBM cells were treated with TMZ or BCNU for 1 hour in serum-free media at the specified concentrations. After treatment, drug-containing medium was removed and replaced with DMEM containing 10% FBS and 10% pen-strep. For ionizing radiation treatment, cells were irradiated in complete media using a gamma cell irradiator for the time period necessary to achieve the specified exposure. For MNNG treatment, cells were treated in complete media, and exposure time determined by its rapid decay in complete media.

Generation of temozolomide resistant GBM cell lines

Selection for TMZ resistance consisted of three rounds of selection with increasing doses of temozolomide (Figure 1A). The first round consisted of exposure to 20 μM TMZ for 3 hours, after which, cells were allowed to reach 90% confluence then passaged three times in the absence of drug. This initial priming stage was necessary for cells to endure the selection process. During the third passage without drug exposure, cells entered the second round of TMZ selection by treatment with 40 μM TMZ for 3 hours. Cells were then allowed to reach 90% confluence after treatment, at which point cells were passaged. This 40μM TMZ treatment followed by attainment of 90% confluency of the treated cells was repeated two additional times to complete the second round of selection. The third round of TMZ selection was identical to the second round with the exception that 60 μM TMZ was used. At the end of the third round cells were passaged three times to enrich for a stable population. This selection protocol was based on previous generation of 5-fluorouracil resistant colorectal cancer cells and was designed

to mimic TMZ treatment in GBM patients (Dallas et al., 2009; Hegi et al., 2005; Stupp et al., 2005).

Metaphase chromosome spreads

Control, p53kd, Control-TMZ^{R3} and p53kd-TMZ^{R3} GBM cells were incubated with 0.1 mg/mL colcemid to arrest cells during metaphase. Metaphase cells were collected by mitotic shake-off and incubated in warm (37°C) hypotonic 75 mM potassium chloride for 15 minutes at 37°C, after which, cells were fixed in Carnoys fixative (3:1 mixture of methanol and acetic acid). Fixed cells were dropped onto microscope slides to burst the cells and create metaphase spreads. Dried slides were stained with Giemsa stain, and the chromosomes of one hundred spreads were counted per condition to establish modal chromosome number.

Immunoblotting

For protein level analysis, cells were harvested during exponential growth phase. For analysis of H2AX activation, cells were seeded at 3 x 10^6 cells in 15 cm plates, with the exception of p53kd-TMZ^{R3} that were seeded at 1.5 x 10^6, and cells were allowed to attach for 24 hours. After attachment, duplicate cell cultures were treated for 1 hour in serum free media with or without 80 μM TMZ. When treatment was finished drug containing medium was removed and DMEM + 10% FBS and 1% pen-strep was added. Two cell cycle times after treatment samples were harvested by scraping cells into ice cold PBS and cells from duplicate plates pooled. Cell pellets were lysed in buffer containing 20 mM Tris HCl pH 8.0, 137 mM NaCl, 10% glycerol, 1% NP-40 and 10 mM EDTA. At the time of lysis, 1 mM DTT, 10 mM sodium fluoride, 1 mM sodium orthovanadate and a protease inhibitor cocktail tablet (Roche) were added to the lysis buffer. Lysates were incubated on ice, sonicated and centrifuged to remove cell debris.

Protein concentration was measured using the Micro BCA assay kit (Pierce). Roughly equal amounts of protein were electrophoresed on 10% bis-tris Novex gels (Invitrogen) and proteins transferred to PVDF membranes (BioRad). Membranes were blocked in Odyssey blocking buffer (Licor) and antibody incubations were carried out for 1 hour at room temperature. For imaging, membranes were probed with secondary antibodies, conjugated to infrared dyes (Sigma) and immunoblots imaged using the Odyssey infrared imaging system (Licor). Immunoblots were quantified using the NIH ImageJ processing software. In the case of protein level analysis, protein levels were normalized to actin as a loading control. For H2AX activation, analysis of S139-phosphorylated H2AX levels were normalized to total H2AX levels. Significance was assessed using the student's t-test.

Flow cytometry based proliferation assay

All U87MG derived cells were seeded at a density of 3 x 10^5 cells in 6 cm plates with the exception of p53kd-TMZ^{R3} cells, which were seeded at 1.5 x 10^5 cells in 6 cm plates, and allowed to attach for 24 hr. Plating the larger, polyploid, p53kd-TMZ^{R3} cells at lower density ensured that all lines were at similar confluence. After attachment, cells were exposed to each agent as described above. Two cell cycle times after treatment, BrdU was added to each plate at a final concentration of 25 μM. Cells were allowed to incorporate BrdU for an additional two cell cycle times to follow proliferation after drug exposure. At the end of BrdU exposure, cells were harvested, stained with Hoechst and propidium iodide and analyzed by FACS as described (Valiathan et al., 2012).

Cell cycle analysis

Cells were seeded at 1 x 10^6 cells, with the exception of p53kd-TMZ^{R3} at 5 x 10^5 cells, in 10 cm plates and allowed to attach for 24 hours. After attachment, cells were mock

treated or treated with 80 μM TMZ as described above. For cell cycle profiling analysis by BrdU incorporation and DNA content staining, Control and p53kd samples were harvested 24, 48, 72, 96, 120, 144, 168 and 192 hours post TMZ exposure. Cell pellets were resuspended in 500 μL cold PBS and 5 mL of cold ethanol was added drop-wise while vortexing and then fixed overnight at 4°C. Fixed cells were washed with PBS containing 1% bovine serum albumin (BSA) and incubated in 2M HCl containing 0.5% Triton-X100 for 30 minutes to unwind DNA. HCl was neutralized with 0.1M sodium borate pH 8.5, washed with PBS containing 1% BSA and 0.5% Tween 20 (PBS-TB) and incubated in PBS-TB containing Alexa Fluor 647 conjugated anti-BrdU for 2 hours at room temperature. At the end of incubation cells were washed twice with PBS containing 0.5% Tween 20 (PBS-T) and resuspended in 300 μL of PBS containing 1% BSA, 50 μg/mL propidium iodide and 500 μg/mL RNAseA. Samples were incubated for 30 minutes at room temperature prior to FACS analysis. For cell cycle response of parental and TMZ^{R3} cells, samples were harvested two cell cycles after TMZ treatment. Cell pellets were resuspended in 500 μL cold PBS and 5 mL of cold ethanol was added drop-wise while vortexing and then fixed overnight at 4°C. For nuclear staining, the fixed cells were washed with PBS containing 1% bovine serum albumin (BSA) and resuspended in 300 μL of PBS containing 1% BSA, 50 μg/mL propidium iodide and 500 μg/mL RNAseA. Samples were incubated for 30 minutes at room temperature prior to FACS analysis.

Isotope dilution tandem mass spectrometry-based quantification of O^6-methylguanine (O^6-meG) lesions

Control, p53kd, Control-TMZ^{R3} and p53kd-TMZ^{R3} cells were seeded at a density of 1 x 10^7 cells in 15 cm plates for mock or TMZ treatment with each condition in replicate. Cells were allowed to attach for 24 hours, after which, medium was removed and replaced with serum-free medium containing 80 μM TMZ. 1 hour later, medium was

replaced with DMEM containing 10% FBS and 1% pen-strep. Three hours after the end of TMZ treatment, medium was removed and cells were washed with ice cold PBS. After washing, cells were scraped into 5 mL of ice cold PBS and the content of replicate plates were pooled. Cells were centrifuged for 5 minutes at 300 x g and pellets were snap frozen in liquid nitrogen. DNA was extracted from pellets using the Roche DNA isolation kit for cells and tissues according to the manufacturer's instructions. Isolated DNA was dried and resuspended in water. DNA concentration was quantified by UV absorption at 260 and 280 nm. 500 fmol of a deuterium labeled O^6-meG internal standard (O^6-CD_3-G) was added for LC-MS/MS quantitation. Acid thermal hydrolysis to depurinate DNA was performed for 40 min at 80°C in 0.1 N hydrochloric acid, neutralized by the addition of 0.1N sodium hydroxide, then subjected to solid phase extraction using Strata X (30mg, 1mL) polymeric reversed phase cartridges. Eluates were vacuum dried, resuspended in 25 µL of 25 mM Ammonium acetate and subjected to LC-MS/MS analysis using Zorbax 300 SB-C18 (150 x 0.5 mm, 5µ) column with an LC elution gradient of A: 25mM Ammonium acetate in water and B: 3:1 methanol:acetonitrile on a TSQ vantage-2 triple quadrupole instrument operated at spray voltage of 3.2 KV, capillary temperature of 250 °C, collision energy of 20V and S-lens value of 85 units. LC Gradient conditions started with 2% B and liner increase to 9.5% B in 9 min, to 25% B in 6 min and then to 2% B in 3 min followed by equilibration for 4 min at 2% B with a flow rate of 10µL/min. Under these conditions O6-Me-G eluted at 11.6 min. O^6-CD_3-G levels were quantified based on the peak area for the MS/MS transitions for O^6-meG and the O^6-CD_3-G internal standard, 166.1 → 149.1 and 169.1 → 152.1, respectively. Student's t-test was used to assess significance between adduct levels in parental and TMZ^{R3} resistant GBM cells.

Assessment of MGMT and DNA MMR activity using Host-Cell Reactivation

A non-replicating plasmid encoding an mPlum fluorescent protein containing a single O^6-meG lesion in the transcribed strand (at a site critical for fluorophore maturation) was transfected into parental and TMZ^{R3} resistant GBM cells. Two outcomes are possible after transcription in the presence of O^6-meG containing mPlum gene: (i) non-fluorescent mPlum will be produced if either RNA polymerase II inserts a cytosine opposite the O^6-meG lesion or if O^6-meG lesions are repaired by MGMT and thus a cytosine will be inserted opposite the resulting base; (ii) a fluorescent mPlum can be generated if O^6-meG is not repaired because RNA polymerase II can occasionally insert a thymine opposite the lesion generating a wild type transcript and functional protein. Thus, cells proficient for O^6-meG repair will produce lower levels of fluorescent protein compared to cells deficient in O^6-meG repair. The O^6-meG repair capacity (i.e. MGMT activity) was normalized to the mean repair capacity of control cells (U87MG cells expressing a scramble hairpin control).

A non-replicating plasmid containing a single G:G mismatch at a site necessary for fluorophore maturation was transfected into cells. If the mismatch is not repaired, or if MMR is directed to the non-transcribed strand, the transcript produced will code for a non-fluorescent mOrange protein. However, if the mismatch is corrected with repair directed to the transcribed strand, a wild type fluorescent mOrange transcript will be produced and fluorescence restored. Thus, cells proficient in MMR will produce higher levels of fluorescent protein compared to MMR deficient cells. The MMR repair capacity was normalized to the mean repair capacity of control cells.

Results

p53 status alters the magnitude and the resolution of TMZ-induced G2/M arrest but not the sensitivity of GBM cells to acute TMZ exposure

p53 is one of the most commonly mutated tumor suppressor genes in GBM (The Cancer Genome Atlas, 2008). Moreover, p53 status has been proposed to alter the response of GBM cells to DNA damaging agents, including TMZ (Dinca et al., 2008; Hirose et al., 2001; Wang et al., 2004). To assess whether p53 alters the response to acute TMZ exposure we employed p53 proficient and p53 deficient U87MG GBM cells generated by expression of lentiviral vectors containing either a scrambled hairpin control (Control) or an shRNA targeting p53 transcripts (p53kd) (Figure 2.1A and 2.1B). Using a flow cytometry based proliferation assay we found that Control and p53kd cells display similar sensitivity to various doses of TMZ (Figure 2.1C). Cell cycle profiling of Control and p53kd cells treated with a single, high 80 μM dose of TMZ revealed a robust accumulation of cells with 4N DNA content beginning two cell cycle post-treatment (Figure 2.2, 48 hours). This arrest appears to be resolved over time starting at 96 hours post-exposure. However, this resolution appears to be lagging in p53kd cells (Figure 2.2). Additionally, TMZ treatment resulted in the accumulation of a small proportion of cells with higher than 4N DNA content a phenotype previously observed in GBM cells treated with damaging agents (Hirose et al., 2001). DNA synthesis detection by BrdU incorporation combined with DNA content staining demonstrates that the TMZ induced increase in 4N cells is due to a collection of cells at late S, which precedes accumulation at the G2/M boundary (Figure 2.3A and 2.3B, panel). Quantification of cell cycle phase accumulation by DNA content staining and BrdU incorporation (Figure 2.4) confirm that both the magnitude and the resolution of the arrest following TMZ exposure appears p53 dependent (Figure 2.5, G2 panel). This arrest is accompanied by activation of H2AX

and, more robustly, activation of Chk2 as assessed by phosphorylation of serine 139 and threonine 68, respectively (Figure 2.6).

Generation of TMZ resistant p53 proficient and p53 deficient GBM cells by periodic exposure to escalating doses of TMZ

To identify changes associated with acquired TMZ resistance in GBM, resistant cell lines were generated by periodic exposure of U87MG GBM cells that were p53-proficient (Control) and p53-deficient (p53kd) (Figure 2.7A) to increasing doses of TMZ. This approach was adapted from a method that was successfully employed to generate 5-fluorouracil resistant colon carcinoma lines (Dallas et al., 2009); details of the selection process are shown in Figure 2.8A. Importantly, the periodic exposures to increasing doses of TMZ emulated standard TMZ chemotherapy regimens currently used for GBM therapy (75 mg/kg/m^2 cycle, followed by a 150 mg/kg/m^2 and finally a high dose of 200 mg/kg/m^2) (Stupp et al., 2005). Moreover, the doses chosen were close to the maximum cerebrospinal fluid (CSF) TMZ concentrations observed during patient dosing (Ostermann et al., 2004).

Previous reports suggest that p53 loss may sensitize GBM cells to TMZ (Blough et al., 2011; Hirose et al., 2001). However, we find that Control and p53kd cells became confluent at similar times following the various TMZ treatment cycles (Figure 2.7B). A flow cytometric cell survival assay (Valiathan et al., 2012) was used to measure the TMZ sensitivity of parental cells (Control and p53kd) and of cells from the third round of TMZ selection (Control-TMZ^{R3} and p53kd-TMZ^{R3}). Control and p53kd cells exhibited very similar TMZ sensitivity, indicating equivalent ability to cope with an acute TMZ challenge. In contrast, both Control-TMZ^{R3} and p53kd-TMZ^{R3} displayed a strong TMZ-resistant phenotype (Figure 2.7C) suggesting that a change in p53 status is not required for

acquisition of TMZ resistance. As the toxicity of TMZ is attributed primarily to the formation of O^6-meG lesions in the DNA, we investigated TMZ induced levels of O^6-meG in parental and TMZ^{R3} cells (proficient and deficient for p53). Isotope dilution tandem mass spectrometry was employed to measure O^6-meG DNA adduct levels in parental and TMZ^{R3} resistant GBM cells after treatment with a high dose of TMZ (80 μM). This analysis revealed that parental and TMZ^{R3} cells acquire very similar levels of O^6-meG upon TMZ exposure, eliminating the possibility that cells become resistant by somehow preventing TMZ from reacting with genomic DNA (Table 2.1).

Various groups have observed polyploid induction in U87MG cells after TMZ treatment (Hirose et al., 2001). We find that this phenotype is exacerbated in U87MG cells made deficient in p53. Polyploid GBM cells were regarded as unstable and primed for mitotic catastrophe (Hirose et al., 2001). Analysis of the cells obtained at the end of each round of TMZ selection showed that polyploidy was induced in the p53 proficient Control cells early in selection; however, this population was selected against during the course of repeated TMZ exposure (Figure 2.8A). However, consistent with the role of p53 in the tetraploid checkpoint (Andreassen et al., 2001), p53kd cells rapidly became polyploid in response to TMZ exposure and maintained polyploidy throughout subsequent rounds of TMZ selection (Figure 2.8A). Metaphase chromosome analysis confirmed the polyploid phenotype (Figure 2.8B and 2.8C). Thus, in contrast to the previously reported instability and transient nature of this polyploid population (Hirose et al., 2001), the p53kd-TMZ^{R3} cells appear to be stably tetraploid even after extended growth in culture (data not shown). Control and p53kd GBM cells underwent a robust cell cycle arrest at the late S/G2-M boundary two cell cycle times after a single TMZ treatment (Figure 2.6, late S and G2 panel and Figure 2.9A and 2.9B). This timing corresponds to the time at which MMR-induced processing at O^6-meG leads to double strand break formation at collapsed replication forks (Li, 2008). In contrast, TMZ^{R3} GBM cells (proficient and

deficient for p53) did not activate a cell cycle checkpoint two cell cycle times after drug exposure consistent with their TMZ resistance. Immunoblot analysis of H2AX phosphorylation after TMZ treatment revealed that TMZ^{R3} cells exhibit decreased H2AX phosphorylation compared to parental lines (Figure 2.10A and 2.10B).

The TMZ resistant phenotype is specific for O^6-meG formation and does not confer resistance to ionizing radiation or 1,3-bis-(2-chloroethyl)-1-nitroso-urea (BCNU)

To assess whether TMZ resistance was accompanied by resistance to other S_N1 alkylating agents and to other types of DNA damaging agents relevant to GBM therapy, cells were exposed to MNNG (an S_N1 alkylating agent), BCNU (a DNA crosslinking bifunctional alkylating agent) and ionizing radiation (an agent that induces DSB's and various oxidized DNA bases). TMZ^{R3} cells displayed strong resistance to MNNG, demonstrating that resistance extends to other S_N1 alkylating agents that induce O^6-meG (Figure 2.11A). TMZ and MNNG resistance could be mediated by the efficient repair of DNA double strand breaks induced by replication past MMR processed O^6-meG lesions. However, parental and TMZ^{R3} cells did not display significant differences in their sensitivity to ionizing radiation, suggesting that TMZ resistance was not due to increased double strand break repair (Figure 2.11B). Prior to the adoption of TMZ as the frontline chemotherapeutic agent for GBM patients, BCNU was the major chemotherapeutic agent used to treat GBM. Since TMZ is well tolerated, can be taken orally, and synergizes with ionizing radiation treatment, it has now become the standard treatment for GBM patients (Stupp et al., 2005). It is well documented that MGMT expression greatly reduces the sensitivity of cells to BCNU, a DNA crosslinking agent whose mechanism of action initially involves formation of O^6-chloroethyl lesions that are

efficiently removed by MGMT (Samson et al., 1986; Yan et al., 2005). Interestingly, parental and TMZ^{R3} cells (proficient and deficient for p53) were equally sensitive to BCNU treatment (Figure 2.11C) suggesting that TMZ^{R3} cells are unlikely to have reactivated MGMT expression. Taken together, the TMZ resistant phenotype of GBM cells obtained after selection appears to be specific for monofunctional S_N1 alkylating agents and likely independent of MGMT-mediated enhanced O^6-meG repair.

TMZ^{R3} cells do not express increased MGMT protein

A few studies have suggested that increased MGMT levels are responsible for the resistance of some recurrent GBM tumors to TMZ (Brandes et al., 2010; Kitange et al., 2012). The U87MG cell line does not express MGMT, due to epigenetic silencing of the MGMT locus by promoter methylation (Lorente et al., 2008), making it feasible that resistance in TMZ^{R3} could be achieved by *MGMT* derepression. Immunoblot analysis of parental and TMZ^{R3} cells confirmed that MGMT was not expressed in any of the TMZ^{R3} cells (proficient and deficient for p53) obtained after selection (Figure 2.12A). To rule out the possibility that MGMT protein levels fell below the limit of detection, or that cells repaired O^6-meG in an MGMT independent manner, we employed an in-cell Host Cell Reactivation (HCR) assay for O^6-meG repair (Figure 2.12C). Parental and TMZ^{R3} cells (proficient and deficient for p53) displayed equally low O^6-meG repair activity demonstrating that increased MGMT activity is not responsible for the TMZ resistant phenotype of TMZ^{R3} cells. T98G cells, a GBM cell line known to expresses MGMT (Agnihotri et al., 2012), serves as a positive control for MGMT activity (Figure 2.12B). Taken together, we infer that MGMT does not play a role in our system of acquired TMZ resistance.

MMR protein levels and activity are deregulated in TMZ^{R3} cells

Deficiencies in MMR are known to prevent toxic processing of O^6-meG (Fu et al., 2012). Indeed immunoblot analysis of parental and TMZ^{R3} cells revealed decreases in the MutSα MMR recognition complex components, MSH6 and MSH2. However, these decreases were surprisingly modest with 50% MSH6 and 70% MSH2 protein remaining (Figure 2.13A, 2.13B and 2.13C). An in-cell HCR assay was employed to determine whether these modest decreases in MSH2 and MSH6 diminished MMR capacity in TMZ^{R3} cells (Figure 2.14B). TMZ^{R3} cells (proficient and deficient for p53) displayed roughly 50% decreased MMR capacity compared to their respective parental cells (Figure 2.14A). We inferred that diminished MMR capacity likely contributes to TMZ resistance in TMZ^{R3} cells, but questioned whether such a modest MMR decrease could entirely account for the extreme resistance of TMZ^{R3} cells.

Discussion

Temozolomide treatment in conjunction with radiotherapy is the current standard of care for GBM patients post surgical resection of the tumor. Unfortunately, the addition of TMZ accounts only for a two-month survival advantage compared to radiotherapy alone (Stupp et al., 2005). Moreover, recurrent tumors frequently display a strong radio- and chemo-resistant phenotype. Here we set out to explore mechanisms by which GBM cells acquire TMZ resistance.

TMZ selection was performed on p53 proficient and p53 deficient cells, as p53 deficiency has been reported to increase the response of GBM cells to TMZ (Blough et al., 2011; Hirose et al., 2001). In our U87MG cells, p53 status did not appear to confer a TMZ sensitivity phenotype after acute TMZ exposure nor did it seem to influence the mechanism by which GBM cells acquire TMZ resistance. It is possible that the residual p53 in our p53 knockdown cell lines is enough to mask this phenotype. It should be noted that in GBM a patient's p53 status does not predict therapeutic response to TMZ (Shiraishi et al., 2002). We did observe a p53 dependent polyploid induction in response to repeated TMZ exposure; however, polyploidy did not affect how cells became resistant to TMZ. In response to chronic TMZ exposure, a fraction of p53 proficient cells became polyploid yet were cleared before the end of the selection process, whereas in p53 deficient cells virtually all cells had became polyploid at the end of selection (Figure 2.8A) consistent with the role of p53 in the tetraploid checkpoint (Andreassen et al., 2001). These results suggest that the polyploid cells obtained from p53 deficient cells after TMZ selection may constitute a stable population that contribute to chemoresistance.

Patient specific variability in response to TMZ is a confounding factor in the efficacy of treatment. MGMT, a protein able to reverse TMZ induced O^6-meG lesions, is the best

studied and most characterized biomarker for TMZ efficacy, with higher efficacy in tumors exhibiting epigenetic silencing at the MGMT locus. The U87MG GBM cell line from which TMZ^{R3} cells were generated does not express MGMT due to epigenetic silencing at the MGMT locus. Therefore, increased MGMT expression by de-repression of the MGMT locus was a potential mechanism by which GBM cells could overcome TMZ sensitivity. However, MGMT expression was not altered in TMZ^{R3} GBM cells (Figure 2.12A and 2.12B). A recent study looking at matched primary and recurrent GBM found that MGMT promoter methylation, as well as protein levels were generally conserved in matched, primary and recurrent tumors (Felsberg et al., 2011). Based on this data, there does not appear to be a strong selective pressure to increase MGMT levels in response to TMZ therapy *in vivo*.

The MMR machinery processes TMZ-induced O^6-meG lesions into toxic DNA strand breaks (Fu et al., 2012; Li, 2008). It is therefore not surprising that MMR mutations are found almost exclusively in recurrent GBM tumors (Cahill et al., 2007; The Cancer Genome Atlas, 2008; Yip et al., 2009). More recently, analysis of matched primary and recurrent GBM tumors have found that disruption of the MMR machinery may be a common characteristic of recurrent disease. The MMR components MSH2, MSH6 and PMS2 are frequently down regulated at the protein level in recurrent GBM when compared to matched primary tumors (Felsberg et al., 2011). Similarly, decreases in MMR components were found in *in vitro* generated TMZ resistant GBM cells in the absence of any inactivating mutations in MMR genes (Happold et al., 2012). In the present study, we directly demonstrate that TMZ resistance correlated with decreased MMR components in GBM cells. Given the central role of MMR in the processing of TMZ-induced O^6-meG lesions we explore in the coming chapter the relationship between minor decreases in the MMR components MSH2 and MSH6 and sensitivity to TMZ.

Figures

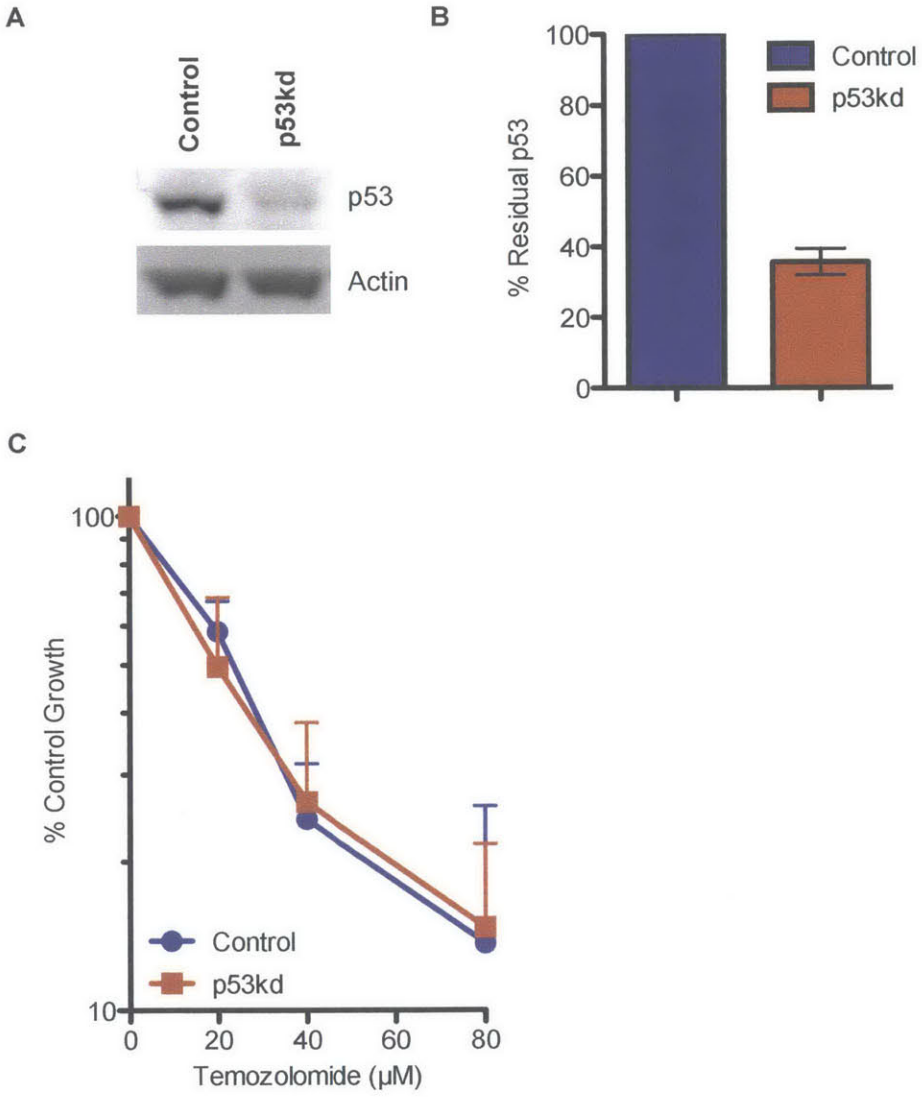

Figure 2.1 p53 status does not alter the sensitivity of GBM cells to TMZ.

(A) Immunoblot for p53 levels in Control and p53kd cells.

(B) Quantification of p53 levels in Control and p53 knockdown cells (Error bars denote standard error of the mean, n=3).

(C) Sensitivity of Control and p53kd GBM cells to TMZ.

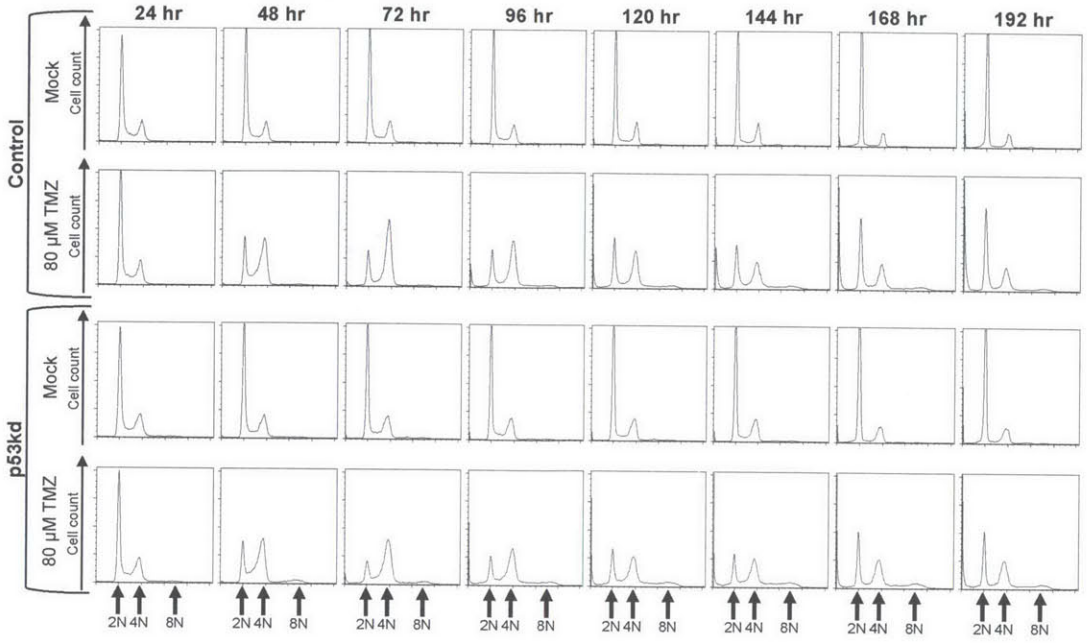

Figure 2.2 TMZ treatment induces an accumulation of cells at 4N two cell cycles post-treatment in Control and p53kd cells.

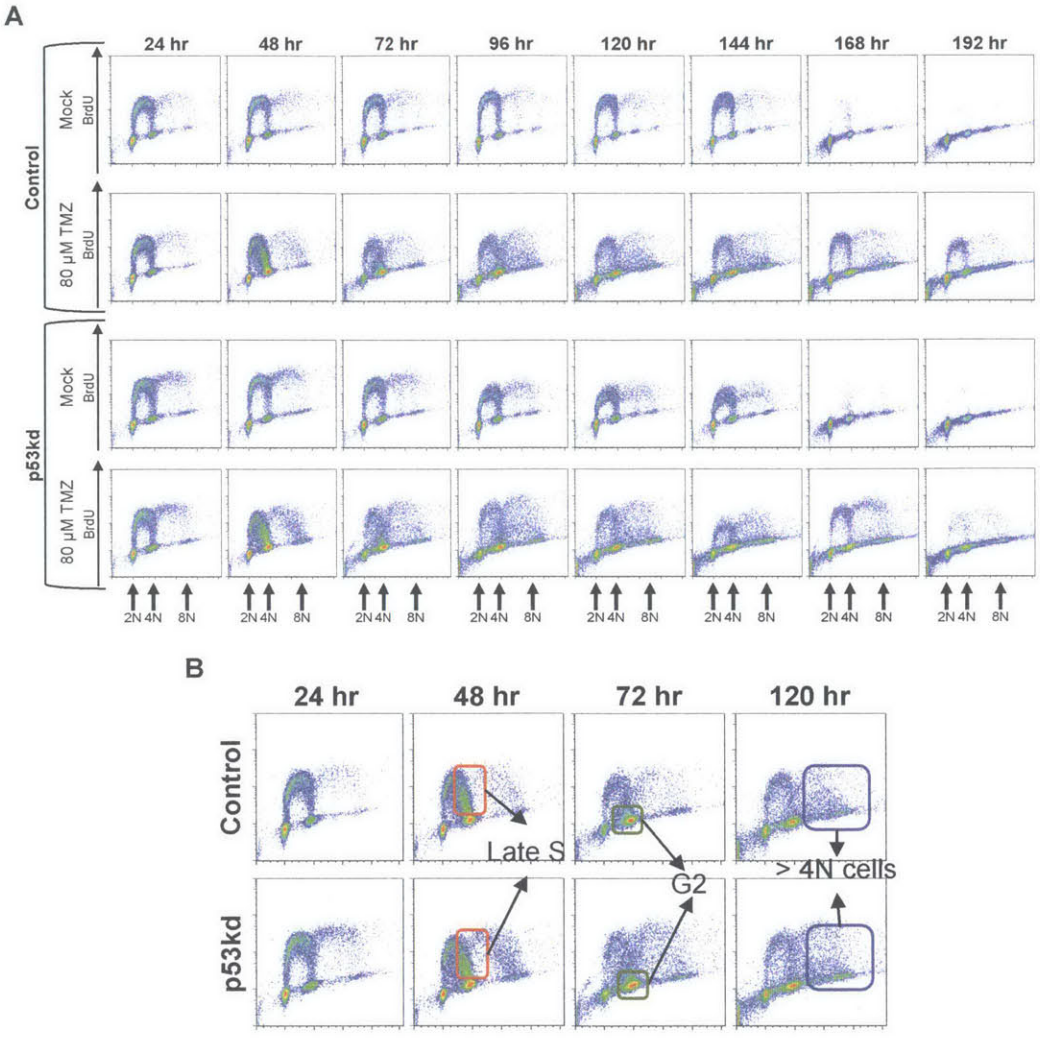

Figure 2.3 BrdU incorporation and DNA content staining reveals robust cell cycle changes in Control and p53kd cells after acute TMZ exposure.

(A) Cell cycle changes in TMZ treated control and p53kd GBM after 24 to 192 hours post TMZ exposure.

(B) Late S accumulation leads into a G2/M arrest and aneuploidy in Control and p53kd cells.

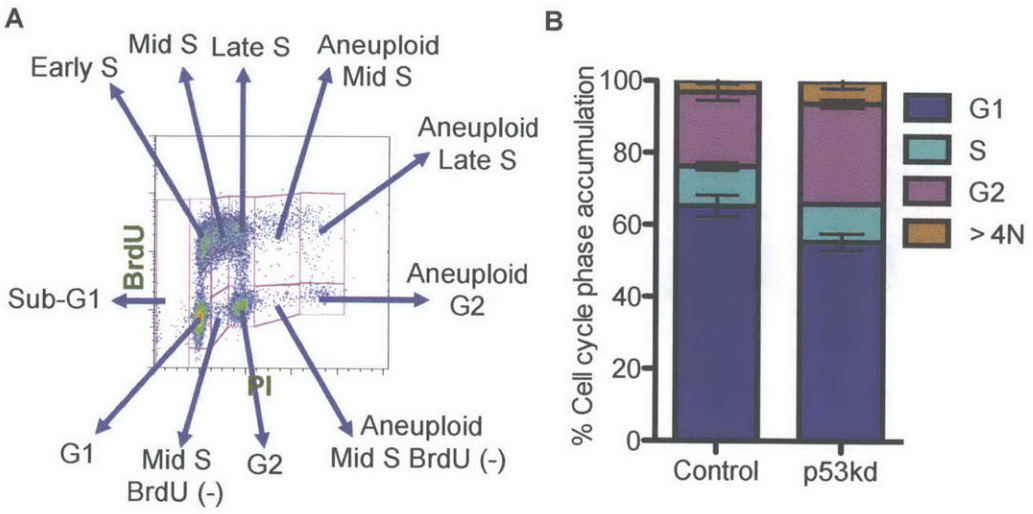

Figure 2.4 Gating used for the quantitation of cell cycle phase accumulation and cell cycle distribution of untreated Control and p53kd cells.

(A) Gates used for the quantitation of the various cell cycles phases in TMZ treated GBM cells.

(B) Cell cycle distribution of Control and p53kd cells. Due to the differences in cell cycle distribution of Control and p53kd cells the quantitation of cell cycle phases was normalized to the untreated cell cycle distribution.

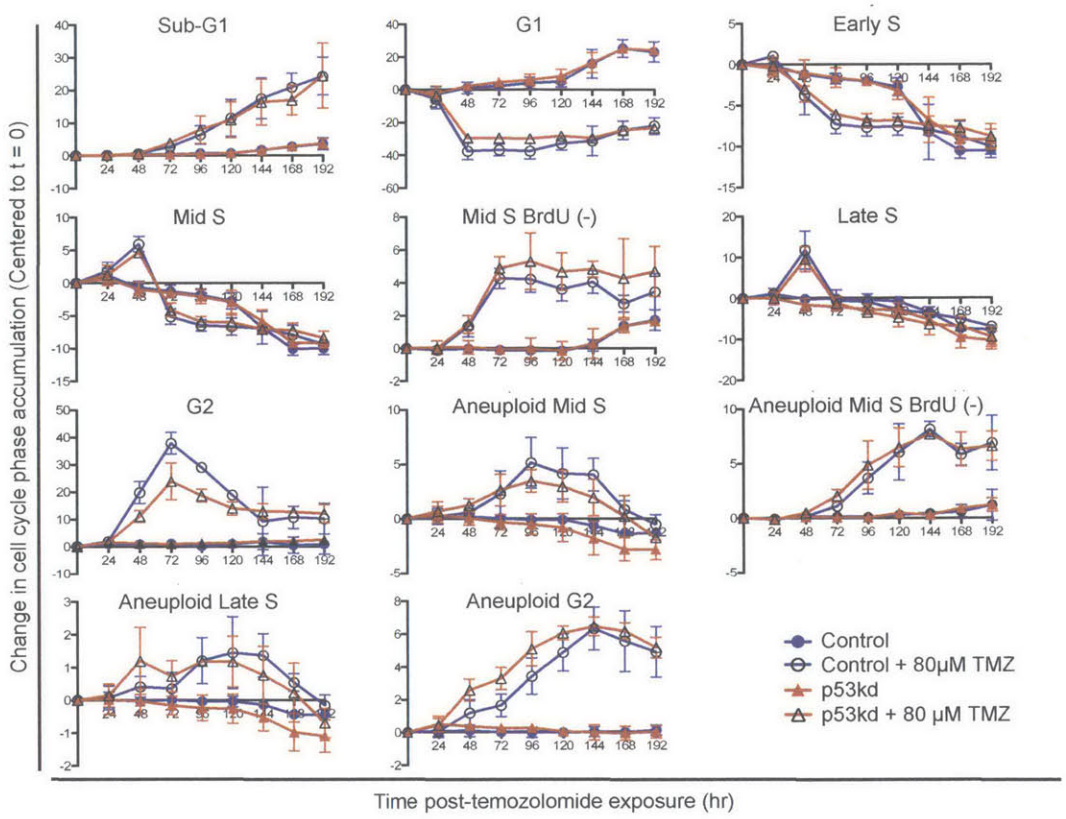

Figure 2.5 Quantitation of cell cycle phase accumulation in TMZ treated Control and p53kd cells as measured by BrdU incorporation and DNA content staining. Each panel above corresponds to the change over time in cell cycle phase accumulation in the gates described in Figure 2.5A. Data was normalized by centering to the cell cycle distribution of untreated Control and p53kd cells to account for differences in cell cycle distribution (Figure 2.5B).

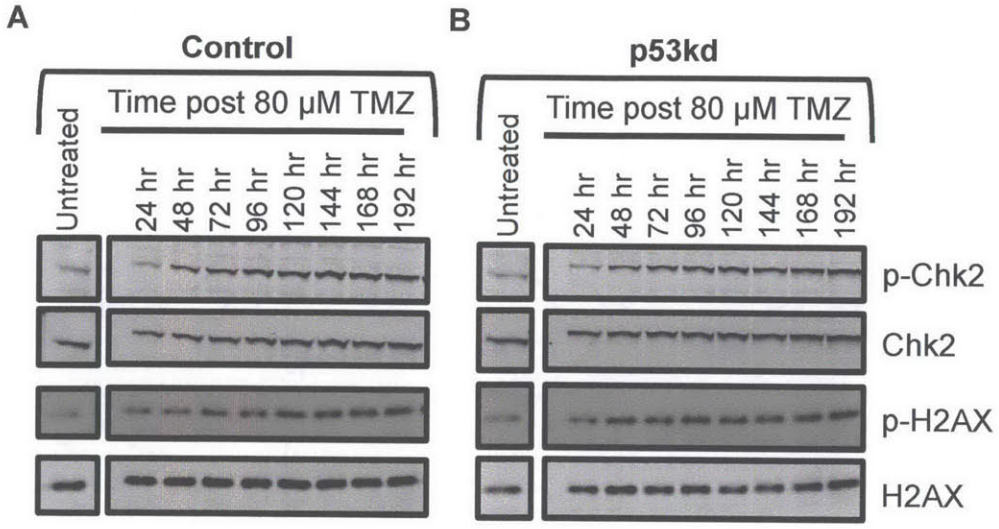

Figure 2.6 TMZ treatment leads to Chk2 and H2AX activation in Control and p53kd GBM cells.

(A) Immunoblot for T68 phosphorylated/total Chk2 and S139 phosphorylated/total H2AX levels in Control cells.

(B) Immunoblot for T68 phosphorylated/total Chk2 and S139 phosphorylated/total H2AX levels in p53kd cells.

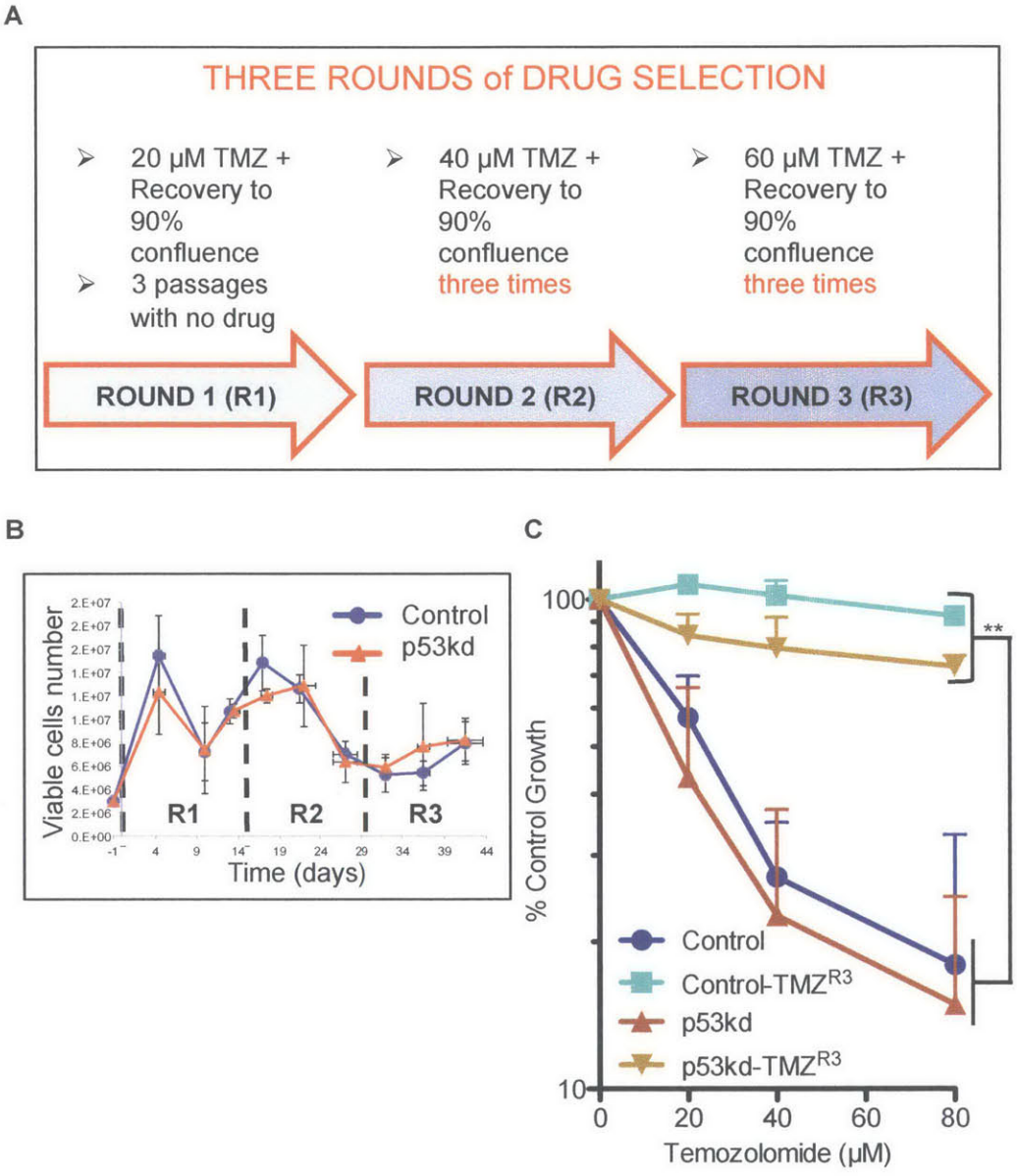

Figure 2.7 Generation of an *in vitro* model of acquired TMZ resistance in GBM.

(A) Treatment scheme for the *in vitro* selection of TMZ resistant GBM cells in p53 proficient and p53 deficient backgrounds.

(B) Timing of the TMZ selection process in Control and p53kd cells. The process begins by plating at day -1. Each mark represents passaging of cells when reaching 90%

confluence. (Horizontal and vertical error bars denote standard deviation from the mean, n=2).

(C) Sensitivity of p53 proficient and p53 deficient GBM cells prior to and after TMZ selection. Two-way ANOVA analysis was used to assess significance between the sensitivity of parental and TMZ^{R3} GBM cells (Error bars denote standard deviation from the mean, n=3, ** $p<0.01$).

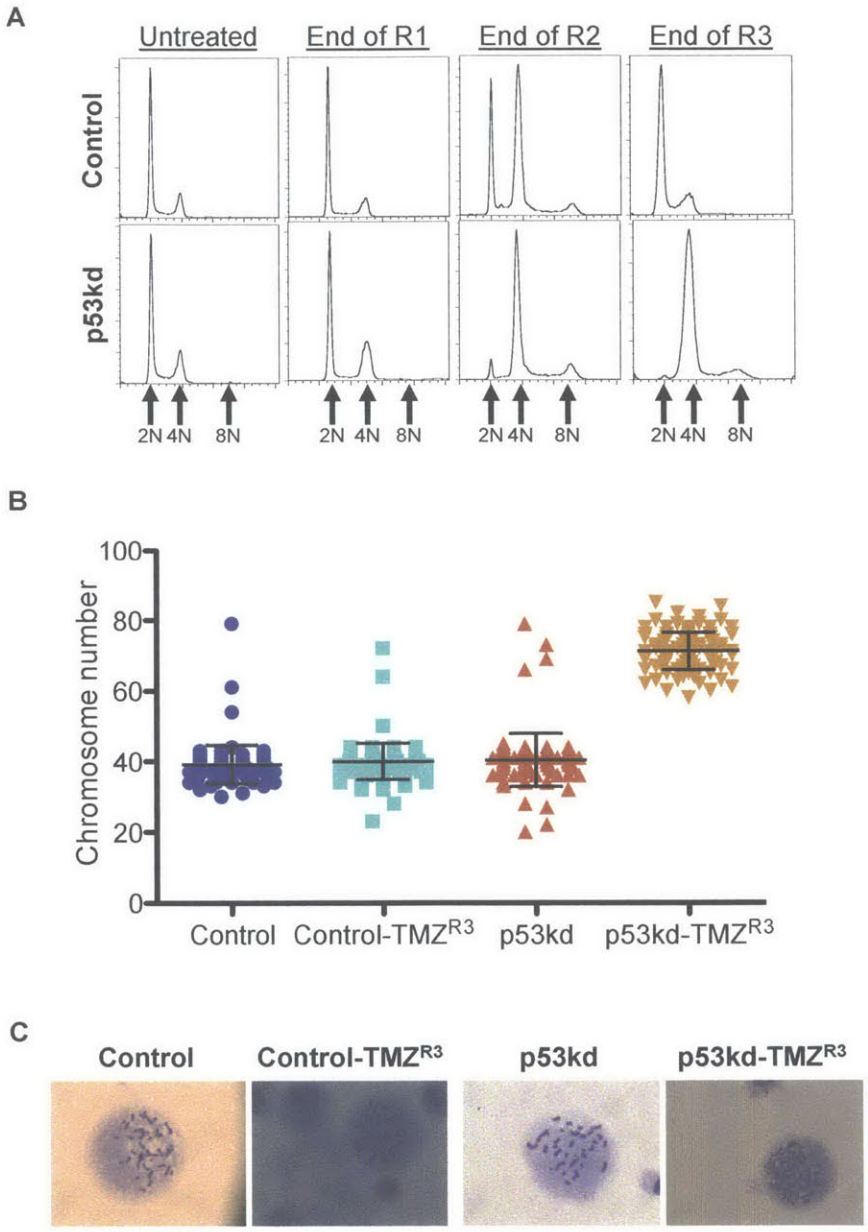

Figure 2.8 TMZ^{R3} cells obtained from a p53 deficient background display increased ploidy.

(A) Cell cycle profiles of Control and p53kd prior to and after the first (R1), second (R2) and third (R3) rounds of TMZ selection.

(B) Quantitation of modal chromosome number from karyotypes of parental and TMZ^{R3} glioblastoma cells (Error bars denote standard deviation from the mean).

(C) Representative karyotypes from p53kd and p53kd-TMZ^{R3} glioblastoma cells.

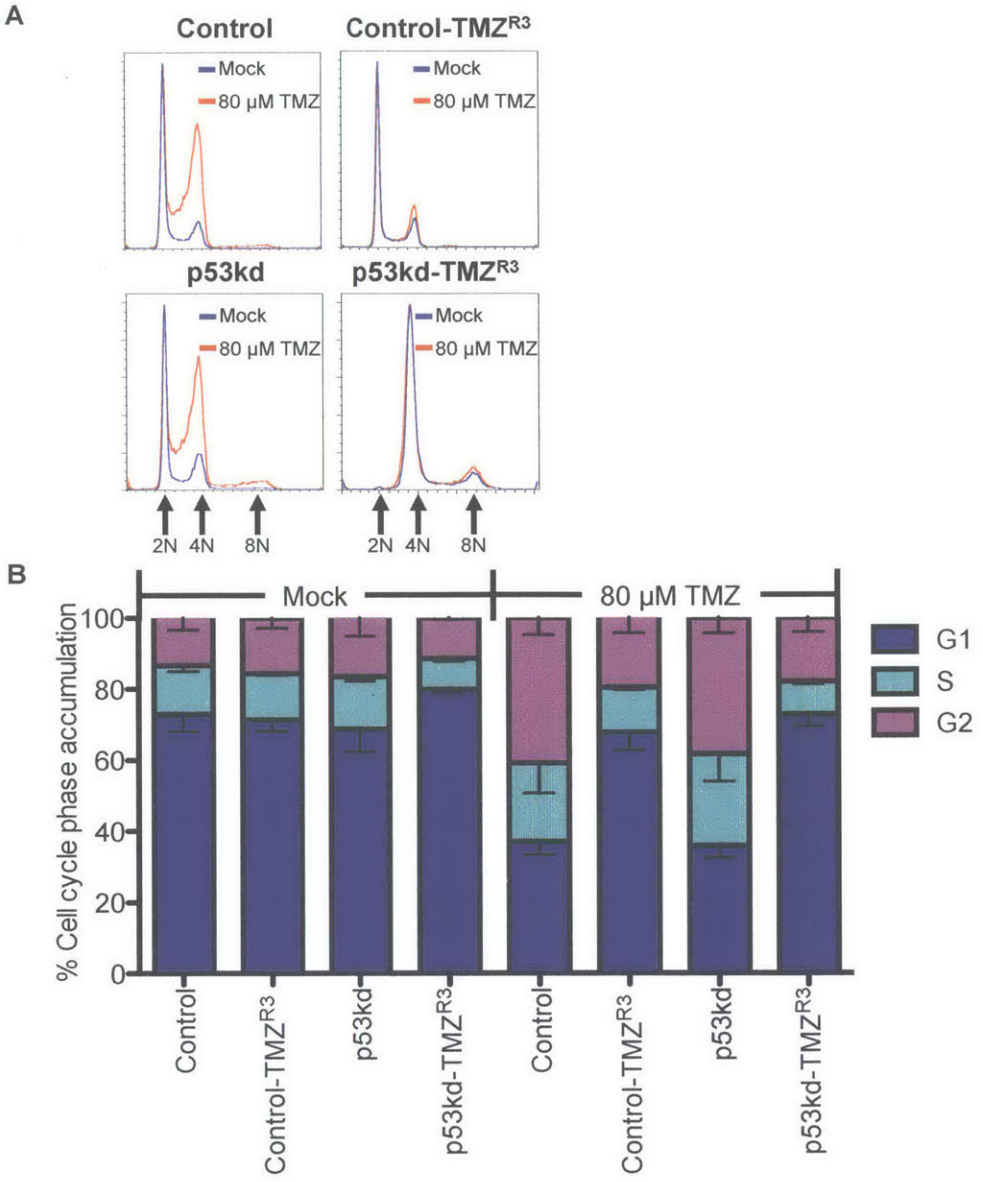

Figure 2.9 TMZ^{R3} GBM cells exhibit decreased G2/M accumulation two cell cycles post-TMZ exposure.

(A) Cell cycle profiles of parental and TMZ^{R3} GBM cells two cell cycles post-TMZ exposure.

(B) Quantitation of cell cycle changes in parental and TMZ^{R3} GBM cells two cell cycles post-TMZ exposure.

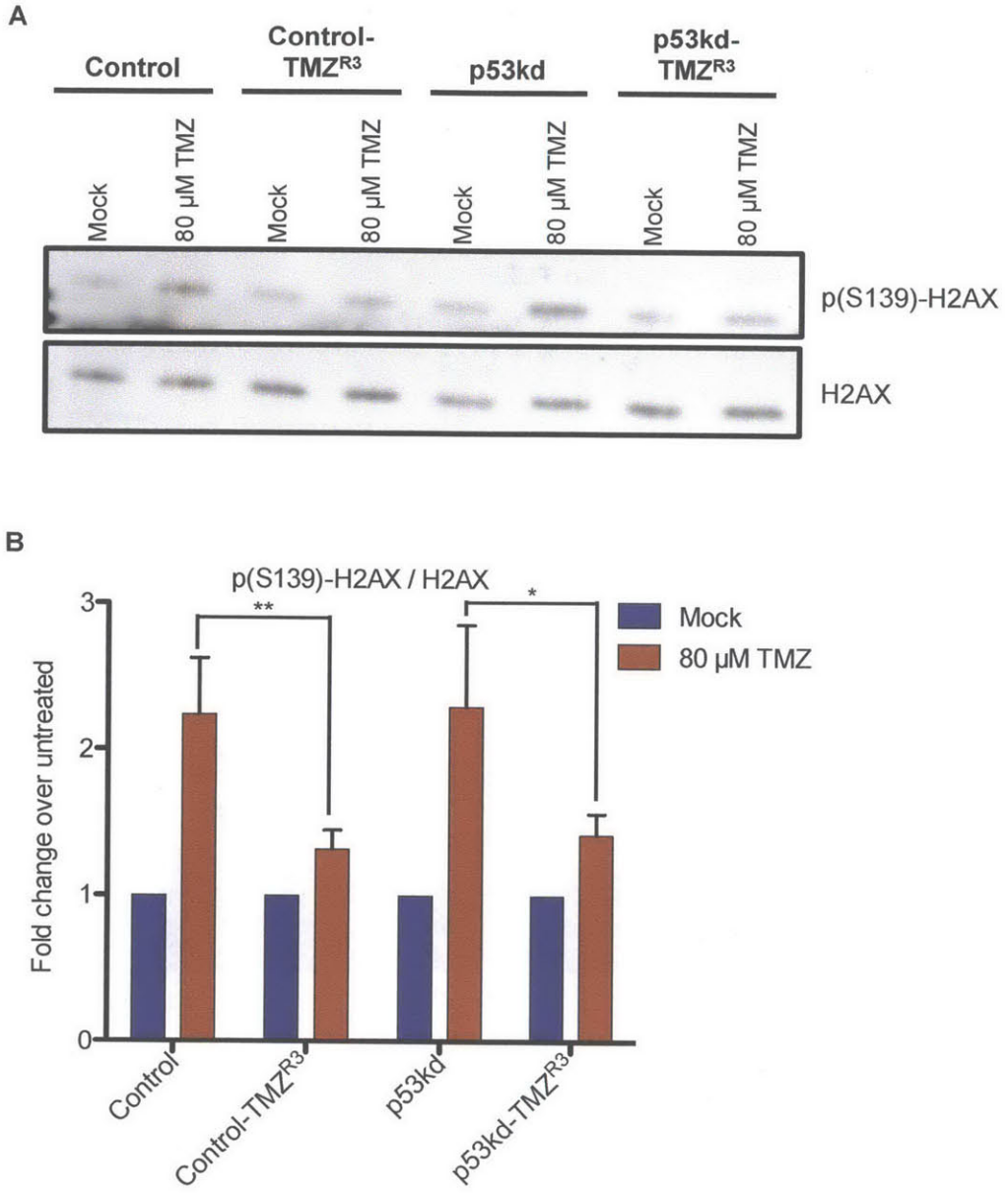

Figure 2.10 TMZ^{R3} GBM cells exhibit decreased H2AX activation two cell cycles post-TMZ exposure.

(A) Immunoblot for S139 phosphorylated and total H2AX in parental and TMZ^{R3} GBM cells two cell cycles post-TMZ exposure.

(B) Quantification of H2AX S139 phosphorylation levels in parental and TMZ^{R3} GBM cells two cell cycles post-TMZ exposure. Student's t-test was used to assess significance between the sensitivity of parental and TMZ^{R3} GBM cells (Error bars denote standard deviation from the mean, n=3, ** $p<0.01$).

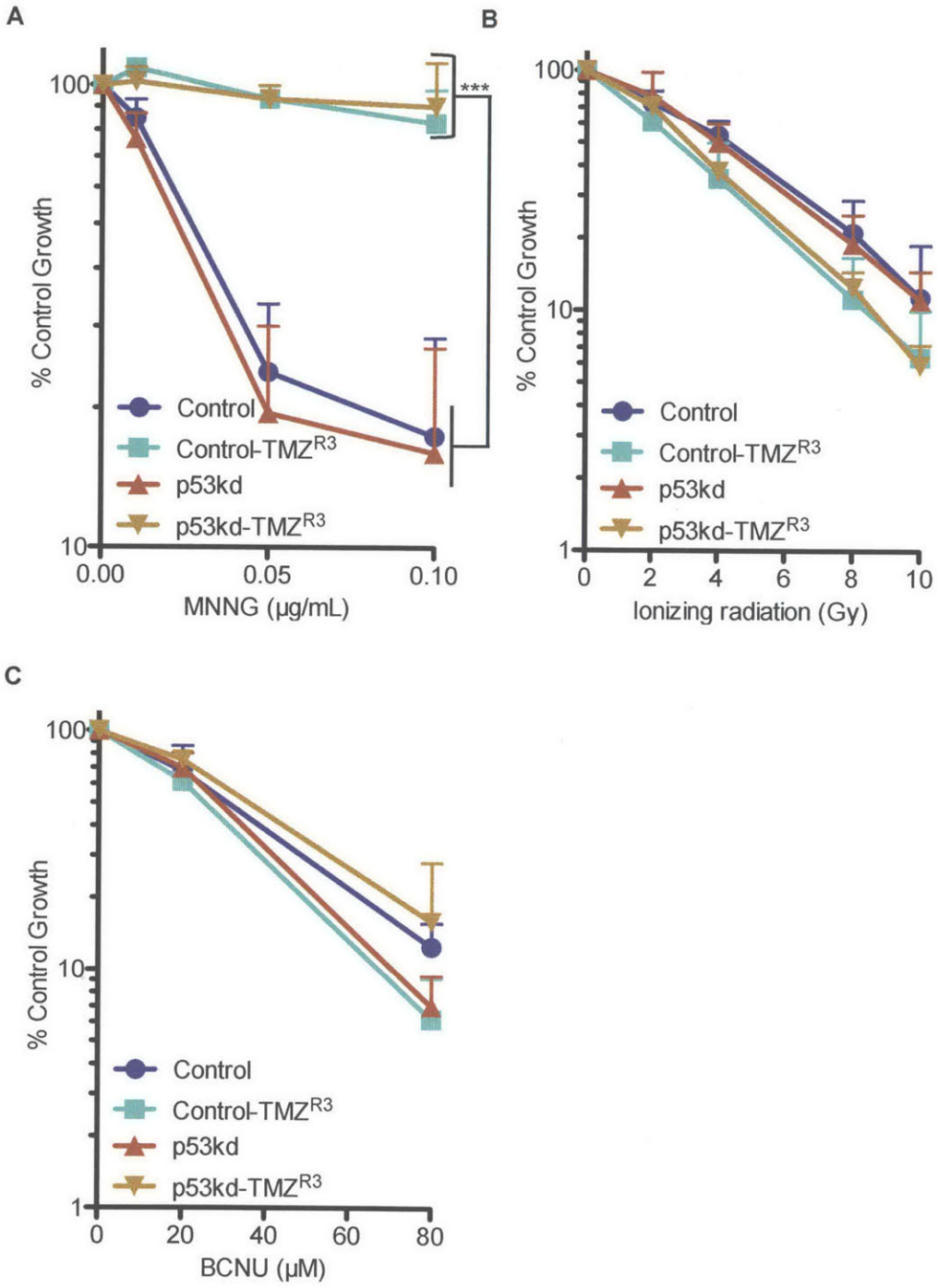

Figure 2.11 TMZ^{R3} GBM cells display cross-resistance to MNNG but not to IR or BCNU.

(A-C) Sensitivity of parental and TMZ^{R3} GBM cells to MNNG (A), IR (B) and BCNU (C). Two-way ANOVA analysis was used to assess significance between the sensitivity of parental and TMZ^{R3} GBM cells (Error bars denote standard deviation from the mean, n=3, ** $p<0.01$).

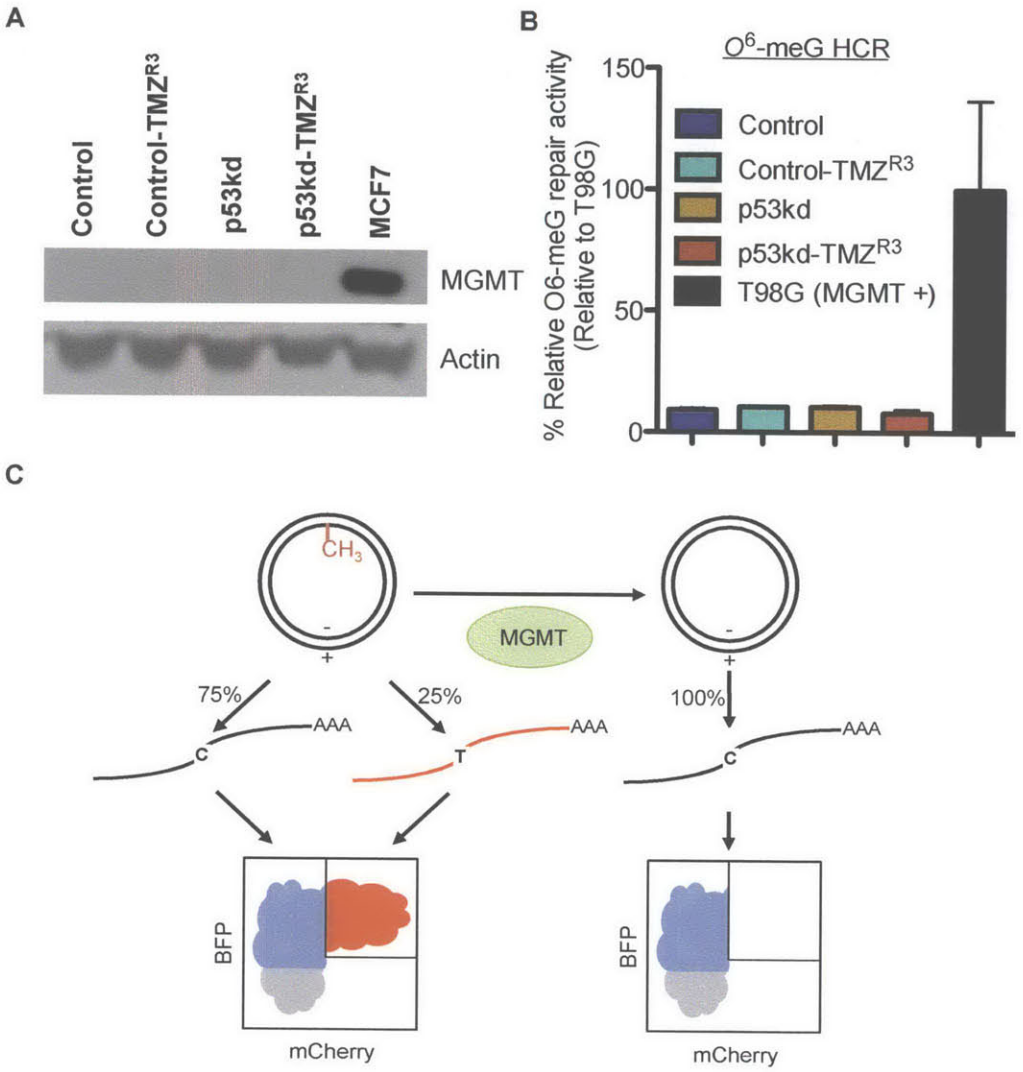

Figure 2.12 The TMZ resistant phenotype in TMZ^{R3} GBM cells is not due to increased repair of O^6-methylguanine lesions.

(A) Immunoblot of MGMT levels in parental and TMZ^{R3} GBM cells.

(B) O^6-meG repair capacity of parental and TMZ^{R3} GBM cells (Error bars denote standard deviation from the mean, n=3).

(C) Direct Reversal of O^6-meG HCR (DR-HCR). This assay reports on the ability of cells to repair a single O^6-meG lesion in the transcribed strand of a plasmid encoding a red fluorescent protein.

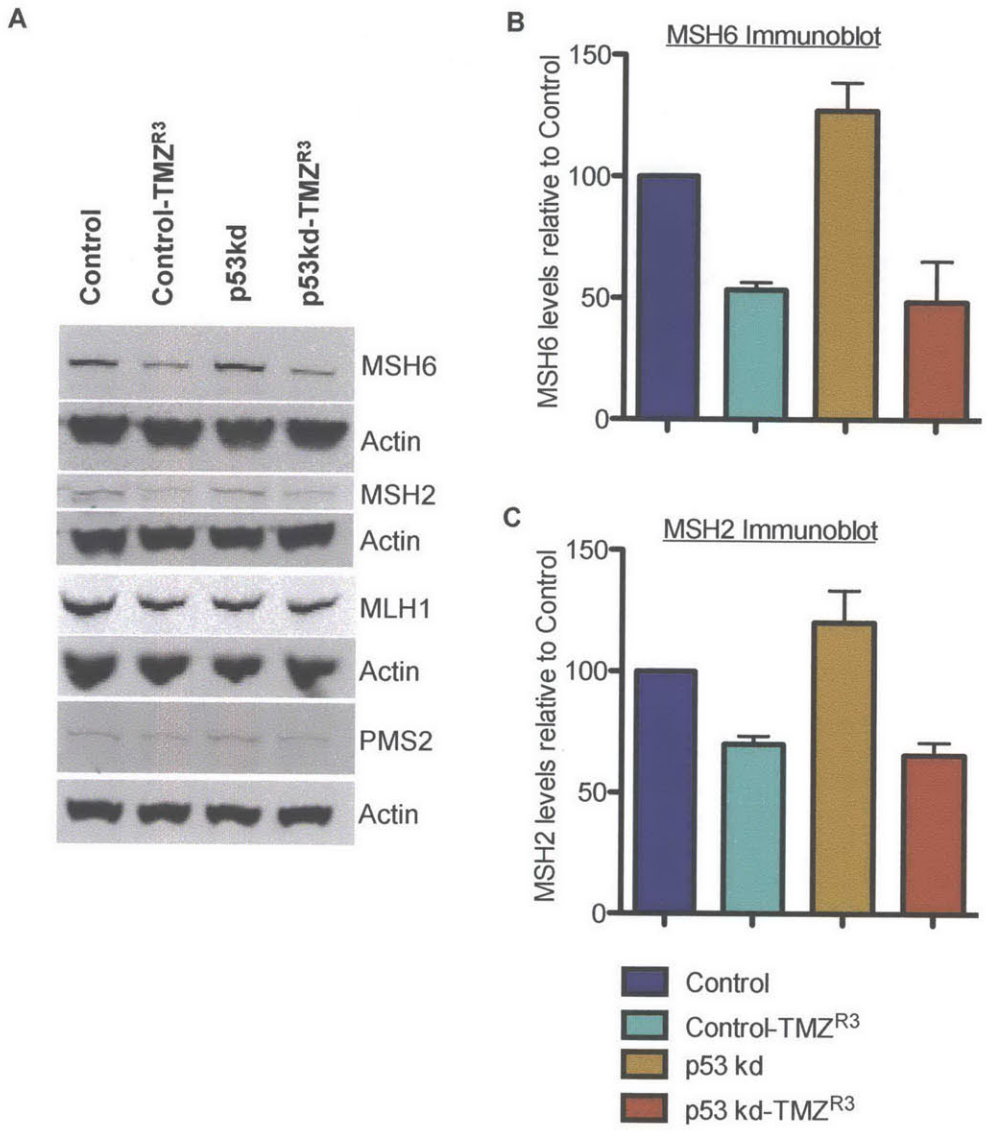

Figure 2.13 TMZ^{R3} GBM cells exhibit decreased MMR component levels

(A) Immunoblot of MSH6, MSH2, MLH1 and PMS2 levels in parental and TMZ^{R3} GBM cells.

(B-C) Quantitation of MSH6 (B) and MSH2 (C) protein levels in parental and TMZ^{R3} GBM cells (Error bars denote standard deviation from the mean, n=3).

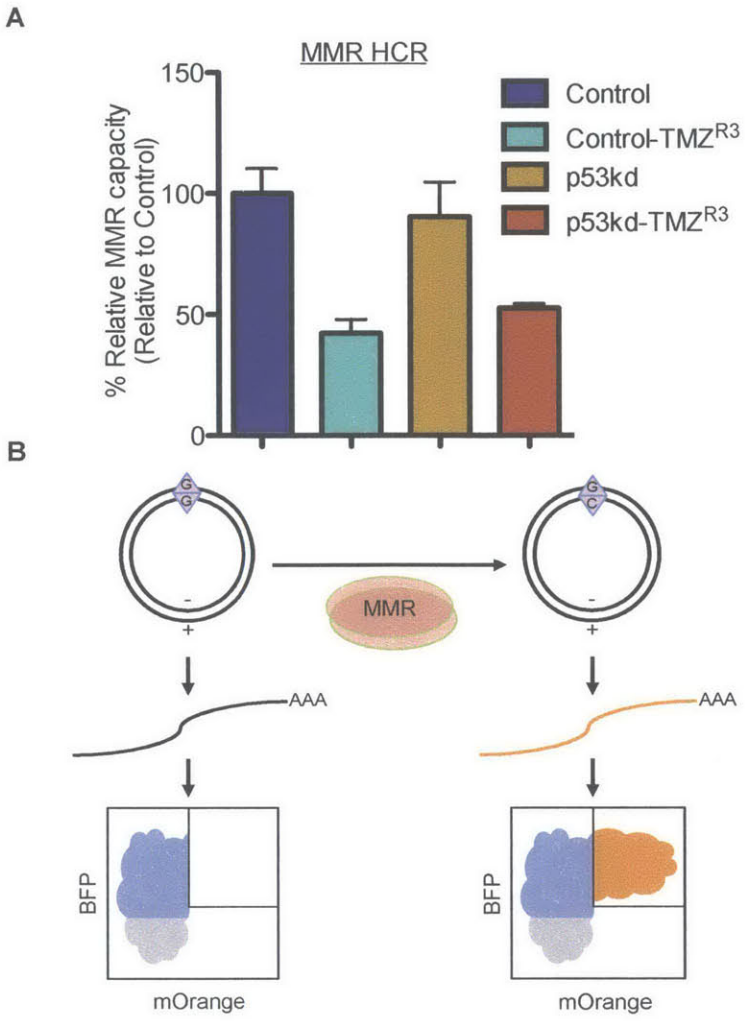

Figure 2.14 Decreased MMR component levels in TMZ^{R3} GBM cells correlates with decreased MMR activity

(A) Mismatch repair capacity against a G:G mismatch in parental and TMZ^{R3} GBM cells. Student's t-test was used to assess significance between the sensitivity of parental and TMZ^{R3} GBM cells (Error bars denote standard deviation from the mean, n=3, * $p< 0.05$; ** $p<0.01$).

(B) Mismatch repair HCR (MMR-HCR). This assay reports on the ability of cells to repair a single G-G mismatch found in the template strand of a plasmid encoding an orange fluorescent protein.

Sample	O^6-methylguanine per 10^7 nts	
	Mock	80 μM TMZ
Control	< LOD	12.15 ± 2.65
Control-TMZ^{R3}	< LOD	10.41 ± 0.51
p53kd	< LOD	11.77 ± 1.11
p53kd-TMZ^{R3}	< LOD	10.78 ± 1.13

Table 2.1 Parental and TMZ^{R3} GBM cells accumulate equal O^6-meG levels upon TMZ exposure.

LOD denotes samples were O^6-meG levels were under the limit of detection.

Hairpin	Vector	Catalog number and clone ID or Seed sequence
Non-silencing control	pGIPZ	RHS4346
shp53	pGIPZ	RHS4430-98486236 ID: V2LHS_217

Table 2.2 shRNA constructs used in this study.

References`

Agnihotri, S., Gajadhar, A. S., Ternamian, C., Gorlia, T., Diefes, K. L., Mischel, P. S., Kelly, J., McGown, G., Thorncroft, M., Carlson, B. L., *et al.* (2012). Alkylpurine-DNA-N-glycosylase confers resistance to temozolomide in xenograft models of glioblastoma multiforme and is associated with poor survival in patients. J Clin Invest *122*, 253-266.

Andreassen, P. R., Lohez, O. D., Lacroix, F. B., and Margolis, R. L. (2001). Tetraploid state induces p53-dependent arrest of nontransformed mammalian cells in G1. Mol Biol Cell *12*, 1315-1328.

Blough, M. D., Beauchamp, D. C., Westgate, M. R., Kelly, J. J., and Cairncross, J. G. (2011). Effect of aberrant p53 function on temozolomide sensitivity of glioma cell lines and brain tumor initiating cells from glioblastoma. Journal of neuro-oncology *102*, 1-7.

Brandes, A. A., Franceschi, E., Tosoni, A., Bartolini, S., Bacci, A., Agati, R., Ghimenton, C., Turazzi, S., Talacchi, A., Skrap, M., *et al.* (2010). O(6)-methylguanine DNA-methyltransferase methylation status can change between first surgery for newly diagnosed glioblastoma and second surgery for recurrence: clinical implications. Neuro-oncology *12*, 283-288.

Cahill, D. P., Levine, K. K., Betensky, R. A., Codd, P. J., Romany, C. A., Reavie, L. B., Batchelor, T. T., Futreal, P. A., Stratton, M. R., Curry, W. T., *et al.* (2007). Loss of the mismatch repair protein MSH6 in human glioblastomas is associated with tumor progression during temozolomide treatment. Clinical cancer research : an official journal of the American Association for Cancer Research *13*, 2038-2045.

Cejka, P., Stojic, L., Mojas, N., Russell, A. M., Heinimann, K., Cannavo, E., di Pietro, M., Marra, G., and Jiricny, J. (2003). Methylation-induced G(2)/M arrest requires

a full complement of the mismatch repair protein hMLH1. The EMBO journal *22*, 2245-2254.

Dallas, N. A., Xia, L., Fan, F., Gray, M. J., Gaur, P., van Buren, G., 2nd, Samuel, S., Kim, M. P., Lim, S. J., and Ellis, L. M. (2009). Chemoresistant colorectal cancer cells, the cancer stem cell phenotype, and increased sensitivity to insulin-like growth factor-I receptor inhibition. Cancer research *69*, 1951-1957.

Dinca, E. B., Lu, K. V., Sarkaria, J. N., Pieper, R. O., Prados, M. D., Haas-Kogan, D. A., Vandenberg, S. R., Berger, M. S., and James, C. D. (2008). p53 Small-molecule inhibitor enhances temozolomide cytotoxic activity against intracranial glioblastoma xenografts. Cancer research *68*, 10034-10039.

Felsberg, J., Thon, N., Eigenbrod, S., Hentschel, B., Sabel, M. C., Westphal, M., Schackert, G., Kreth, F. W., Pietsch, T., Loffler, M., *et al.* (2011). Promoter methylation and expression of MGMT and the DNA mismatch repair genes MLH1, MSH2, MSH6 and PMS2 in paired primary and recurrent glioblastomas. Int J Cancer *129*, 659-670.

Fu, D., Calvo, J. A., and Samson, L. D. (2012). Balancing repair and tolerance of DNA damage caused by alkylating agents. Nature reviews Cancer *12*, 104-120.

Happold, C., Roth, P., Wick, W., Schmidt, N., Florea, A. M., Silginer, M., Reifenberger, G., and Weller, M. (2012). Distinct molecular mechanisms of acquired resistance to temozolomide in glioblastoma cells. Journal of neurochemistry *122*, 444-455.

Hegi, M. E., Diserens, A. C., Gorlia, T., Hamou, M. F., de Tribolet, N., Weller, M., Kros, J. M., Hainfellner, J. A., Mason, W., Mariani, L., *et al.* (2005). MGMT gene silencing and benefit from temozolomide in glioblastoma. N Engl J Med *352*, 997-1003.

Hirose, Y., Berger, M. S., and Pieper, R. O. (2001). p53 effects both the duration of G2/M arrest and the fate of temozolomide-treated human glioblastoma cells. Cancer research *61*, 1957-1963.

Kitange, G. J., Mladek, A. C., Carlson, B. L., Schroeder, M. A., Pokomy, J. L., Cen, L., Decker, P. A., Wu, W. T., Lomberk, G. A., Gupta, S. K., *et al.* (2012). Inhibition of Histone Deacetylation Potentiates the Evolution of Acquired Temozolomide Resistance Linked to MGMT Upregulation in Glioblastoma Xenografts. Clinical Cancer Research *18*, 4070-4079.

Li, G. M. (2008). Mechanisms and functions of DNA mismatch repair. Cell research *18*, 85-98.

Lorente, A., Mueller, W., Urdangarin, E., Lazcoz, P., von Deimling, A., and Castresana, J. S. (2008). Detection of methylation in promoter sequences by melting curve analysis-based semiquantitative real time PCR. Bmc Cancer *8*.

Ostermann, S., Csajka, C., Buclin, T., Leyvraz, S., Lejeune, F., Decosterd, L. A., and Stupp, R. (2004). Plasma and cerebrospinal fluid population pharmacokinetics of temozolomide in malignant glioma patients. Clinical Cancer Research *10*, 3728-3736.

Samson, L., Derfler, B., and Waldstein, E. A. (1986). Suppression of human DNA alkylation-repair defects by Escherichia coli DNA-repair genes. Proceedings of the National Academy of Sciences of the United States of America *83*, 5607-5610.

Shiraishi, S., Tada, K., Nakamura, H., Makino, K., Kochi, M., Saya, H., Kuratsu, J., and Ushio, Y. (2002). Influence of p53 mutations on prognosis of patients with glioblastoma. Cancer *95*, 249-257.

Stupp, R., Mason, W. P., van den Bent, M. J., Weller, M., Fisher, B., Taphoorn, M. J., Belanger, K., Brandes, A. A., Marosi, C., Bogdahn, U., *et al.* (2005). Radiotherapy plus concomitant and adjuvant temozolomide for glioblastoma. N Engl J Med *352*, 987-996.

The Cancer Genome Atlas, T. (2008). Comprehensive genomic characterization defines human glioblastoma genes and core pathways. Nature *455*, 1061-1068.

Valiathan, C., McFaline, J. L., and Samson, L. D. (2012). A rapid survival assay to measure drug-induced cytotoxicity and cell cycle effects. DNA repair *11*, 92-98.

van Nifterik, K. A., van den Berg, J., van der Meide, W. F., Ameziane, N., Wedekind, L. E., Steenbergen, R. D., Leenstra, S., Lafleur, M. V., Slotman, B. J., Stalpers, L. J., and Sminia, P. (2010). Absence of the MGMT protein as well as methylation of the MGMT promoter predict the sensitivity for temozolomide. British journal of cancer *103*, 29-35.

Wang, Y., Zhu, S., Cloughesy, T. F., Liau, L. M., and Mischel, P. S. (2004). p53 disruption profoundly alters the response of human glioblastoma cells to DNA topoisomerase I inhibition. Oncogene *23*, 1283-1290.

Yan, L., Donze, J. R., and Liu, L. L. (2005). Inactivated MGMT by O-6-benzylguanine is associated with prolonged G(2)/M arrest in cancer cells treated with BCNU. Oncogene *24*, 2175-2183.

Yip, S., Miao, J., Cahill, D. P., Iafrate, A. J., Aldape, K., Nutt, C. L., and Louis, D. N. (2009). MSH6 mutations arise in glioblastomas during temozolomide therapy and mediate temozolomide resistance. Clinical cancer research : an official journal of the American Association for Cancer Research *15*, 4622-4629.

Chapter III: Minor decreases in MSH2 leads to major changes in the response of glioblastoma to chemotherapy

José L. McFaline, Christian J. Braun, Monica Stanciu, Zachary Nagel, Patrizia Mazzucato, Edvinas Cerniauskas, Kelly Barford, Jacqueline A. Lees, Michael T. Hemann, Forest M. White and Leona D. Samson.

Experimental contributions: C.B. and M.S. performed the *in vivo* GBM mouse model experiments on Figures 3.13 and 3.14. Z.N. and P.M. performed the Host Cell reactivation experiment on Figures 3.11.

Chapter III: Minor decreases in MSH2 leads to major changes in the response of glioblastoma to chemotherapy

Introduction

The toxicity attributed to TMZ is primarily due to MMR induced processing of O^6-meG lesions. Therefore, TMZ resistance can be achieved by deficiencies in the MMR machinery that prevent futile MMR cycling. Unfortunately, GBM tumors almost always recur and are usually no longer responsive to treatment (Hou et al., 2006). Recurrent, but not primary, GBM tumors frequently harbor mutations in MMR genes (Cahill et al., 2007; The Cancer Genome Atlas Research Network, 2008; Yip et al., 2009). A recent study by the German Glioma network found widespread decreases in MMR protein levels in recurrent GBM relative to their initial tumors suggesting that MMR deficiencies are more common than previously appreciated (Felsberg et al., 2011; Hou et al., 2006).

The stability of the various MMR components is dependent on their stability and nuclear localization (Halabi et al., 2012; Hayes et al., 2009; Wu et al., 2003). It is plausible that even minor decreases in one or more of MMR machinery components can have dramatic consequences in terms of MMR activity and TMZ resistance. Various groups have sought out to investigate the role of MMR in the resistant phenotype of recurrent GBM on the basis of microsatellite stability or a hypermutation phenotype, the hallmarks of total MMR deficiency (Maxwell et al., 2008; The Cancer Genome Atlas Research Network, 2008). Unfortunately, these studies have not taken into account how subtle changes in MMR activity may drive TMZ resistance without displaying the classic markers of MMR deficiency. Recently, it has been shown that, in contrast to MSH2 and MLH1 loss, MSH2 and MLH1 knockdown does not drive microsatellite instability in human colorectal cancer cells (Barber, 2012). Therefore, the classical approaches to

identify total MMR deficiency may be inadequate for systems where minor decreases in MMR, unlikely to alter microsatellite stability or mutation rates, are enough to give a selective advantage to tumor cells. As such, mechanisms other than direct mutations in the MMR machinery, such as decreased MMR protein levels may drive resistance to TMZ in GBM. In our *in vitro* model of acquired TMZ resistance decreases in MSH6 and MSH2 were associated with decreased TMZ sensitivity. Strikingly, we show that remarkably small decreases in some MMR components, primarily MSH2, can lead to dramatic TMZ resistance of GBM cells *in vitro*. Moreover, we demonstrate that a modest decrease in MSH2 leads to a significant growth advantage for GBM tumors in an *in vivo* model of GBM chemotherapy. Lastly, analysis of *MSH6* and *MSH2* transcript levels in TMZ treated GBM patients from the TCGA database identify MSH2 as a potent predictor of survival post-TMZ therapy.

Various studies have explored the use of BCNU, the standard of care for GBM chemotherapy prior to TMZ, as a plausible treatment for recurrent GBM with mixed results. Various studies have found that patients with recurrent GBM indeed respond to BCNU treatment (Brandes et al., 2004; Reithmeier et al., 2010). The use of BCNU in primary GBM has also been explored. Treatment of primary GBM patients with BCNU wafers (Gliadel), TMZ and radiotherapy increased survival compared to Gliadel and radiotherapy alone (McGirt et al., 2009). In this chapter, we further explore the effect of MMR deficiency on the sensitivity of GBM cells to BCNU exposure. Our results suggest that MMR deficiency has no effect on BCNU-induced toxicity and suggest it as a treatment for MGMT and MMR deficient recurrent disease. Further, dual treatment of TMZ and BCNU in primary disease may decrease the rate of recurrence by eliminating cells that escape TMZ toxicity due to decreased MMR.

Materials and methods

Reagents

TMZ, 1,3-Bis(2-chloroethyl)-1-nitrosourea (BCNU), Hoechst, and propidium iodide were purchased from Sigma-Aldrich. TMZ was dissolved in DMSO, BCNU was dissolved in ethanol. Aliquots of stock solutions were stored at -80°C.

Cell culture

Human U87MG GBM cells were purchased from ATCC. Mouse GL261 GBM cells lines were a kind gift from Dr. David Zagzag (Department of Pathology, NYU School of Medicine) as previously described in (Newcomb and Zagzag, 2009). All cell lines were cultured in DMEM medium supplemented with 10% fetal bovine serum (FBS) and 1% penicillin/streptomycin (pen-strep). Cells were maintained under standard incubation conditions.

shRNA constructs

For knockdown experiments in the human U87MG cell line, pGIPZ lentiviral vectors expressing a scrambled hairpin control or hairpins targeting human p53, MSH2 or MSH6 transcripts were purchased from Open Biosystems. For GL261 knockdown experiments, shRNA constructs were designed and cloned into TMP retroviral vectors as previously described (Dickins et al., 2005). Sequences targeted by shRNAs are provided in Table 3.1.

Generation of MSH2 and MSH6 knockdown cells

Lentiviral shRNA constructs and packaging plasmids (psPAX2 and pMD2.G) were co-transfected into 293T cells to produce lentiviral particles. Subsequently, U87MG cells

were infected with lentivirus and shRNA expressing cells selected by puromycin treatment.

Acute drug treatments

MSH2 and MSH6 knockdown GBM cells were treated with TMZ and BCNU for 1 hour in serum-free media at the specified concentrations. After treatment, drug-containing medium was removed and replaced with DMEM containing 10% FBS and 10% pen-strep.

Flow cytometry based proliferation assay

All U87MG derived cells were seeded at a density of 3 x 10^5 cells in 6 cm plates with the exception of p53kd-TMZ^{R3} cells, which were seeded at 1.5 x 10^5 cells in 6 cm plates, and allowed to attach for 24 hr. Plating the larger, polyploid, p53kd-TMZ^{R3} cells at lower density ensured that all lines were at similar confluence. After attachment, cells were exposed to each agent as described above. Two cell cycle times after treatment, BrdU was added to each plate at a final concentration of 25 μM. Cells were allowed to incorporate BrdU for an additional two cell cycle times to follow proliferation after drug exposure. At the end of BrdU exposure, cells were harvested, stained with Hoechst and propidium iodide and analyzed by flow cytometry as described (Valiathan et al., 2012).

Mean lethal dose (D_0)

A mean lethal dose was estimated from dose response curves of TMZ treated MSH6 and MSH2 knockdown cells as previously described (Jagger, 1976). A threshold value, represented by 'NR' (no response), was set for MSH6 and MSH2 knockdown cells that do not respond to TMZ on Figure 3.9A and 3.9C.

Cell cycle analysis

Cells were seeded at 1 x 10^6 cells per 10 cm plate, with the exception of p53kd-TMZ^{R3} at 5 x 10^5 cells, and allowed to attach for 24 hours. After attachment, cells were mock treated or treated with 80 μM TMZ as described above. Samples were harvested two cell cycle times after treatment. Cell pellets were resuspended in 500 μL cold PBS and 5 mL of cold ethanol was added drop-wise while vortexing and then fixed overnight at 4°C. For nuclear staining, the fixed cells were washed with PBS containing 1% bovine serum albumin (BSA) and resuspended in 300 μL of PBS containing 1% BSA, 50 μg/mL propidium iodide and 500 μg/mL RNAseA. Samples were incubated for 30 minutes at room temperature prior to flow cytometry analysis.

Assessment of DNA MMR activity using Host-Cell Reactivation

A non-replicating plasmid containing a single G:G mismatch at a site necessary for fluorophore maturation was transfected into cells. If the mismatch is not repaired, or if MMR is directed to the non-transcribed strand, the transcript produced will code for a non-fluorescent mOrange protein. However, if the mismatch is corrected with repair directed to the transcribed strand, a wild type fluorescent mOrange transcript will be produced and fluorescence restored. Thus, cells proficient in MMR will produce higher levels of fluorescent protein compared to MMR deficient cells. The MMR repair capacity was normalized to the mean repair capacity of control cells.

GL261 *in vitro* and *in vivo* competition assay

The effects of decreased MSH2 levels on the sensitivity of murine GL261 GBM cells were assessed when cultured *in vitro* as well as when injected into mouse brains to recapitulate GBM tumors *in vivo* using a competition assay. For both competition assays, GL261 cells were infected with the shRNA vectors described above such that 20

to 40% of cells expressed GFP, a marker for shRNA hairpin expression. For the *in vitro* competition assay, 1.5 x 10^4 cells per well were seeded in 12 well plates. 24 hours after seeding cell culture medium was exchanged for fresh TMZ containing media or vehicle media. Cells were harvested 96 hours after treatment. Single cell suspensions of GL261 cells were analyzed and the percentage of GFP-positive cells was quantified in the surviving cell population using a BD Biosciences LSRII flow cytometer. For the *in vivo* competition assay, 5 x 10^5 GL261 tumor cells in 3 µl of serum-free media were injected into the left frontal lobe of syngeneic C57BL6/J female recipient mice under general anesthesia and preemptive analgesia. The site of injection was located on the left hemisphere, 2 mm left of the bregma along the coronal suture. After injection, the skull was sealed with sterile bone wax, and wounds closed using tissue glue. Mice were monitored daily for three days and treated with analgesics. 8 days after surgery mice were randomly distributed into TMZ or vehicle treatment groups. Animals were treated with 50 mg/kg body weight TMZ (purchased from Sigma-Aldrich, Number: 34219-25MG) per i.p. injection. TMZ was initially dissolved in sterile DMSO and then diluted in 0.9% normal saline solution. Mice of the non-treatment group were injected with the vehicle solution alone. Animals were monitored daily for clinical signs of disease onset and were euthanized when approved euthanasia criteria were reached. After euthanasia, brains were removed, then tumors macroscopically localized and excised. Tumor samples were dissociated manually. Single cell suspensions were produced using Brain Tumor Dissociation Kit (P) (Company: Miltenyi Biotec, 130-095-942) and the gentleMACS Dissociator (Miltenyi Biotec, 130-093-235); suspensions of GL261 were analyzed and the percentage of GFP-positive cells was obtained in the surviving cell population by flow cytometry. For both *in vitro* and *in* vivo competition assays the Mann-Whitney test was used to assess significance of GFP+ cell enrichment between untreated and TMZ treated mice.

Analysis of The Cancer Genome Atlas data to assess the effects of lower levels of select transcripts on the survival of TMZ treated GBM patients

The UNC transcriptional TCGA data sets GBM_agilentg4502a_07_1__unc_edu__Level_3__unc_lowess and GBM_agilentg4502a_07_2__unc_edu__Level_3__unc_lowess were downloaded from the Broad Firehose data portal. Clinical patient data were downloaded from the NCI TCGA data matrix. Patients treated with TMZ and for whom days from diagnosis to death data was available were z-scored for their MSH2, MSH3, MSH6, PMS2, MLH1 and MGMT expression levels. Patients whose expression levels for a particular transcript was 0.5 z-score above (high expressor) or below (low expressor) the mean were used to create Kaplan Meier Survival curves. The log rank test, available in the Prism software (GraphPad), was used to determine whether the median survival of the low versus high expressor groups were significantly different from each other using a cutoff of $p \leq 0.05$. The effects of select transcript levels on the survival of TMZ treated TCGA GBM patients were also assessed out to the 95^{th} percentile for patient survival; this cutoff allows us to eliminate patients whose survival is at the tail end of the normal distribution for patient survival in TMZ treated GBM (Figure 3.16). The Kolomogorov-Smirnov test was used to confirm the normality of the distribution.

Results

Very limited knockdown of MSH2 protein levels leads to extensive TMZ chemoresistance in GBM cells in vitro

Using a panel of lentiviral vectors encoding short hairpin RNAs targeting *MSH2* or *MSH6* transcripts, we created a library of U87MG GBM cells with varying degrees of MSH2 or MSH6 knockdown (Figure 3.1). The TMZ sensitivity of MSH6 knockdown cells was bimodal with a transition to TMZ resistance in cells with 35% or less residual MSH6 protein (Figure 3.2A). TMZ resistance correlated with decreased late-S/G2-M accumulation after TMZ treatment (Figure 3.3A and 3.3B). Strikingly, the TMZ sensitivity of MSH2 knockdown cells revealed that a modest 20% decrease in MSH2 protein levels (80% residual MSH2) led to robust TMZ resistance compared to Control cells expressing a scrambled hairpin control (Figure 3.2C). Again, the TMZ resistant phenotype correlated with decreased late-S/G2-M accumulation after TMZ treatment (Figure 3.4A and 3.4B). It is important to note that, like the TMZ^{R3} cells, none of the MSH2 and MSH6 knockdown cells showed any resistance to BCNU compared to control (Figure 3.2B and 3.2D). It therefore seems likely that BCNU treatment could be an effective alternative for GBM patients with recurrent disease previously treated with TMZ.

From the TMZ dose response curves we can assign a single measure for TMZ sensitivity, namely the mean lethal dose (D_0) at which, on average, there is one lethal event per cell (Jagger, 1976). The relationship between MSH6 protein levels and the D_0 for TMZ further highlights the sharp transition from sensitivity to resistance as the MSH6 protein levels drop below 50% of control levels (Figure 3.5A). In contrast, the equivalent

analysis for D_0 versus MSH2 protein levels revealed that even the smallest decrease in MSH2 conferred significant TMZ resistance upon GBM cells (Figure 3.5B).

It is well documented that MSH2 and MSH6 stability is influenced by their dimerization (Halabi et al., 2012). MSH2 has two dimerization partners, namely MSH6 and MSH3, generating the MutSα and MutSβ heterodimers, respectively. In contrast MSH6 only dimerizes with MSH2 (Pena-Diaz and Jiricny, 2012) and only MutSα recognizes and binds O^6-meG:T mismatches (Li, 2008). Given that MSH2 has two binding partners we investigated MSH2 stability in the MSH6 knockdown GBM cells; resistance to TMZ was only seen when MSH6 loss began to destabilize MSH2 as reflected by decreased MSH2 levels (Figure 3.5A, 3.6A and 3.6C). Analysis of MSH6 stability in the MSH2 knockdown cells revealed that MSH6 protein levels decreased linearly with decreasing MSH2 protein levels (Figure 3.5B, 3.6B and 3.6D). Therefore, it appears that resistance to TMZ was observed at MSH6 or MSH2 knockdown levels where destabilization of the binding partner becomes apparent, which is presumably accompanied by decreased MutSα dimer levels and decreased binding to O^6-meG-T mispairs. To investigate how TMZ resistance correlated to MMR activity in MSH knockdown cells, MMR-HCR was used to measure MMR activity in MSH knockdown cell lines that displayed sensitivity to TMZ (MSH6 kd #2, 51% residual MSH6) and resistance to TMZ (MSH6 kd #5, 10% residual MSH6; MSH2 kd #2, 63% residual MSH2 and MSH2 kd #5, 16% residual MSH2). The MMR activity of MSH6 kd #2 was statistically indistinguishable from cells expressing a scrambled hairpin control. In contrast, decreased MMR activity was observed for MSH knockdowns that displayed resistance to TMZ (Figure 3.7). These observations can be explained if MSH6 monomer levels are in excess compared to free MSH2, making MSH2 the limiting factor in MutSα formation (Figure 3.8); this model is further elaborated in the discussion.

Small reductions in Msh2 decrease the in vivo response of GBM tumors to TMZ treatment

To determine whether the effect of minor decreases in MSH2 on the response of cultured GBM cells to TMZ are relevant when treating tumors, we employed the GL261 syngeneic mouse model of GBM. GL261 glioma cells are derived from a chemically induced brain tumor in C57B6/J mice and form robust tumors when injected into the brain of syngeneic C57B6/J mice. Detailed characterization of the GL261 gliomas has shown that they have characteristics consistent with human GBM (Newcomb and Zagzag, 2009). GL261 GBM cells were infected with retroviral particles containing vectors expressing both GFP and one of the following: a vector control, Msh2 hairpin 1 and Msh2 hairpin 2, leading to 0%, 10% or 40% *MSH2* mRNA knockdown, respectively, and 0%, 25% or 50% MSH2 protein knockdown, respectively (Figure 3.9B and 3.9C). Three outcomes were possible upon TMZ treatment: the expression of the Msh2 hairpins could (i) confer growth advantage, (ii) retard growth, or (iii) have no effect. For these outcomes the fraction of GFP expressing cells would be enriched, depleted or remain constant, respectively, after TMZ treatment relative to control (Figure 3.9A).

shRNA expressing GL261 tumor cells experienced TMZ exposure in cell culture (*in vitro*), or in the mouse brain (*in vivo*) (for details see Material and Methods). Msh2 hairpin 2 expressing cells displayed a large growth advantage upon TMZ treatment *in vitro*. Msh2 hairpin 1 expressing cells displayed a trend toward having a growth advantage but this was only significant for the 45 μM dose (Figure 3.10A). As expected, cells expressing the vector control appeared neutral in response to TMZ treatment (Figure 3.10A). More importantly, *in vivo*, significant enrichment upon TMZ treatment was observed for GFP cells expressing either Msh2 hairpin, with hairpin 2 conferring a stronger growth advantage than hairpin 1 (Figure 3.10B). As for the *in vitro* experiment,

no *in vivo* enrichment was observed in GFP cells expressing the vector control. Thus, it appears that even *in vivo*, very modest decreases in Msh2 levels endow GBM tumors with a significant growth advantage during TMZ treatment.

MSH2 transcript levels are predictive for the overall survival of TMZ treated primary GBM patients

Our results suggest that moderate decreases in MSH2 levels alter the response of GBM tumors to TMZ therapy. This led us to hypothesize that if there were a range of *MSH2* and *MSH6* expression levels in primary GBM tumors, one would expect patients with low expression to be less responsive to TMZ chemotherapy. To test our hypothesis, we ranked *MSH2* and *MSH6* transcript levels of resected primary tumors among GBM patients who had been treated with TMZ. Transcript levels were derived from The Cancer Genome Atlas (TCGA) data and ranked by a z-score of +/- 0.5 as described in Material and Methods (The Cancer Genome Atlas Research Network, 2008). We observed a trend for low *MSH6* transcript levels being associated with decreased survival in TMZ treated TCGA patients, but the difference did not reach significance for the overall survival of TMZ treated GBM patients (Figure 3.11A). However, when we exclude patients whose survival falls on the tail end of the normal distribution (top 5^{th} percentile) for patient survival after TMZ treatment, low *MSH6* levels did significantly correlate with decreased GBM patient survival after TMZ treatment (Figure 3.12 and Figure 3.13A). Strikingly, low *MSH2* transcript levels showed a highly significant correlation with decreased overall survival of TMZ treated GBM patients and this correlation was even stronger when looking at TMZ treated patients minus the top 5^{th} percentile for patient survival after TMZ treatment (Figure 3.11B and 3.13B). Moreover,

for this subset (representing 95% of the patients), there was a significant correlation between *MSH2* transcript levels and survival down to +/- 0.25 z-score (Figure 3.13C). *MGMT* methylation status and transcript levels are currently the most accepted molecular biomarkers for the survival of GBM patients (Hegi et al., 2005; Walid, 2008). In this particular TCGA data set, low *MGMT* transcript levels were indeed significantly correlated with patient survival when we exclude patients whose survival falls on the tail end of the normal distribution (Figure 3.14A and 3.14B). Taken together, it appears *MSH2* levels are not only a strong predictor of GBM patient response to initial TMZ therapy, but also a more robust predictor than *MGMT* transcript levels.

Discussion

Despite aggressive treatment glioblastoma tumors recur and frequently display radio- and chemo-resistance (Hou et al., 2006). Identifying and understanding the factors associated with resistance is critical for the design of therapy aimed at the treatment of recurrent disease. MMR is responsible for creating the toxic strand breaks associated with TMZ-induced O^6-meG lesions (Fu et al., 2012; Li, 2008; Mojas et al., 2007). The role of MMR in mediating TMZ resistance in recurrent GBM remains unclear and is plagued with opposing views. However, MMR mutations are found almost exclusively in recurrent GBM giving strong support that there is selective pressure to decreased MMR in GBM tumors, which are frequently treated, with TMZ, the current standard of care in disease treatment (Cahill et al., 2007; The Cancer Genome Atlas Research Network, 2008; Yip et al., 2009). In our previous study, we observed that the acquisition of TMZ resistance correlated with decreased MMR components, primarily MSH6 and MSH2, in GBM cells *in vitro*. Recently, a study by the German Glioma Network investigated promoter methylation and protein levels of various MMR components in 43 matched primary and recurrent GBM (Felsberg et al., 2011), to our knowledge, the largest study of its kind. No significant differences were identified in methylation status of MMR components before and after recurrence. In line with our *in vitro* results, the majority of recurrent tumors showed a significant decrease at the protein level in one or more of the MMR components, namely MSH2, MSH6 and PMS2 (Felsberg et al., 2011). Further, decreases in MMR components have been shown to occur in *in vitro* generated TMZ resistant cells in the absence of inactivating mutations (Happold et al., 2012). More importantly, we demonstrate that even minor decreases in the MutSα component MSH2 can lead to modest decreases in MMR activity and very large decreases in the sensitivity of GBM tumor cells to TMZ. We demonstrated this relationship in *in vitro* and *in vivo*

models of GBM. Furthermore, by mining the TCGA database, we show that MSH2 transcript levels are a sensitive indicator for initial therapeutic response of TMZ treated GBM patients. This finding highlights the fact that MutSα levels and mismatch repair activity play an important role in the response of primary glioblastoma tumors to TMZ treatment.

In contrast to MSH2, the expression of MSH6, the other component of the MutSα complex that recognize O6-meG lesions, needs to be depleted to a much greater extent to achieve the same level of resistance (Figure 3.9A and 3.9B). It is possible that this effect is cell line specific and dependent on the steady state levels of MSH2, MSH6 and MSH3, which presumably exist in a dynamic equilibrium. However, the finding that MSH2 transcript levels are more predictive for patient response after TMZ treatment than MSH6 transcript levels supports our conclusion that small changes in MSH2 can lead to more robust changes in the processing of TMZ-induced lesions and therefore to significant changes in the survival of GBM patients after TMZ therapy. MSH3 and MLH1, components of the MutSβ and MutLα heterodimers, respectively, were not found to correlate with survival in TMZ treated GBM patients (Figure 3.15A and 3.15B). Surprisingly, and in contrast to MSH2 and MSH6, low PMS2 transcript levels were found to be associated with increased survival in TMZ treated GBM patients (Figure 3.15C). At this time we do not have a hypothesis as to how PMS2 may effect the response to TMZ treatment, yet the observation that decreased levels are associated with survival suggest this effect may be independent of its role in MMR.

The stability of both MSH2 and MSH6 is dependent on their dimerization state (Halabi et al., 2012). MSH2 can dimerize with MSH6 as well as with MSH3 to form the MutSα and MutSβ recognition complexes, respectively. The MutSα dimer is responsible for the recognition of single base pair mismatches and loops formed by 1 base deletions/insertions, while MutSβ recognizes loops formed by the deletion/insertion of

multiple bases (Halabi et al., 2012; Kantelinen et al., 2010; Li, 2008). We observed that changes in MSH2 protein levels led to linear changes in MSH6 protein levels, while MSH6 had to be depleted to a larger extent to affect MSH2 stability (Figure 3.9C and 3.9D). When comparing to TMZ sensitivity, it appears that resistance is encountered when enough MSH2 or MSH6 is lost to destabilize its binding partner, presumably leading to decreased MutSα levels and decreased recognition of O^6-meG:T mispairs. These results suggest that MSH2 is rate limiting in the formation of the MutSα complex. By comparison, the MSH2/3 heterodimer, termed MutSβ, does not recognize single base pair mismatches and would therefore not recognize TMZ-induced G:T mismatches (Kantelinen et al., 2010). To the best of our knowledge, the degradation rates of the MSH proteins, as well as the affinities of MSH2 binding to MSH3 or MSH6, have not been characterized. Our observations are consistent with MSH2 being found mostly in dimer form while MSH6 and MSH3 are in excess. At low levels of MSH6 knockdown, depletion of the monomeric pool would not lead to an appreciable change in MutSα levels, whereas MSH2 knockdown would quickly deplete MutSα levels, decrease total MSH6 levels due to decreased stability of MSH6 in its monomeric form and, ultimately, decreased recognition of O^6-meG:T mispairs (Figure 3.12). Moreover, it may be possible that a higher binding affinity of MSH3 for MSH2 would further favor MutSβ heterodimer formation compared to MutSα when MSH2 is limiting.

A number of recurrent GBM tumors display a hypermutator phenotype and microsatellite instability consistent with inactivating mutations in MMR components (The Cancer Genome Atlas Research Network, 2008). However, the small occurrence of microsatellite instability in recurrent GBM tumors has been used to rule out or minimize a role for MMR in the TMZ resistant phenotype of recurrent disease (Maxwell et al., 2008). These approaches are adequate in determining MMR mutation in colon cancer where MSH2 and MLH1 loss of function (either by mutation or epigentic silencing) are frequent

drivers of the disease but appear inadequate for identifying MMR deficiencies in GBM. Moreover, recent work has suggested that, in contrast to MSH2 mutation, decreased MSH2 protein levels is not an effective inducer of microsatellite instability (Barber, 2012). Therefore, current approaches to measure microsatellite instability are unlikely to be a robust marker of decresed MutSα activity due to minor decreases in MSH2 expression, as presented.

The study presented here indicates that MSH2 transcript and protein levels strongly predict the response of GBM tumors to TMZ treatment. However, discerning a small change in MSH2 expression to categorize TMZ sensitive and TMZ resistant GBM tumors may make it challenging to use MSH2 levels as a clinical marker. As an alternate strategy, Nagel and colleagues have recently developed flow cytometry-based in-cell functional assays to measure various DNA repair activities including MMR and MGMT activity (Figure 2.13C and 2.15B) (Nagel et al., 2014). The combination of these functional assays on isolated tumor samples has the potential to better inform therapeutic strategies. Our results have shown that even a small decrease in MSH2 protein levels can lead to a statistically significant decrease in MMR activity, and a large, statistically significant change in TMZ resistance. Further characterization of MMR activity and sensitivity to TMZ may provide a threshold of MMR activity under which TMZ treatment would not be recommended.

The ultimate goal of this work is to identify alternate strategies for the treatment of recurrent GBM. Taken together with our results in Chapter 2, it appears BCNU is a logical choice for the treatment of recurrent GBM after failed TMZ therapy. Importantly, we have shown this both in *in vitro* generated resistance cells and GBM cells made resistant by MSH6 and MSH2 knockdown. Therefore, it appears MMR deficiencies selected for during treatment do not alter the sensitivity of GBM cells to BCNU. A number of studies have found that patients with recurrent disease indeed respond to

BCNU treatment albeit with high toxicity associated with BCNU exposure (Brandes et al., 2004; Reithmeier et al., 2010). A case could also be made for dual treatment with TMZ and BCNU. Dual treatment of primary GBM patients with BCNU containing wafers (Gliadel) at the site of resection, TMZ and IR demonstrated a survival advantage over Gliadel and radiotherapy alone (McGirt et al., 2009). This strategy has the potential of eliminating cells during selection for MMR deficiency as a result of TMZ exposure. In conclusion, our results, suggests that patient stratification on the basis of low MGMT expression and low MMR activity identifies a subset of patients with recurrent GBM that would derive maximum benefit from BCNU treatment.

Figures

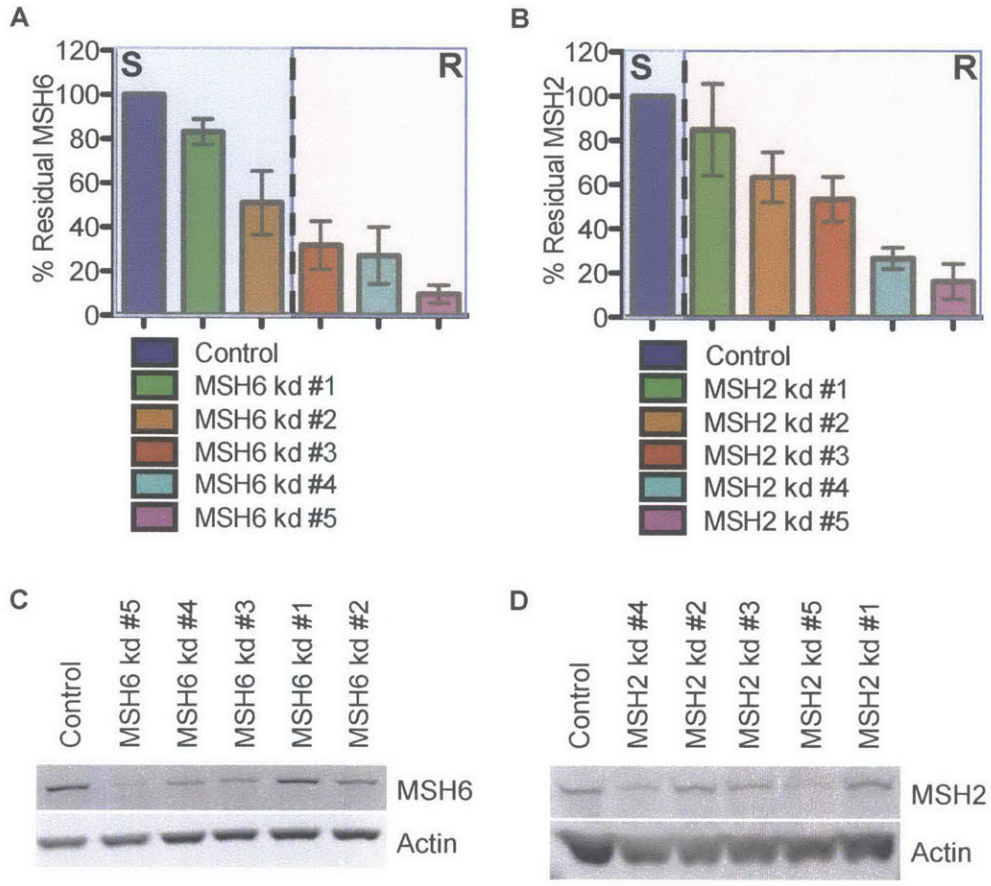

Figure 3.1 Panel of MSH6 and MSH2 knockdown GBM cells.

(A-B) Quantification of MSH6 (A) and MSH2 (B) protein levels in a panel of MSH6 and MSH2 knockdown GBM cells as measured by quantitative immunoblotting. Blue and red shaded regions denote MSH6 and MSH2 knockdown cells where sensitivity (**S**) or resistance (**R**) to TMZ was observed as measured in Figure 3.2 (Error bars denote standard error of the mean, n=3).

(C-D) Immunoblot of MSH6 (C) and MSH2 (D) levels in MSH6 knockdown cells.

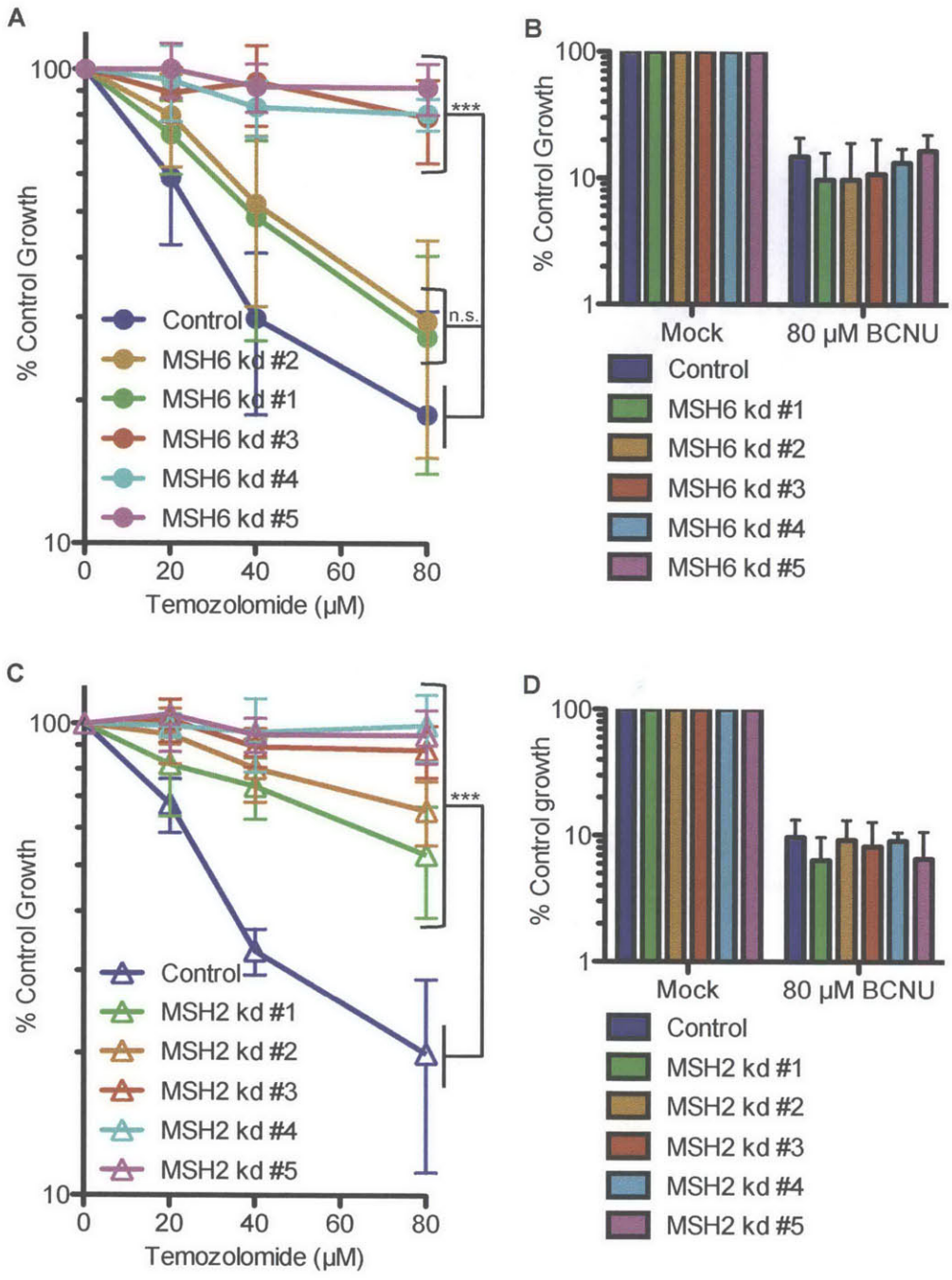

Figure 3.2 Modulation of MSH6 and MSH2 levels and TMZ sensitivity.

(A) Sensitivity of MSH6 knockdown cells to TMZ. Two-way ANOVA analysis was used to assess significance between the sensitivity of parental and TMZ^{R3} GBM cells (Error bars denote standard deviation from the mean, n=5, *** $p<0.001$).

(B) Sensitivity of MSH6 knockdown cells to BCNU (Error bars denote standard deviation from the mean, n=3).

(C) Sensitivity of MSH6 knockdown cells to TMZ. Two-way ANOVA analysis was used to assess significance between the sensitivity of parental and TMZ^{R3} GBM cells (Error bars denote standard deviation from the mean, n=5, *** $p<0.001$).

(D) Sensitivity of MSH6 knockdown cells to BCNU (Error bars denote standard deviation from the mean, n=3).

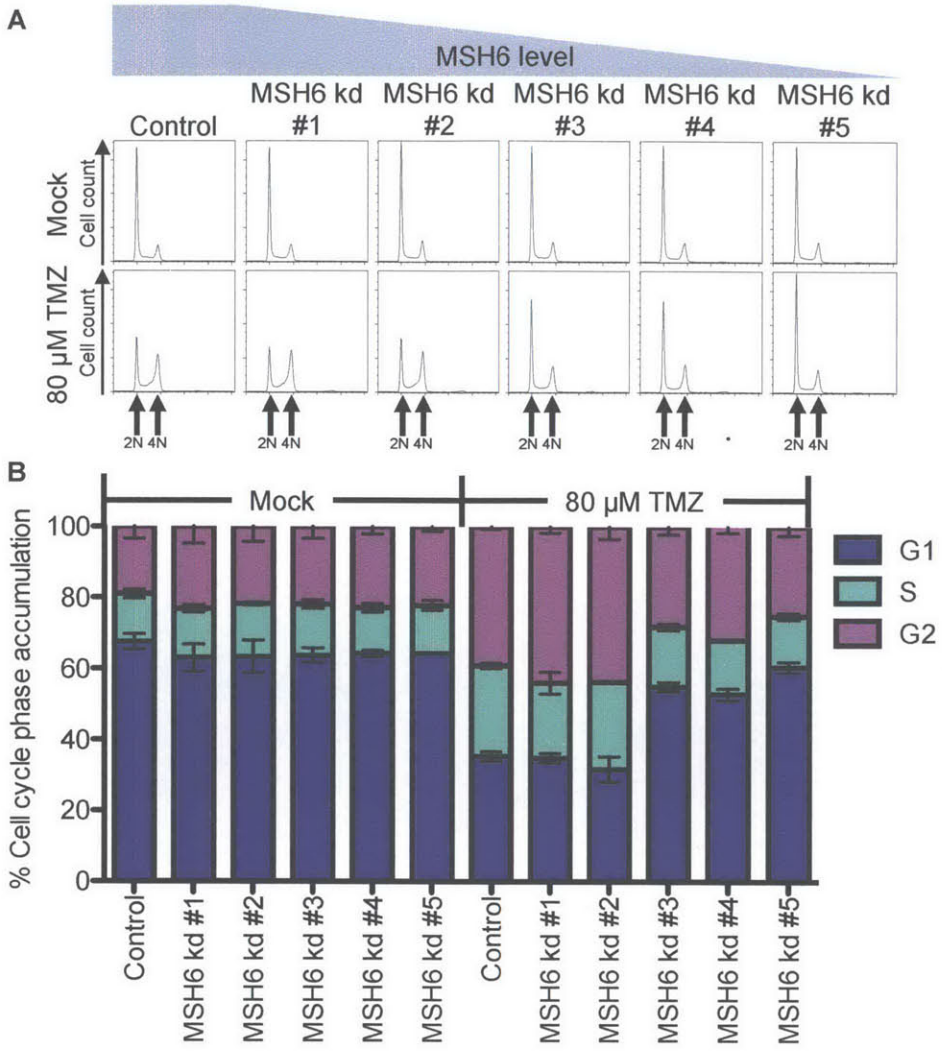

Figure 3.3 Extent of G2/M accumulation post-TMZ exposure correlates with sensitivity in MSH6 knockdown cells.

(A) Cell cycle profiles of MSH6 knockdown GBM cells two cell cycles post-TMZ exposure.

(B) Quantitation of cell cycle changes in MSH6 knockdowns GBM cells two cell cycles post-TMZ exposure.

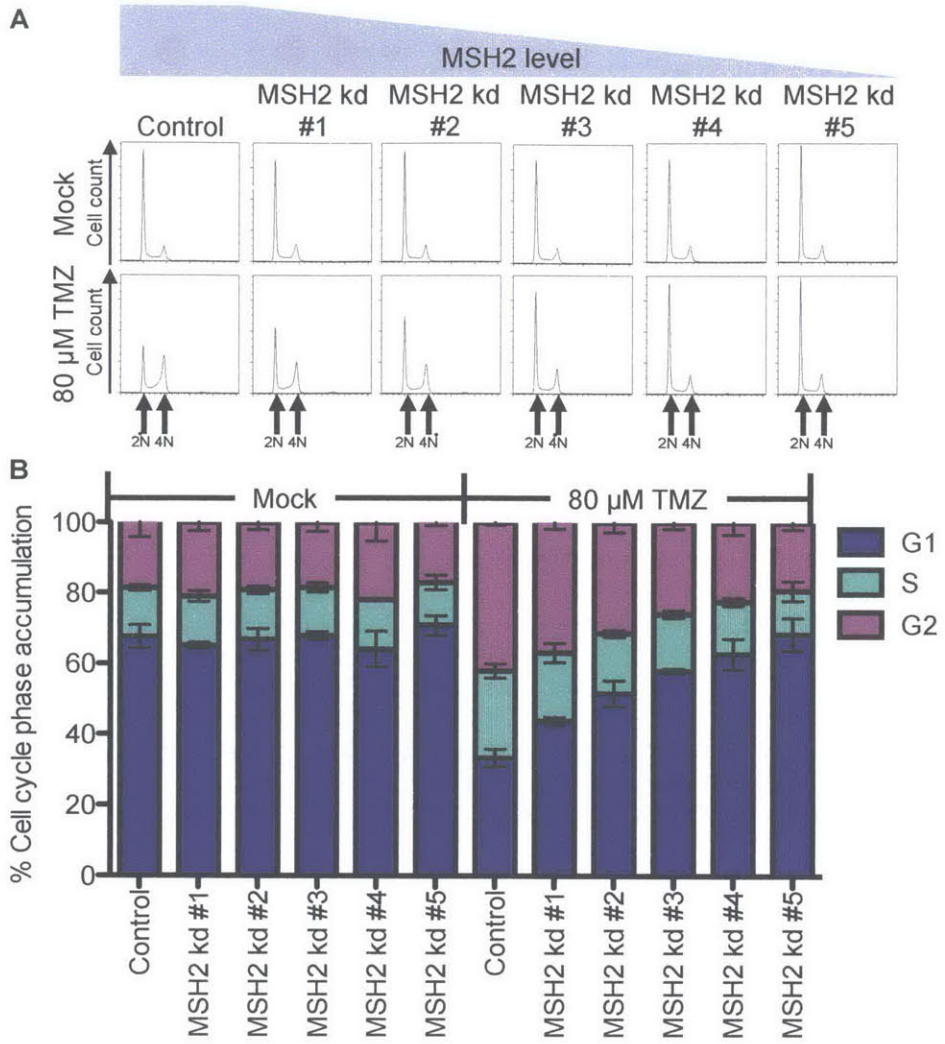

Figure 3.4 Extent of G2/M accumulation post-TMZ exposure correlates with sensitivity in MSH2 knockdown cells.

(A) Cell cycle profiles of MSH2 knockdown GBM cells two cell cycles post-TMZ exposure.

(B) Quantitation of cell cycle changes in MSH2 knockdowns GBM cells two cell cycles post-TMZ exposure.

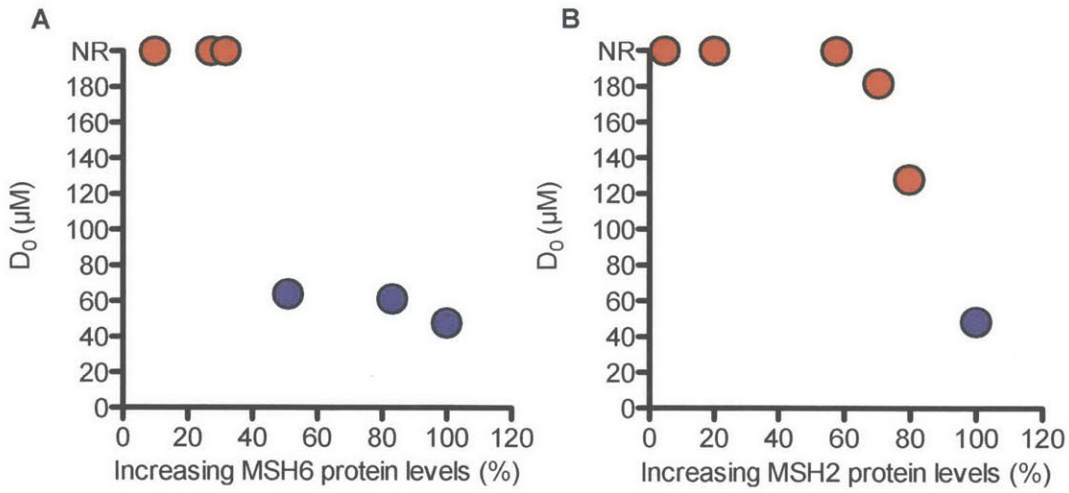

Figure 3.5 Relationship between MSH levels and response to TMZ.

(A/B) Relationship between MSH6 (A) and MSH2 (B) protein levels and sensitivity to TMZ in MSH2 and MSH6 knockdown cells. 'NR' (No response) denotes a threshold for knockdown cells that do not respond to TMZ (Horizontal error bars denote standard error of the mean; vertical error bars denote standard error of the mean, n=3).

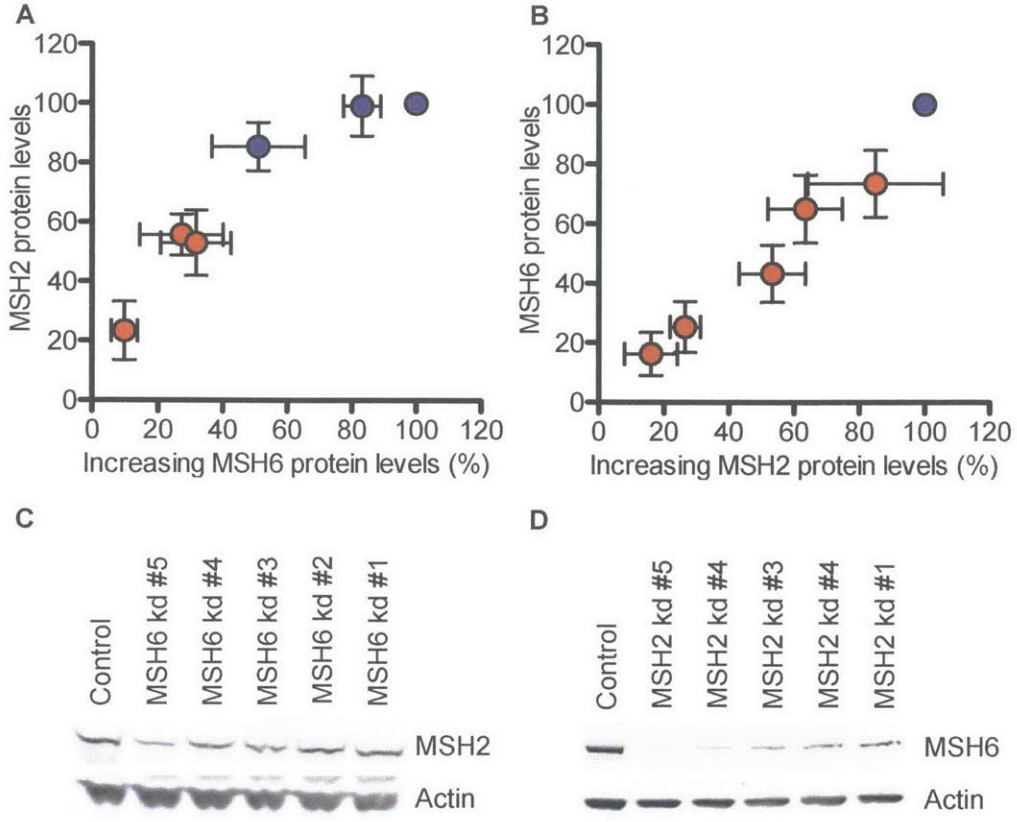

Figure 3.6 Small decreases in MSH2 protein alter MSH6 protein levels and lead to decreased mismatch repair activity.

(A/B) Effects of MSH6 (A) and MSH2 (A) knockdown on the stability of its dimerization partner. Immunoblot analysis was used to assess MSH2 and MSH6 protein levels in MSH6 and MSH2 knockdown cells, respectively. Blue and red shaded regions denote areas of MSH6 and MSH2 knockdown where sensitivity (**S**) or resistance (**R**) to TMZ was observed (Error bars denote standard error of the mean, n=3).

(C) Immunoblot for MSH2 levels in MSH6 knockdown cells.

(D) Immunoblot for MSH6 levels in MSH2 knockdown cells.

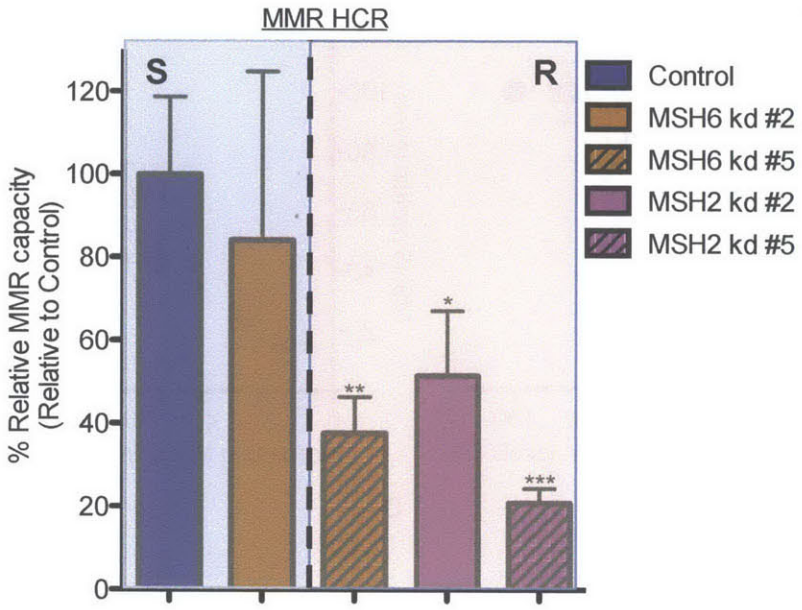

Figure 3.7 Decreased MMR activity correlates with TMZ resistance in MSH6 and MSH2 knockdown GBM cells.

Mismatch repair capacity against a GG mismatch substrate in select MSH6 and MSH2 knockdown GBM cells. Blue and red shaded regions denote areas of MSH6 and MSH2 knockdown where sensitivity (**S**) or resistance (**R**) to TMZ was observed. Student's t-test was used to assess significance between the sensitivity of parental and TMZ^{R3} GBM cells (Error bars denote standard deviation from the mean, n=3, * $p< 0.05$; ** $p<0.01$; *** $p< 0.001$).

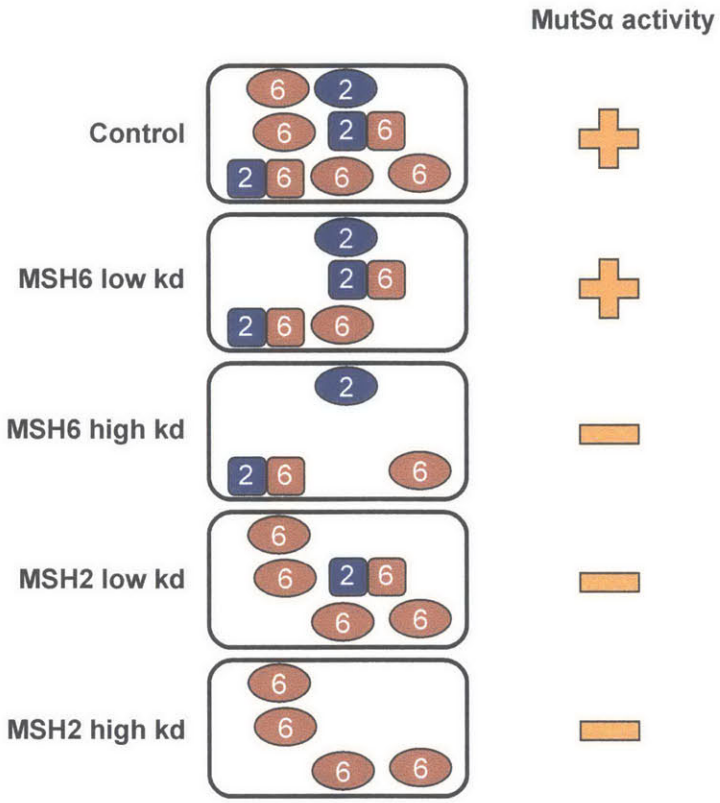

Figure 3.8 Model for MSH induced decreased MMR activity.

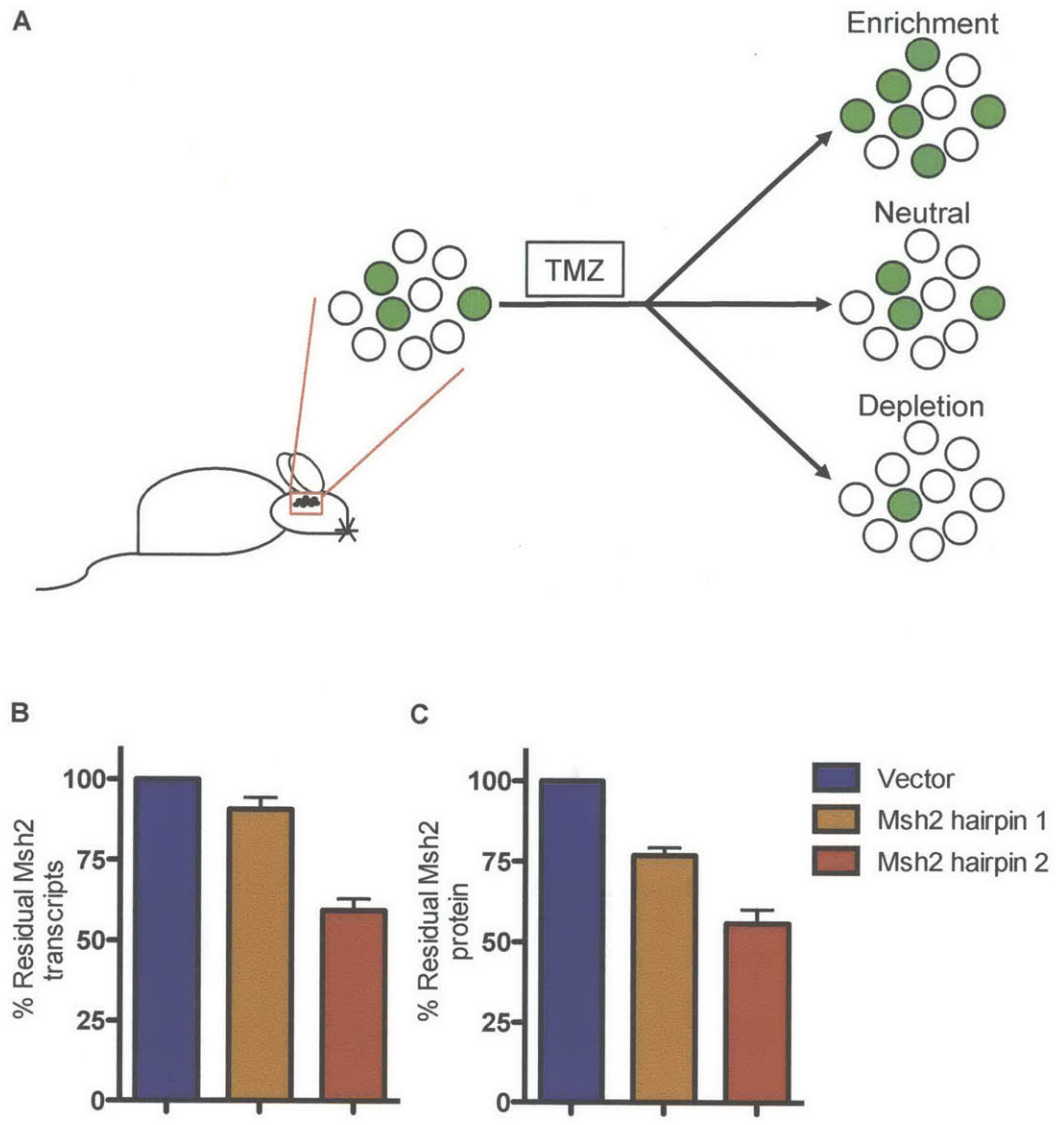

Figure 3.9 Investigating the effects of minor Msh2 decreases on the response of GBM tumors to TMZ.

(A) A competition assay to assess the effects of decreased Msh2 levels on the response of GL261 GBM tumors to TMZ. GL261 cells expressing GFP as a marker of hairpin expression are labeled green.

(B/C) Msh2 transcript (B) and protein (C) levels in GL261 GBM cells expressing a vector control or one of two hairpins targeting Msh2 transcripts (Error bars denote standard error of the mean, n=3).

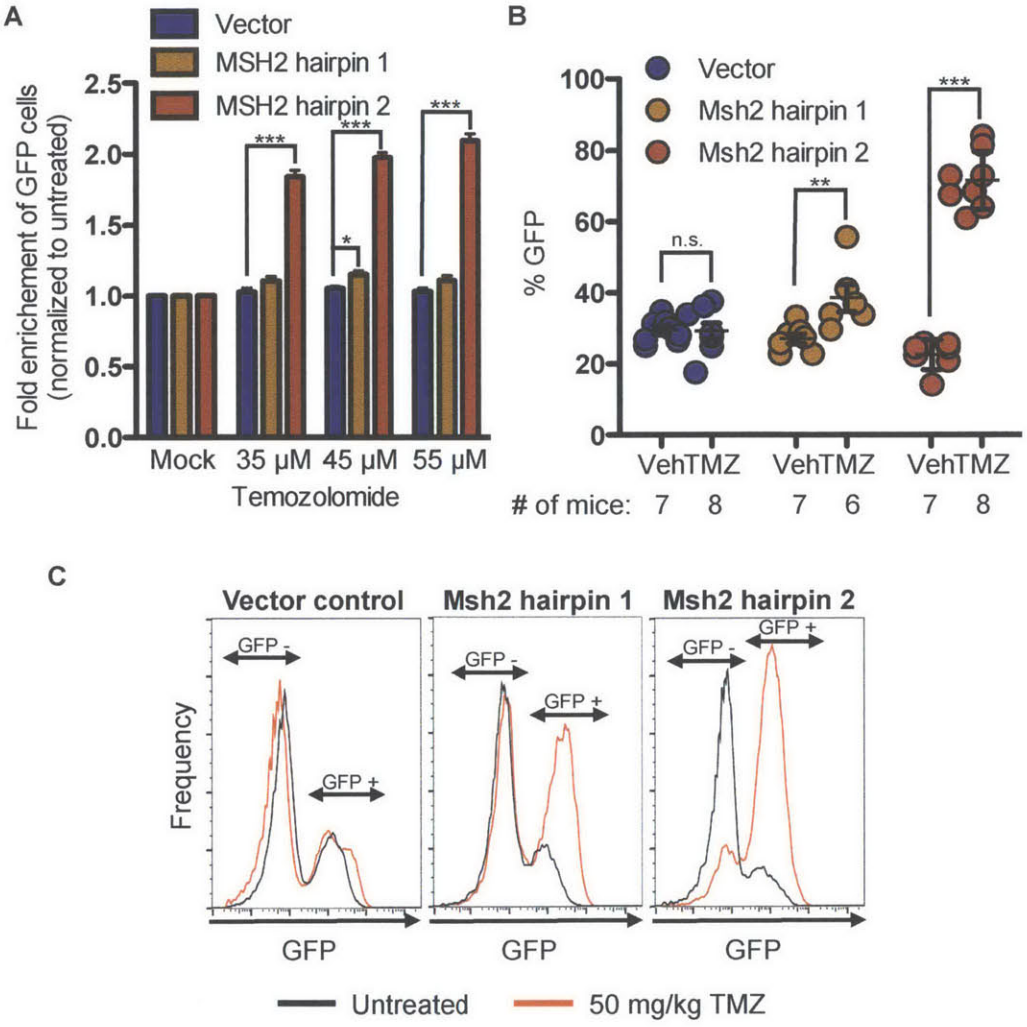

Figure 3.10 Small decreases in Msh2 confer a growth advantage to GBM tumors after TMZ challenge.

(A) TMZ-induced changes in the proportion of GFP expressing cells in GI261 GBM cells expressing a vector control or one of two hairpins targeting Msh2 transcript as measured *in vitro*. Flow cytometry was used to assess changes in the percentage of GFP positive cells 72 hours post-TMZ treatment. The Mann-Whitney test was used to assess significant enrichment of GFP cells between GI261 tumors expressing a vector control or

one of two hairpins targeting Msh2 transcripts (Error bars denote standard deviation from the mean, n=3, * $p< 0.05$; *** $p< 0.001$).

(B) *In vivo* enrichment of Msh2 knockdown cells in a TMZ treated GBM tumor model. C56BL6/J mice harboring GI261-derived GBM tumors were treated with TMZ 8 days post-tumor initiation. Changes in the percentage of GFP positive cells was assessed by flow cytometry of dissociated tumors from mice euthanized after euthanasia criteria were observed. The Mann-Whitney test was used to assess significant enrichment of GFP cells between GI261 tumors expressing a Vector control or one of two hairpins targeting Msh2 transcripts ((Error bars denote standard deviation from the mean, * $p< 0.05$; *** $p< 0.001$).

(C) Representative histogram obtained from dissociated GI261 tumors expressing a vector control or one of two hairpins targeting Msh2 transcripts.

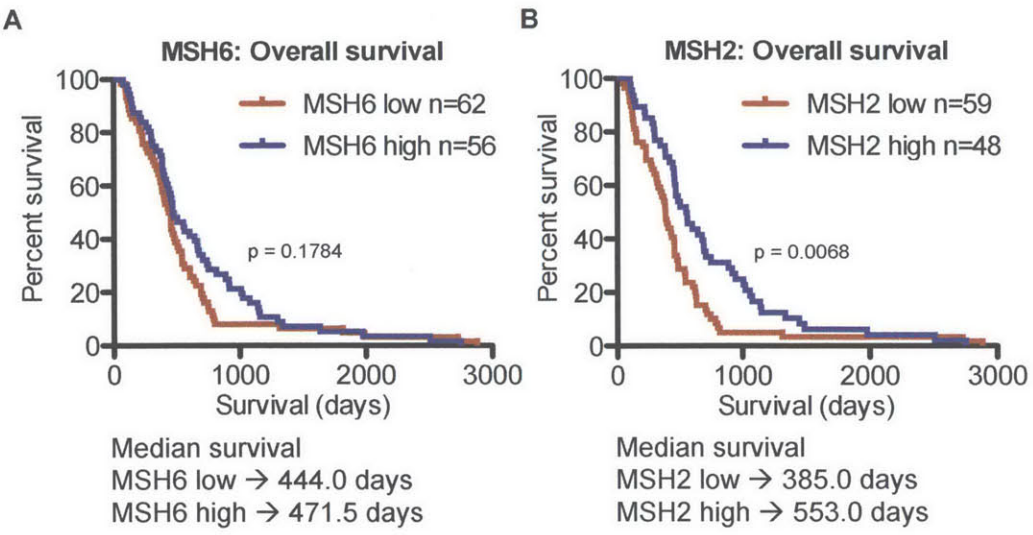

Figure 3.11 MSH2 levels are predictive for the survival of TMZ treated GBM patients.

(A-B) Effects of MSH2 and MSH6 transcript levels on the overall survival of TMZ treated GBM patients. Patients were stratified as high or low expressers by a z-score cutoff of 0.5. The log rank test was employed to assess significance between the median survivals of both populations.

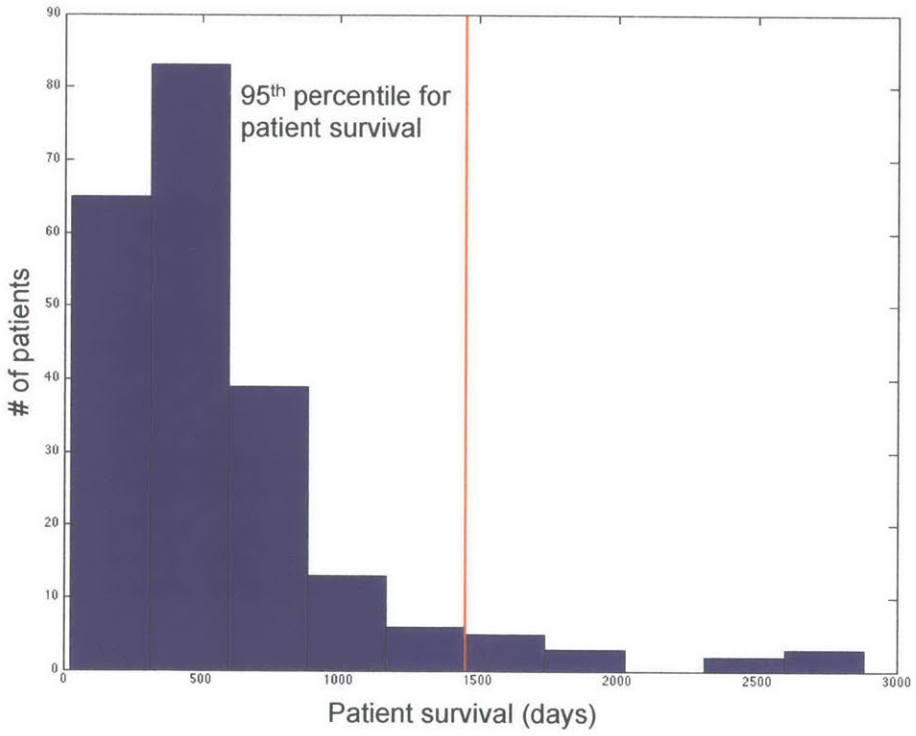

Figure 3.12 Distribution of patient survival in TMZ treated TCGA GBM patients.

Histogram depicting the survival of TMZ treated GBM patients. Survival data was obtained from the clinical data set for GBM patients in the NIH TCGA data matrix. The vertical red line demarcates the separation of the patients who fall into the upper 95th percentile for patient survival after TMZ treatment.

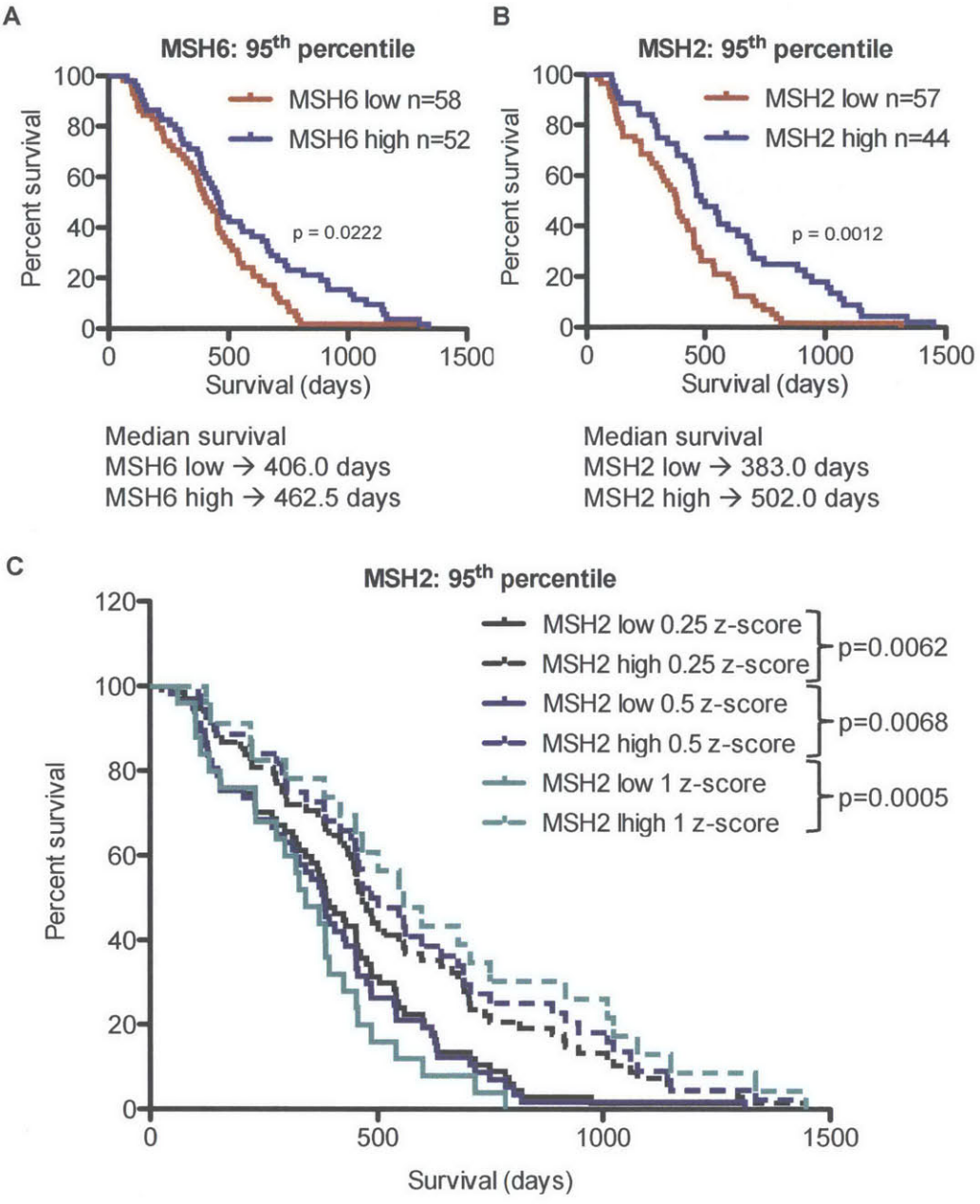

Figure 3.13 MSH2 and MSH6 are predictive for survival in TMZ treated 95th percentile GBM patients.

(A-B) Effects of MSH6 (A) and MSH2 (B) transcript levels on the survival of TMZ treated GBM patients that fall into the 95th for patient survival after TMZ treatment. Patients were

stratified as high or low expressers by a z-score cutoff of 0.5. The log rank test was employed to assess significance between the median survivals of both populations.

(C) Survival of 95th percentile GBM patients defined as high or low MSH2 at various z-score cutoffs. The log rank test was employed to assess significance between the median survivals of both populations.

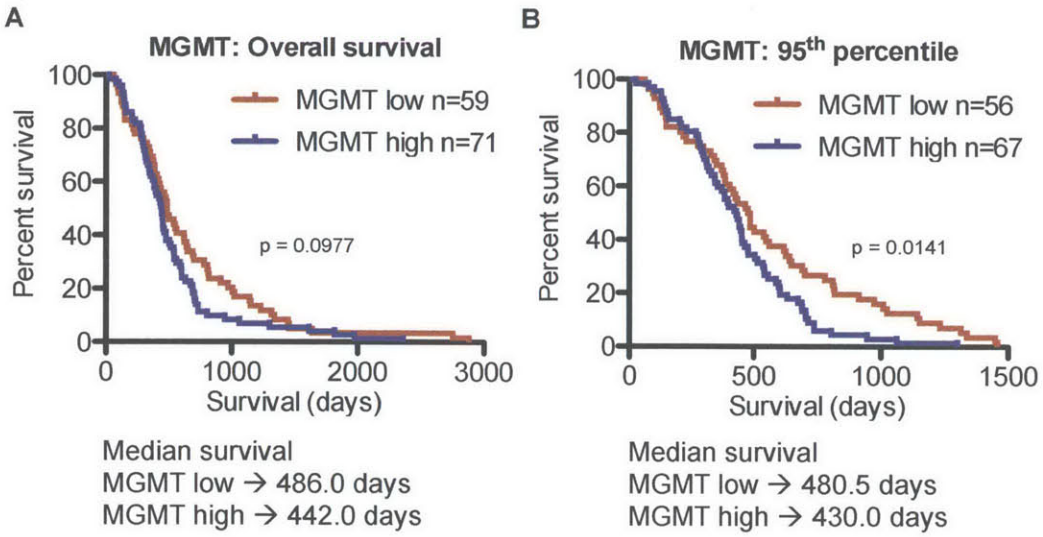

Figure 3.14 MGMT levels are predictive of survival in TMZ treated 95th percentile GBM patients.

(A) Effect of high or low MGMT transcript levels on the overall survival of TMZ treated GBM patients using a z-score cutoff of 0.5.

(B) Effect of high or low MGMT transcript levels on the survival of patients that fall into the 95th for patient survival after TMZ treatment using a z-score cutoff of 0.5.

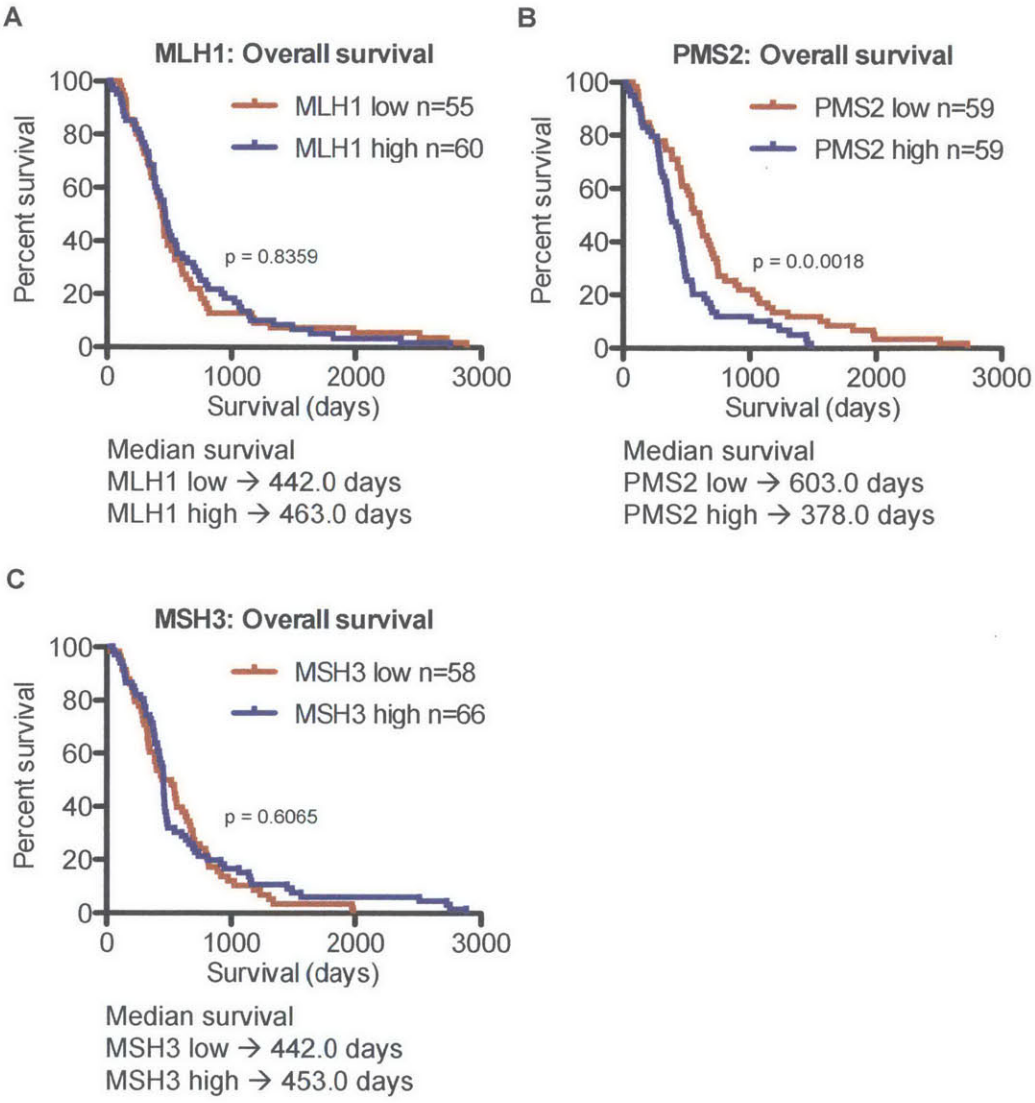

Figure 3.15 Overall survival of GBM patients stratified by MSH3, MLH1 and PMS2 tumor transcript levels.

(A-C) Overall survival of GBM patients stratified as high or low MLH1 (A), PMS2 (B) and MSH3 (C) expressers using a z-score cutoff of 0.5. The log rank test was employed to assess significance between the median survivals of both populations.

Hairpin	Vector	Catalog number and clone ID or Seed sequence
Non-silencing control	pGIPZ	RHS4346
shMSH2 #1	pGIPZ	RHS4430-101025896 ID: V3LHS_390385
shMSH2 #2	pGIPZ	RHS4430-101520518 ID: V3LHS_390381
shMSH2 #3	pGIPZ	RHS4430-101519140 ID: V3LHS_390383
shMSH2 #4	pGIPZ	RHS4430-101521023 ID: V3LHS_390382
shMSH2 #5	pGIPZ	RHS4430-101034588 ID: V3LHS_390386
shMSH6 #1	pGIPZ	RHS4430-101130892 ID: V3LHS_318784
shMSH6 #2	pGIPZ	RHS4430-98481628 ID: V2LHS_82746
shMSH6 #3	pGIPZ	RHS4430-99299091 ID: V2LHS_258239
shMSH6 #4	pGIPZ	RHS4430-98513265 ID: V2LHS_82749
shMSH6 #5	pGIPZ	RHS4430-99166454 ID: V2LHS_82747
Vector control	TMP	----
MSH2 hairpin 1	TMP	CAGGATGCCATTGTTAAAGAA
MSH2 hairpin 2	TMP	AACGATGTGCTGGCTCACTTA

Table 3.1 shRNA constructs used in this study.

References

Barber, A. (2012) The roles of MLH1 and MSH2 in growth and drug resistance in human colorectal cancer cells, University of Guelph, Ontario, Canada.

Brandes, A. A., Tosoni, A., Amista, P., Nicolardi, L., Grosso, D., Berti, F., and Ermani, M. (2004). How effective is BCNU in recurrent glioblastoma in the modern era? A phase II trial. Neurology *63*, 1281-1284.

Cahill, D. P., Levine, K. K., Betensky, R. A., Codd, P. J., Romany, C. A., Reavie, L. B., Batchelor, T. T., Futreal, P. A., Stratton, M. R., Curry, W. T., *et al.* (2007). Loss of the mismatch repair protein MSH6 in human glioblastomas is associated with tumor progression during temozolomide treatment. Clinical cancer research : an official journal of the American Association for Cancer Research *13*, 2038-2045.

Dickins, R. A., Hemann, M. T., Zilfou, J. T., Simpson, D. R., Ibarra, I., Hannon, G. J., and Lowe, S. W. (2005). Probing tumor phenotypes using stable and regulated synthetic microRNA precursors. Nature genetics *37*, 1289-1295.

Felsberg, J., Thon, N., Eigenbrod, S., Hentschel, B., Sabel, M. C., Westphal, M., Schackert, G., Kreth, F. W., Pietsch, T., Loffler, M., *et al.* (2011). Promoter methylation and expression of MGMT and the DNA mismatch repair genes MLH1, MSH2, MSH6 and PMS2 in paired primary and recurrent glioblastomas. Int J Cancer *129*, 659-670.

Fu, D., Calvo, J. A., and Samson, L. D. (2012). Balancing repair and tolerance of DNA damage caused by alkylating agents. Nature reviews Cancer *12*, 104-120.

Halabi, A., Ditch, S., Wang, J., and Grabczyk, E. (2012). DNA mismatch repair complex MutSbeta promotes GAA.TTC repeat expansion in human cells. The Journal of biological chemistry *287*, 29958-29967.

Happold, C., Roth, P., Wick, W., Schmidt, N., Florea, A. M., Silginer, M., Reifenberger, G., and Weller, M. (2012). Distinct molecular mechanisms of acquired

resistance to temozolomide in glioblastoma cells. Journal of neurochemistry *122*, 444-455.

Hayes, A. P., Sevi, L. A., Feldt, M. C., Rose, M. D., and Gammie, A. E. (2009). Reciprocal regulation of nuclear import of the yeast MutSalpha DNA mismatch repair proteins Msh2 and Msh6. DNA repair *8*, 739-751.

Hegi, M. E., Diserens, A. C., Gorlia, T., Hamou, M. F., de Tribolet, N., Weller, M., Kros, J. M., Hainfellner, J. A., Mason, W., Mariani, L., *et al.* (2005). MGMT gene silencing and benefit from temozolomide in glioblastoma. The New England journal of medicine *352*, 997-1003.

Hou, L. C., Veeravagu, A., Hsu, A. R., and Tse, V. C. (2006). Recurrent glioblastoma multiforme: a review of natural history and management options. Neurosurgical focus *20*, E5.

Jagger, J. (1976). Ultraviolet inactivaton of biological systems, Vol 2: Academic Press).

Kantelinen, J., Kansikas, M., Korhonen, M. K., Ollila, S., Heinimann, K., Kariola, R., and Nystrom, M. (2010). MutSbeta exceeds MutSalpha in dinucleotide loop repair. British journal of cancer *102*, 1068-1073.

Li, G. M. (2008). Mechanisms and functions of DNA mismatch repair. Cell research *18*, 85-98.

Maxwell, J. A., Johnson, S. P., McLendon, R. E., Lister, D. W., Horne, K. S., Rasheed, A., Quinn, J. A., Ali-Osman, F., Friedman, A. H., Modrich, P. L., *et al.* (2008). Mismatch repair deficiency does not mediate clinical resistance to temozolomide in malignant glioma. Clinical cancer research : an official journal of the American Association for Cancer Research *14*, 4859-4868.

McGirt, M. J., Than, K. D., Weingart, J. D., Chaichana, K. L., Attenello, F. J., Olivi, A., Laterra, J., Kleinberg, L. R., Grossman, S. A., Brem, H., and Quinones-

Hinojosa, A. (2009). Gliadel (BCNU) wafer plus concomitant temozolomide therapy after primary resection of glioblastoma multiforme. Journal of neurosurgery *110*, 583-588.

Mojas, N., Lopes, M., and Jiricny, J. (2007). Mismatch repair-dependent processing of methylation damage gives rise to persistent single-stranded gaps in newly replicated DNA. Genes & development *21*, 3342-3355.

Nagel, Z. D., Margulies, C. M., Chaim, I. A., McRee, S. K., Mazzucato, P., Ahmad, A., Abo, R. P., Butty, V. L., Forget, A. L., and Samson, L. D. (2014). Multiplexed DNA repair assays for multiple lesions and multiple doses via transcription inhibition and transcriptional mutagenesis. Proceedings of the National Academy of Sciences of the United States of America *111*, E1823-1832.

Newcomb, E. W., and Zagzag, D. (2009). The murine Gl261 glioma experimental model to assess novel brain tumor treatments. In CNS Cancer: Models, Markers, Prognostic Factors, Targets, and Therapeutic Approaches, E.G. Van Meir, ed. (Humana Press), pp. 227-241.

Pena-Diaz, J., and Jiricny, J. (2012). Mammalian mismatch repair: error-free or error-prone? Trends Biochem Sci *37*, 206-214.

Reithmeier, T., Graf, E., Piroth, T., Trippel, M., Pinsker, M. O., and Nikkhah, G. (2010). BCNU for recurrent glioblastoma multiforme: efficacy, toxicity and prognostic factors. Bmc Cancer *10*, 30.

The Cancer Genome Atlas Research Network, T. (2008). Comprehensive genomic characterization defines human glioblastoma genes and core pathways. Nature *455*, 1061-1068.

Valiathan, C., McFaline, J. L., and Samson, L. D. (2012). A rapid survival assay to measure drug-induced cytotoxicity and cell cycle effects. DNA repair *11*, 92-98.

Walid, M. S. (2008). Prognostic factors for long-term survival after glioblastoma. The Permanente journal *12*, 45-48.

Wu, X., Platt, J. L., and Cascalho, M. (2003). Dimerization of MLH1 and PMS2 limits nuclear localization of MutLalpha. Molecular and cellular biology *23*, 3320-3328.

Yip, S., Miao, J., Cahill, D. P., Iafrate, A. J., Aldape, K., Nutt, C. L., and Louis, D. N. (2009). MSH6 mutations arise in glioblastomas during temozolomide therapy and mediate temozolomide resistance. Clinical cancer research : an official journal of the American Association for Cancer Research *15*, 4622-4629.

Chapter IV: Phosphoproteomic profiling of parental and TMZ^{R3} GBM cells

José L. McFaline, Hannah Johnson, Amanda del Rosario, Leona D. Samson and Forest M. White

Experimental contributions: H.J. processed GBM samples for LC-MS/MS analysis. H.J. and A.D. analyzed LC-MS/MS results for phosphopeptide identification.

Chapter 4: Phosphoproteomic profiling of parental and TMZ^{R3} GBM cells

Introduction

In the previous chapters, we characterized the response of GBM cells to both acute and repeated TMZ exposure. Repeated exposure of GBM cells to TMZ led to the selection of GBM cells that display a remarkable degree of TMZ resistance. Candidate-based screening of these TMZ resistant cells identified minor deficiencies in MMR as a driver of the resistant phenotype. This selection process was likely to lead to many more changes than just MMR alterations. It is to be expected that multiple mechanisms evolved to endure the increased genomic instability resulting from O^6-meG persistence, as well as cope with other, seemingly less toxic, lesions produced by TMZ during the repeated exposure experienced by TMZ^{R3} cells.

The response of cells to stimuli can be mediated by any one of a variety of changes in the cell including changes in transcription, translation and post-translational modifications, and some responses may involve more than one of these. Post-translational modifications, including phosphorylation, are usually first responders to such stimuli leading to altered cellular growth, survival, proliferation, migration and even the response to DNA damage and repair. The DNA damage response is orchestrated through activation of numerous components, at the center of which lie the PI3-K like kinases: DNA protein kinase (DNA-PK), Ataxia Telangiectasia mutated (ATM) and Ataxia Telangiectasia and Rad3 related (ATR) (Sirbu and Cortez, 2013). Substrate phosphorylation by the PI3K-like kinases modulates the structure, activity, and protein-protein interactions of a variety of downstream mediators, eventually leading to the activation of effector kinases to mount a global response to DNA damage (Ciccia and Elledge, 2010). These pathways have been shown to interact, affect, and be affected by

the canonical cell survival and proliferation pathways (Guo et al., 2013; Lee et al., 2006; Nikitin et al., 2014).

Multiple signaling pathways modulate the response of GBM cells to various DNA damaging agents, including TMZ. Epidermal growth factor receptor variant 3 (EGFRvIII), a constitutively active EGFR mutant, is one of the most frequent genetic alterations identified in GBM (Gan et al., 2013). EGFRvIII, through modulation of DNA-PK, increases the rate of double strand break repair in GBM cells following IR exposure (Mukherjee et al., 2009). Loss of PTEN activity, the negative regulator of AKT, is prevalent in GBM occurring in up to 60% of tumors (Koul, 2008). Conflicting reports have surfaced regarding the effects of increased AKT signaling (due to PTEN loss) on the sensitivity to TMZ. Hirose and colleagues find that increased AKT activity, via expression of an inducible gain of function AKT fusion protein, leads to abrogation of the TMZ–induced G2/M arrest and increased survival of GBM cells following TMZ exposure *in vitro* (Hirose et al., 2005). In contrast, McEllin and colleagues demonstrated in primary astrocytes that PTEN loss, the negative regulator of AKT, resulted in increased sensitivity to MNNG, a TMZ analogue (McEllin et al., 2010). However, in their system, McEllin and colleagues found that expression of a constitutively activated version of AKT did not recreate the phenotype induced by PTEN loss suggesting that AKT does not play a role in the response to alkylation damage. This discrepancy is likely due to the high doses of MNNG used to overcome MGMT expression in the latter study, as the number of base excision repair lesions becomes significant with increasing amounts of MNNG. With this in mind, it is possible that increased AKT activity decreases the toxicity associated with O^6-meG lesions, the most toxic lesion at low TMZ doses, yet does not alter the toxicity of base excision repair substrates accumulating at higher doses. Additionally Chk1, p38αMAPK and JNK MAPK inhibition have all been shown to sensitize GBM cells to TMZ (Hirose et al., 2001; Hirose et al., 2003; Ohba et al., 2009).

In the present study, we performed phosphoproteomic profiling of parental and TMZ^{R3} GBM cells to identify changes in the phosphorylation network that accompany the acquisition of TMZ resistance. Analysis of the phosphotyrosine and global phosphor-serine/threonine networks revealed modest changes in the phosphorylation of numerous targets. Analysis of variance was used to filter our datasets for phosphorylation sites that vary both by p53 status and TMZ sensitivity. Efforts to identify the kinases responsible for these changes suggest various kinases particularly the platelet derived growth factor receptor tyrosine kinase α (PDGFRα), cyclin dependent kinases (CDKs) and mitogen activated protein kinases (MAPKs) as possibly deregulated in TMZ^{R3} GBM cells. Overall, protein phosphorylation analysis has identified putative target kinases whose activity may mediate the response of GBM cells to TMZ exposure.

Materials and Methods

Sample preparation, protein isolation and tryptic digestion

Parental (control and p53kd) and TMZ resistant (control-TMZ^{R3} and p53kd-TMZ^{R3}) GBM cells were seeded at 2 x 10^7 cells per 15 cm plates, while p53kd-TMZ^{R3} cells were seeded at 1.5 x 10^7 cells per 15 cm plate. Cells were allowed to attach for 24 hours after seeding. After attachment, media was removed and cells were stimulated by addition of DMEM containing 10% FBS. Cells were exposed to FBS for 8h at which time media was removed, plates set on ice, washed with cold PBS and cells lysed by scraping into 8M urea containing 1 μM sodium orthovanadate and 10 μM sodium fluoride. Proteins were isolated, chemically modified and digested to peptides as described previously (Huang et al., 2007). A total of 4 biological replicates were processed per cell line.

iTRAQ labeling, phosphopeptide enrichment and phosphopeptide identification by LC-MS/MS

iTRAQ labeling, phosphotyrosine enrichment and peptide isoelectric focusing were performed (Johnson et al., 2012). For global phosphorylation analysis, fractions obtained by isoelectric focusing were subjected to phosphopeptide enrichment by metal affinity using NTA (Ficarro et al., 2009). Phosphopeptide enriched samples were resolved by reversed phase chromatography and peptides sequenced and iTRAQ labels were quantified by MS/MS using an Orbitrap Elite (Thermo) for the phosphotyrosine analyses or a QExactive (Thermo) for the global phosphoserine/threonine analyses (Johnson et al., 2012). Only phosphorylation sites that were identified in two or more biological replicates were included in further analyses.

Analysis of variance

Two-way analysis of variance (ANOVA) of pY and global pS/T was performed using MATLAB computing language software package (Simulink) grouping parental and TMZ^{R3} cells into groups depending on their p53 status (low vs. high) or TMZ sensitivity (sensitive vs. resistant) (Figure 4.4). ANOVA analysis compares the mean and variance of each group for each phosphopeptide and determines whether the variation observed between the groups (i.e. p53 low and p53 high or TMZ sensitive or resistant) is significantly different (e.g. whether the mean of p53 low samples is significantly different from p53 high samples). Phosphorylation sites were classified as varying significantly due to p53 status, TMZ sensitivity or both if the probability that the variance was not different between the groups was less that $p = 0.05$.

Kinase enrichment analysis

Kinase enrichment analysis (KEA) was done using the KEA web tool developed at the System Biology Center at the Mount Sinai School of Medicine (Lachmann and Ma'ayan, 2009). Briefly, KEA identifies kinases whose substrates are over-represented on a list of proteins The algorithm uses previously described kinase-substrate interactions to identify whether substrates for a given kinase are over-represented on the submitted list. A p-value was obtained using the Fisher exact test which determines the probability of a particular kinase being enriched as a function of the fraction of kinase substrates in the queried dataset versus the fraction of kinase substrate in the kinase-substrate interaction database. This avoids identification of kinases solely on the basis of being over or under-represented in the database. A cutoff of p=0.05 was used to classify kinases as significantly enriched in our datasets.

Motif enrichment analysis

Motif enrichment analysis was done using the Motif-X web tool available developed at the Harvard Medical School (Chou and Schwartz, 2011; Schwartz and Gygi, 2005). Briefly, motif-x identifies sequences that are overrepresented in a list of peptides and calculates a p-value based on a comparison of the number of times the motif appears in our dataset to the number of times it appears in a background database. To search for motifs, an occurrence threshold (the minimum number of times a motif has to be observed), significance threshold and background database must be specified. For this study, we used a minimum occurrence value of 5, a significance under p=0.0001 and the IPI human proteome database as our background. In the iterative approach taken by motif-X, the foreground and background size decreases as peptides with enriched motifs are removed from the datasets and the algorithm again searches for motifs enriched in the remaining list. As motif-X does not allow simultaneous centering on both serine and

threonine residues, phosphoserine and phosphothreonine containing peptides were analyzed independently.

Hierarchical clustering of GBM samples

Hierarchical clustering of GBM samples in conjunction with either pY or global pS/T data was performed using MATLAB computing language software package (Simulink) using a euclidean distance measure.

K-means clustering of phosphorylation sites with similar dynamics

K-means clustering of global pS/T data was performed using MATLAB computing language software package (Simulink) using the correlation between phosphosites as a distance measure. The k-means algorithm was set to be replicated 1 x 10^5 times and the solution that maximizes the distance between cluster and minimizes the distance between sites in a given cluster was chosen. To plot, phosphorylation levels in each sample were normalized to the square root of the sum of squares for each site, the black line in each cluster denotes the mean of all sites in a given cluster (Figure 4.11 and 4.12).

Results

Phosphoproteomic profiling of parental and TMZ resistant GBM cells

To identify molecular changes that accompany the acquisition of TMZ resistance in GBM cells, phosphoproteomic network analysis was performed. Total protein was isolated from parental and TMZ^{R3} GBM cells after stimulation with 10% FBS. Proteins were

digested to peptides, chemically modified and labeled with isobaric tags (iTRAQ) to allow relative quantification of phosphopeptides. To identify changes at the phosphotyrosine (pY) and global phosphorylation (pS/T) levels, isotope labeled peptides were: (i) subjected to immunoprecipitation using pan anti-pY antibodies followed by immobilized metal affinity chromatography (IMAC) to enrich for pY containing peptides or (ii) fractionated via isoelectric focusing then subjected to IMAC enrichment to investigate global pS/T changes (Figure 4.1, Materials and Methods). Using this approach, we identified 136 pY and 1750 pS/T containing peptides across 1506 proteins. Hierarchical clustering of the phosphoproteomic profiles of each GBM line efficiently grouped replicates together (Figure 4.2) with p53kd-TMZ^{R3} cells characterized as being less similar than all other GBM cells. Interestingly, control and control-TMZ^{R3} clustered closer together, suggesting that p53 status has a profound effect on network phosphorylation levels. However, these changes do not appear to alter the sensitivity of GBM cells to acute TMZ treatment or their ability to acquire resistance during repeated TMZ exposure. Most phosphopeptides identified display small differences in phosphorylation with the great majority of sites displaying less than 2 fold change in phosphorylation. Even though modest changes are observed, unbiased clustering results allows us to conclude that the obtained phosphoproteomic profiles represent molecular signatures that can classify our TMZ sensitive and resistant GBM cell lines.

ANOVA analysis identifies phosphotyrosine sites that vary significantly by p53 status and/or TMZ sensitivity

Analysis of variance (ANOVA) can identify phosphorylation sites whose mean differs significantly between samples due to their classification into distinct categorical variables

(Figure 4.3, Materials and Methods). Here we described two variables: one based on p53 status (low or high p53) and one based on TMZ sensitivity (sensitive or resistant to TMZ). Using this approach we identified 35 pY sites that vary significantly by p53 status (Figure 4.4) and/or TMZ sensitivity (Figure 4.5). For phosphorylation sites that vary significantly by p53 status, two main clusters were apparent for sites that were either decreased or increased in p53 deficient GBM cells, with the largest fold changes observed mainly in p53kd-TMZ^{R3} cells (Figure 4.4). These differences included significant decreases in the phosphorylation sites Y204 and Y187 in the activation loops of extracellular regulated MAP kinase 1 (ERK1) and ERK2, respectively (Figure 4.4). These residues, when phosphorylated, are associated with increased ERK activity (Roskoski, 2012). As described previously, both control-TMZ^{R3} and p53kd-TMZ^{R3} GBM cells display a significant increase in doubling time compared to the parental cells, with the effect being much more pronounced in p53kd-TMZ^{R3} cells (32 hour and 40 hour T_D, respectively, compared to 24 hours for parental lines). Therefore, decreased ERK signaling may be one of the mechanisms leading to decreased proliferation in p53kd-TMZ^{R3} GBM cells. This decrease in proliferation may give the p53kd-TMZ^{R3} GBM cells the time necessary to repair TMZ-induced lesions after repeated exposure to drug.

Tyrosine phosphorylation sites that were modulated by TMZ sensitivity were broadly divided into two categories: (i) those that changed significantly in both of the TMZ^{R3} cell lines compared to parental cells and (ii) those that changed significantly in only one of the two TMZ^{R3} cell lines compared to parental (Figure 4.6) Among the pY sites associated with TMZ sensitivity in both TMZ^{R3} lines, the largest increase between parental and TMZ^{R3} cells was observed for the phosphorylation of Y742 on PDGFRα (Figure 4.6). This site is conserved with the PDGFRβ (Y751) receptor where is has been characterized as an auto-phosphorylation site and therefore associated with increased PDGFR signaling (Kazlauskas and Cooper, 1989). Further, phosphorylation of this site

has been shown to mediate binding to the regulatory p85 subunit of phosphoinositide 3-kinase (PI3K) (Kashishian et al., 1992; Kazlauskas and Cooper, 1989). The PDGF pathway is the second most commonly hyperactivated receptor tyrosine kinase pathway in GBM with overactivation, usually due both to gene amplification and PDGF ligand overexpression (Nazarenko et al., 2012). Furthermore, increased PDGFR signaling characterizes the proneural subtype of GBM (Dunn et al., 2012). A recent studied showed that patients with proneural GBM display an increased overall survival as a group compared to the other GBM subtypes (classical, neural and mesenchymal) (Phillips et al., 2006). However this effect appears independent of response to therapy as these patients are classified as non-responders to therapy suggesting that the survival advantage observed is solely due to decreased progression of the tumors and not increased therapeutic response (Verhaak et al., 2010). Therefore, it appears plausible that increased PDGFRα signaling, like that seen in proneural GBM, leads to decreased sensitivity to TMZ in TMZ^{R3} cells. Currently, we are focusing on identifying the effect of increased and decreased PDGFR activity on the sensitivity of GBM cells to acute and repeated TMZ exposure.

Phosphorylation of integrin alpha 3 (ITGA3) on Y1051 constitutes another target of interest (Figure 4.6). Although this phosphorylation site is not characterized, integrin signaling has been implicated in various aspects of GBM including migration, invasion and sensitivity to TMZ. ITGA3 protein expression correlates with increased invasion of glioma stem-like cells (Nakada et al., 2013). In respect to TMZ treatment, decreased integrin signaling, specifically depletion of integrin α5, has been shown to increase the sensitivity of GBM cells to TMZ (Janouskova et al., 2012). Integrins mediate downstream effects through activation of focal adhesion kinase 1 (FAK1) and other shared downstream targets (Giancotti and Ruoslahti, 1999). Therefore, ITGA3 is a strong

candidate for molecular changes leading to the decreased TMZ sensitivity of TMZ^{R3} cells.

Identification of phosphoserine/threonine sites that vary significantly by p53 status and/or TMZ sensitivity

We employed the ANOVA approach described previously to identify sites in our global phosphorylation data sets that vary significantly by p53 status, TMZ sensitivity or both. ANOVA filtering identified 490 pS/T sites (28%) that vary significantly by p53 status and 188 sites (11%) that vary significantly by TMZ sensitivity. As expected, unbiased clustering of sites that vary significantly by p53 status or TMZ sensitivity grouped samples by p53 proficiency or response to TMZ, respectively (Figure 4.7A and 4.7B).

Similarly to the pY data, our pS/T results highlighted molecular changes that accompany the slow proliferation rate observed in p53kd-TMZ^{R3} cells. Decreased CDK7 T170 phosphorylation was observed in this cell line (Figure 4.8A). CDK7 is the catalytic component of the CDK activating kinase complex (CAK) where T170 phosphorylation increases CAK activation and activation of downstream CDKs (Garrett et al., 2001). Moreover, T170 phosphorylation and CAK activation has been proposed to be a part of a positive feedback loop with both CDK1 and CDK2 able to phosphorylate T170 (Garrett et al., 2001). Therefore, decreased T170 phosphorylation may serve as a biomarker for deregulated CDK signaling, and presumably a mechanism for decreased cell cycle progression, in p53kd-TMZ^{R3} GBM cells.

Interestingly, the phosphorylation at S554 of the pre-mRNA 3'-end processing factor FIP1L1 was increased in TMZ^{R3} GBM cells (Figure 4.8B). FIP1L1 is an uncharacterized protein whose genomic localization is upstream of PDGFRα and has been shown to

undergo genomic rearrangements in cancer to create a FIP1L1-PDGFRα fusion protein that displays constitutive PDGFRα kinase activity (Walz et al., 2009). Deletion of CHIC2, a gene that resides between the FIP1L1 and PDGFRα gene, can be used as a marker for the presence of this fusion protein in TMZ^{R3} GBM cells (Pardanani et al., 2003). The decreased phosphorylation on T389 of the general transcription factor II F (GTF2F1) was also of interest (Figure 4.8C). This particular phosphorylation, in combination with S385 phosphorylation, leads to decreased transcriptional elongation by RNA polymerase II (Rossignol et al., 1999). Therefore, this modification indicates potential for transcriptional changes induced in TMZ^{R3} cells upon acquisition of TMZ resistance.

Kinase enrichment and substrate motif analysis of TMZ^{R3} GBM cells

To further identify factors that accompany the acquisition of TMZ resistance, we employed Kinase Enrichment Analysis (KEA) of the full list of 188 pS/T containing phosphorylation sites that vary significantly by TMZ sensitivity. Kinase enrichment analysis (KEA) identifies kinase substrates over-represented in a list of proteins (Lachmann and Ma'ayan, 2009). The results of this analysis identified a variety of kinases including GSK3, CDK1 (CDC2), CDK2 and various MAP kinases as having an over-representation of substrates in proteins with phosphorylation sites that vary by TMZ sensitivity (Table 4.1).

To more directly identify kinases responsible for phosphorylating sites that vary significantly by TMZ sensitivity, we performed motif scanning using Motif-X motif building software (Chou and Schwartz, 2011; Schwartz and Gygi, 2005). Consistent with our KEA results, the top enriched motifs were PX(S)P and (S)P (where X is any amino acid and the residue in parenthesis is the phosphorylated site), the canonical CDK/MAPK

substrate motifs (Table 4.2) (Songyang et al., 1996). Importantly, these motifs were not the most enriched in the full data set prior to ANOVA filtering, where the acidophilic kinase motif, (S)DEE, mainly associated with casein II kinase (Pearson and Kemp, 1991; Songyang et al., 1996), was most enriched (Table 4.3). This further strengthens the hypothesis that CDK/MAPK substrates are relevant to TMZ sensitivity and not a result of CDK/MAPK substrates being the dominant motif in our dataset.

Although this approach highlights kinases that may be responsible for phosphorylating the sites identified in this study, it does not take into account the differences in phosphorylation between the various GBM lines. To overcome this issue, k-means clustering of sites that vary due to TMZ sensitivity was used to group sites with similar dynamics (Figure 4.9). This approach revealed 6 clusters: two clusters where phosphorylation decreased between parental and TMZ^{R3} cells (clusters 1 and 2), two clusters where phosphorylation increased between parental and TMZ^{R3} cells (clusters 3 and 6) and two clusters where phosphorylation increased either in Control-TMZ^{R3} (cluster 5) or p53 kd-TMZ^{R3} (cluster 6) compared to Control and p53kd GBM cells, respectively (Figure 4.9). All clusters analyzed are enriched for the CDK/MAPK PX(S/T)P or (S/T)P motif. Additionally, clusters 1, 3 and 6 are enriched for the RXX(S) motif, frequently associated with AKT substrates (Table 4.4) (Alessi et al., 1996; Manning and Cantley, 2007). The prevalence of PX(S/T)P or (S/T)P motifs in each of the studied clusters represents a challenge in identifying the particular kinase(s) responsible for the various changes observed between parental and TMZ^{R3} GBM cells. Although the PX(S/T)P and (S/T)P substrate motifs are shared by a number of proteins substrates, namely the CDK/MAPK family, additional substrate specificity is also the result of residues located at varying positions relative to the phosphorylation site termed docking site motifs that bind MAPKs directly or to cyclins that partner with CDKs (Bhaduri and Pryciak, 2011; Schulman et al., 1998; Sheridan et al., 2008). Future work will focus on

identifying these conserved residues within substrates in the various clusters to narrow the list of kinases responsible for the observed dynamics.

K means clustering analysis of phosphorylation sites that vary by p53 status identified five clusters of sites that decreased in the absence of p53 (clusters 1-5) and one cluster where phosphorylation increased upon p53 loss (cluster 6) (Figure 4.10). Additionally, clusters 2 and 3 displayed increased and decreased phosphorylation, respectively, as a function of decreased TMZ sensitivity while cluster 4 showed increased phosphorylation specifically in control-TMZ^{R3} cells and cluster 5 displayed decreased phosphorylation in p53kd-TMZ^{R3}, cells compared to their parental counterparts. Motif analysis again identified PX(S/T)P, (S/T)P and RXX(S) motifs as being overrepresented in all clusters with the exception of cluster 6, which was not enriched for the RXX(S) motif (Table 4.5). Cluster 6, containing phosphorylation sites that decreased after p53 loss, was enriched for (S)XXE, a motif associated with casein II kinase (Pearson and Kemp, 1991; Songyang et al., 1996) suggesting p53 loss leads to increased CKII activity. Unexpectedly, various clusters appeared to also vary due to TMZ sensitivity, with cluster 2 and cluster 3 displaying increased and decreased phosphorylation in resistant cells, respectively. In addition, cluster 4 showed increased phosphorylation specifically in control-TMZ^{R3} cells and cluster 5 displayed decreased phosphorylation in p53kd-TMZ^{R3}, cells compared to their parental counterparts. Cluster 2, whose sites display increased phosphorylation in TMZ resistant cells, showed an enrichment for the R(S) motif, a motif associated with PKA and the SRPK kinase family (Giannakouros et al., 2011; Pearson and Kemp, 1991; Prasad et al., 1999). This motif was also enriched in cluster 4, where phosphorylation increased with resistance, yet only for control-TMZ^{R3} cells. Lastly, cluster 3, where phosphorylation was generally decreased in resistant cells compared to parental, had an enrichment for the (S)XS motif, most often associated with TGFβ receptor type 1 (Table 4.5) (Wrighton et al., 2009).

Discussion

The acquisition of TMZ resistance likely involves a variety of changes to the genetic landscape that has implications farther from just the repair, or lack thereof, of TMZ-induced lesions. These changes probably alter mechanisms not only at the repair level but also the ability of cells to arrest in response to repair damage, allowing them to ignore damage induced death signals and ultimately resume proliferation after repeated genomic insults. In this chapter, we explored what changes accompany TMZ resistance by comparing the phosphoproteome of TMZ sensitive and resistant GBM cells. We identified numerous changes at the phosphotyrosine, phosphoserine and phosphothreonine levels. Hierarchical clustering of phosphoproteomic profiles was able to group all replicates as expected and clustered p53 proficient cells (control and control-TMZ^{R3}) closer together regardless of TMZ sensitivity (Figure 4.2). Therefore, it appears that p53 loss leads to alteration of the global phosphorylation network but not to any change in TMZ sensitivity. To filter sites driving the above signatures, ANOVA analysis was performed to identify sites that vary significantly by p53 status, TMZ sensitivity or both. At both the pY and pS/T level, our analyses suggested a mechanism for the decreased proliferation of p53kd-TMZ^{R3} cells by a combination of decreased pro-growth and cell cycle progression signals. These cells displayed decreased phosphorylation of pY residues associated with increased kinase activity on ERK1 and ERK2, two major regulators of cell proliferation (Roskoski, 2012). Furthermore, these cells displayed decreased phosphorylation of a stimulatory site on CAK, a complex responsible for CDK activation and therefore progression through the cell cycle (Garrett et al., 2001). ANOVA analysis of pY sites also revealed increased levels of an auto-phosphorylation site of PDGFRα in both control-TMZ^{R3} and p53kd-TMZ^{R3} cells suggesting PDGFR activity is selected for during repeated TMZ exposure. This is a particularly exciting result as

PDGFR signaling is the second most commonly altered receptor tyrosine kinase pathway in GBM (Nazarenko et al., 2012). Currently, we are investigating how PDGFR signaling may affect the response of GBM cells to TMZ by exposure of GBM cells to the PDGFR ligand PDGF-BB, to increase PDGFR activity, as well as incubation with the PDGFR inhibitor sutent, to decrease PDGFR activity. Other targets of interest include integrin α3 phosphorylation at Y1051. Although this site is uncharacterized, integrin signaling has been shown to decrease the response of GBM cells to TMZ (Janouskova et al., 2012). Integrins signal by activating a conserved group of downstream targets, including FAK1 (Giancotti and Ruoslahti, 1999). FAK1 inhibitors are readily available and future work will focus on investigating the effect of FAK1 inhibition on the sensitivity of GBM cells to TMZ. Interestingly, integrin induced FAK1 activation has been shown to correlate with increased phosphorylation of PDGFRβ on Y751, the residue analogous to Y742 on PDGFRα, in a PDGF independent manner (Veevers-Lowe et al., 2011).

Analysis of pS/T data remains challenging due to the complexity and magnitude of the dataset. In this study, we used ANOVA filtering followed by k-means clustering to identify sites that vary by p53 status and TMZ sensitivity and subsequently group those that share similar dynamics. Analyzing these clusters for conserved sequence motifs revealed that PX(S/T)P and (S/T)P motifs, likely CDK/MAPK substrates, were enriched in all clusters. The CDK and MAPK families share a similar preference for (S)P and PX(S)P sequence motifs (Songyang et al., 1996). Additional specificity is added by residues farther from the phosphorylation site that interact with docking grooves both on MAPKs themselves and the substrate binding sites on the cyclin proteins that compose the active cyclin-CDK complexes (Bhaduri and Pryciak, 2011; Schulman et al., 1998; Sheridan et al., 2008). More in depth computational analysis identifying enriched motifs at various lengths from the phosphorylation site may uncover some of these docking sites and provide insights into the specific CDKs or MAPKs involved in regulating the

identified sites. Alternatively, pan CDK inhibitors or inhibitors that target the 4 major CDK cell cycle regulators of the classical cell cycle model (CDK1/CDK2/CDK4/CDK6) (Hochegger et al., 2008) and inhibitors to each of the major MAPK families (ERK/p38MAPK/JNK) (Roux and Blenis, 2004) can be used to investigate the effects of these kinases on the response to TMZ. The RXX(S) motif, a motif most often associated with AKT, was enriched in three of the six of these clusters. Conflicting reports have emerged regarding the role of AKT in the response of GBM cells to TMZ with studies suggesting increased AKT activity mediates survival, and in other cases no role, after TMZ treatment (Hirose et al., 2005; McEllin et al., 2010). This difference may reflect roles for AKT in responding to O^6-meG specifically which may be masked by treating cells at high concentrations of drug where BER lesions contribute significantly to toxicity. Regardless, it appears deregulated AKT signaling is a likely candidate for a network change that alters the response of GBM cells to repeated TMZ exposure. Lastly, clustering and motif analysis on sites that vary due to p53 status highlights two clusters that are altered on the basis of TMZ sensitivity. These clusters were enriched for R(X) and S(X)S motifs, respectively, the former being associated with PKA and SRPK substrates and the latter with transforming growth factor β (TGFβ) receptor type 1 substrates. Our ANOVA analysis for variance due to TMZ sensitivity likely missed these due to the variation in baseline phosphopeptide levels as a function of p53 loss (Figure 4.10).

Future goals

This study demonstrates that profiling of baseline phosphorylation levels can be used to identify pathways deregulated between TMZ sensitive and TMZ resistant cells. Using our

results, we will perform a small inhibitor screen targeting kinases implied from our results as possibly altered in TMZ^{R3} cells, namely PDGFRα, FAK1 and members of the CDK and MAPK family. Inhibition in resistant cells can allow us to determine if inhibition of any of these targets decreases cellular viability and whether they re-sensitizes TMZ^{R3} cells to TMZ treatment. Additionally, dual inhibitor and TMZ treatment of TMZ sensitive GBM cells can explore whether any of these targets potentiate or resist initial TMZ-induced toxicity. It is possible that deregulation of one or more of the above mentioned pathways mediates TMZ resistance by altering the levels of MMR components, resulting in decreased MMR activity and resistance to TMZ. Therefore, using a fluorescence-based in-cell HCR assay for MMR activity we will explore whether activity of these kinases regulates MMR directly.

Figures

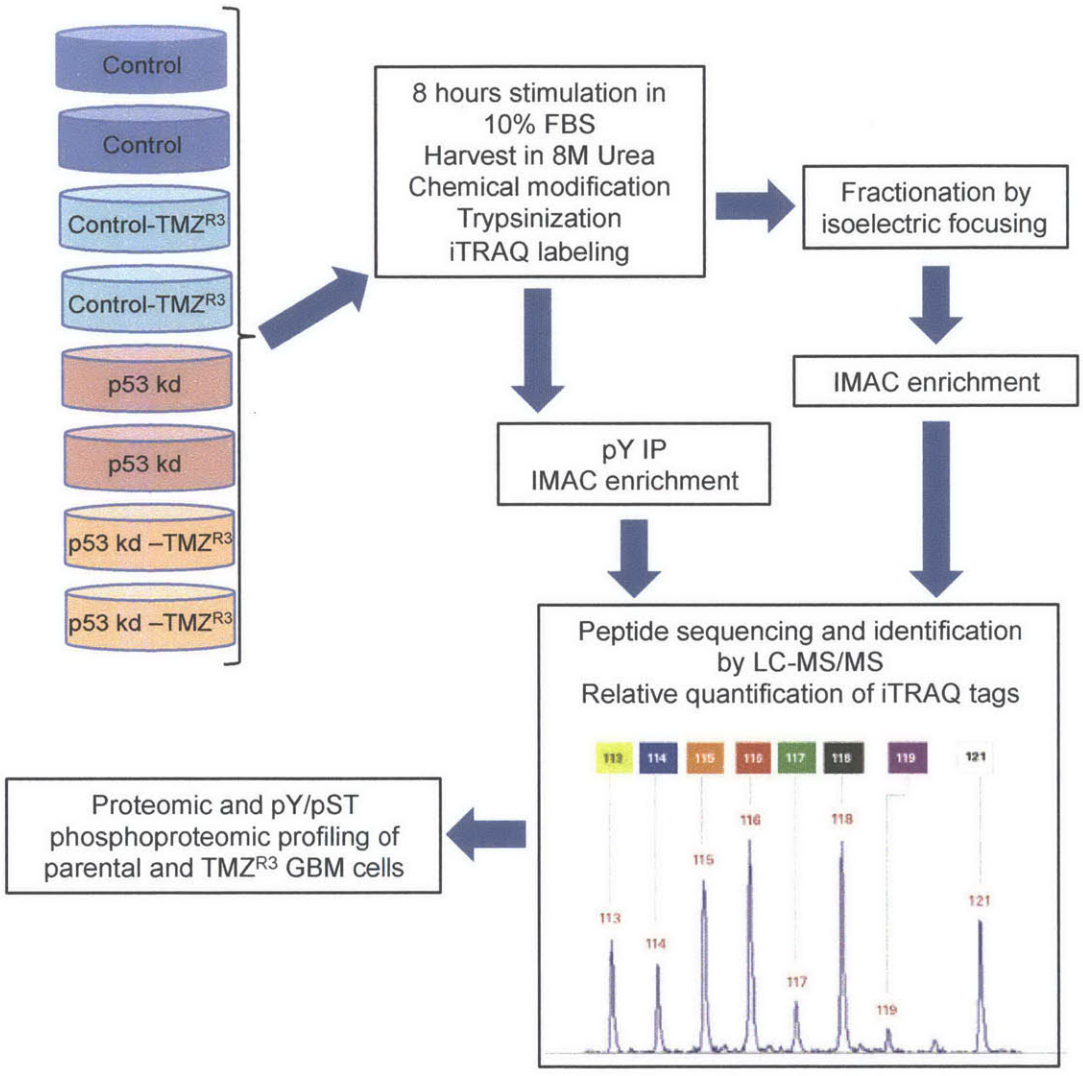

Figure 4.1 Phosphoproteomic profiling of parental and TMZ^{R3} GBM cells.

Parental and TMZ^{R3} GBM cells were stimulated with 10% FBS for 8 hours, and harvested in 8 M urea containing protein phosphatase inhibitors. Protein was isolated and digested to peptides and labeled with isobaric tags. Labeled peptides where then enriched either for pY containing peptides or for phosphopeptides as described in

Materials and Methods. Phosphopeptides were resolved by HPLC and subsequently sequenced and relative levels quantified by LC-MS/MS.

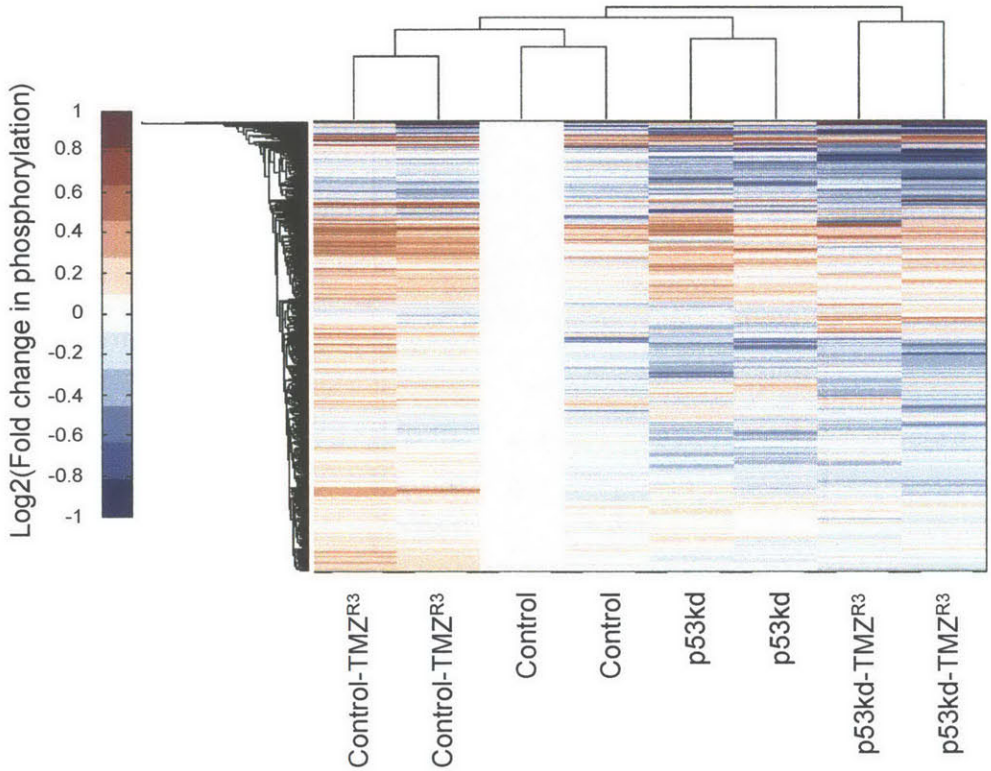

Figure 4.2 Hierarchical clustering of phosphopeptides identified in this study.

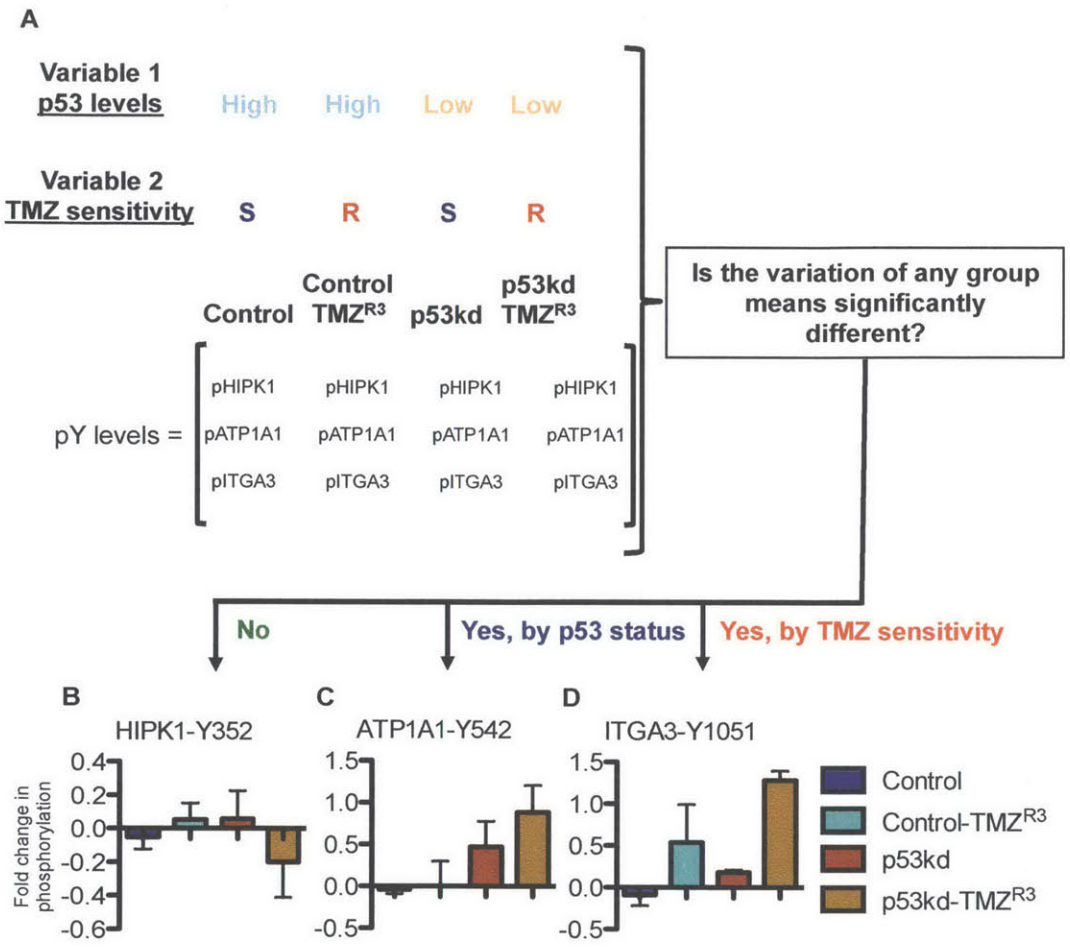

Figure 4.3 ANOVA approach for identifying phosphopeptides that vary significantly by p53 status or TMZ treatment.

(A) For ANOVA analysis, GBM samples were identified according to their p53 status and TMZ sensitivity. For all of the phosphopeptides quantified, ANOVA determines if the variation in phosphopeptide levels is significantly different between the means of the various groups at a predetermined statistical cutoff ($p < 0.05$). There may be no significant difference between the group means (B) or a difference due to p53 status (C), TMZ sensitivity (D) or both (not shown). In group 2, S and R denote sensitivity and

resistance to TMZ, respectively. G1 and G2 designate different groups within a given variable.

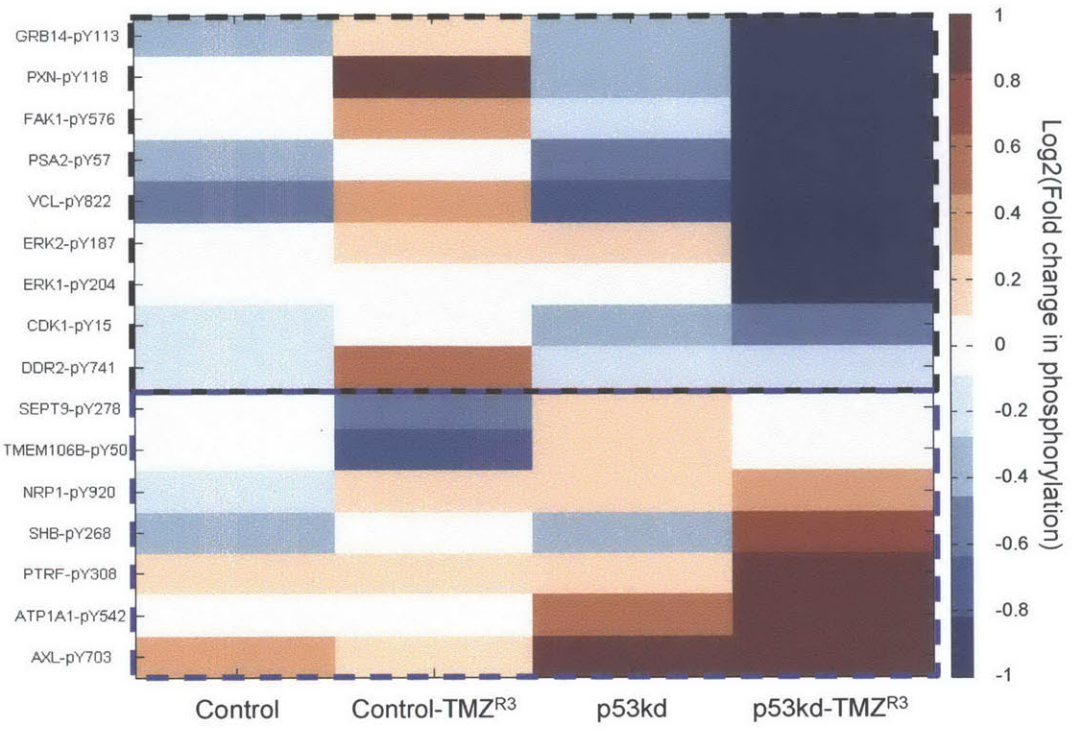

Figure 4.4 pY containing phosphopeptides that vary due to p53 status.

Heatmap displaying 17 phosphorylation sites identified as varying significantly due to p53 status as determined by ANOVA analysis. Samples are rank ordered according to pY levels in p53kd-TMZ^{R3} cells.

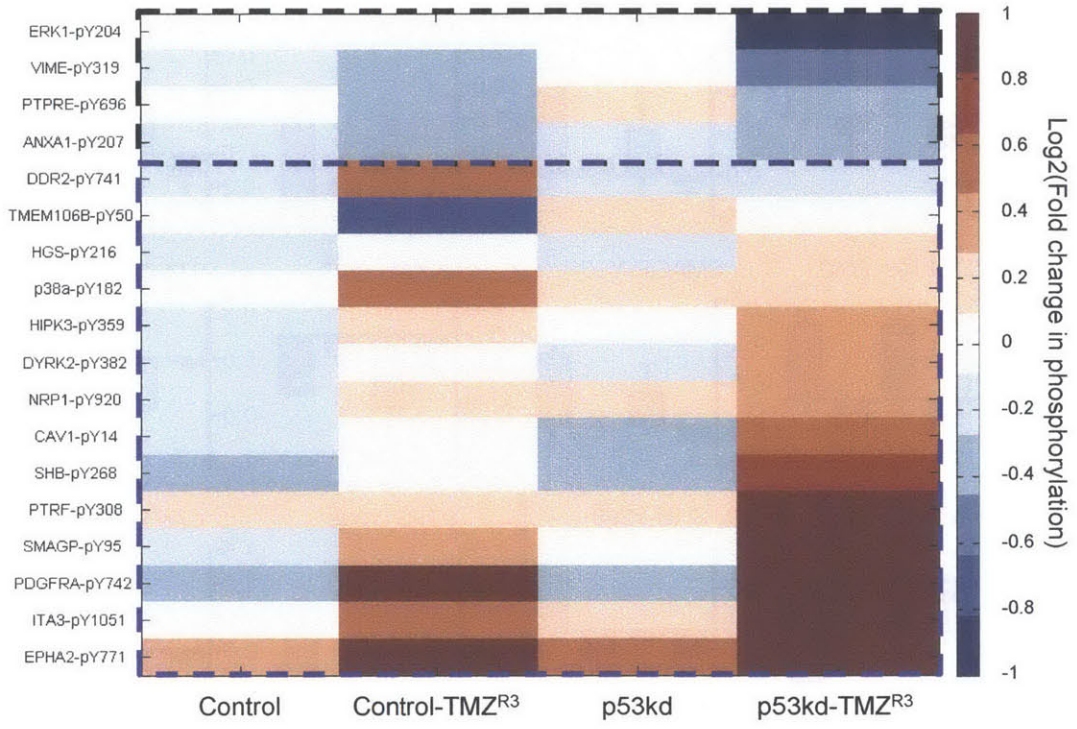

Figure 4.5 pY containing phosphopeptides that vary due to TMZ sensitivity.

Heatmap displaying 18 phosphorylation sites identified as varying significantly due to TMZ sensitivity as determined by ANOVA analysis. Samples are rank ordered according to pY levels in p53kd-TMZ^{R3} cells.

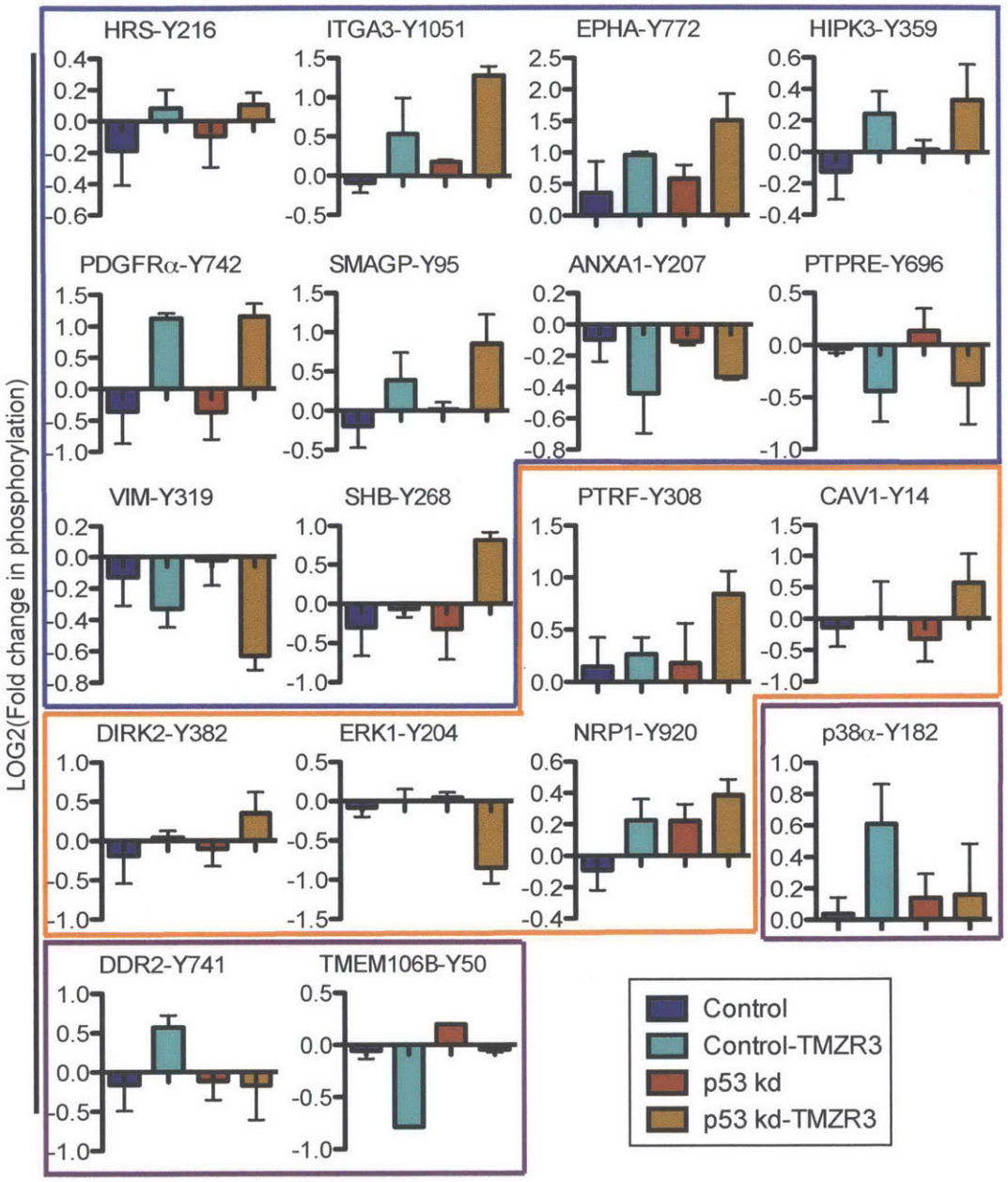

Figure 4.6 Grouping of pY containing phosphopeptides that vary due to TMZ sensitivity.

Bar graphs depicting the relative phosphorylation levels of pY peptides identified as varying due TMZ sensitivity. Sites enclosed inside blue lines are increased or decreased in both TMZ^{R3} backgrounds compared to parental lines, orange lines enclose sites that

vary in p53kd-TMZR3 cells and purple lines enclose sites that vary in Control-TMZ^{R3} cells.

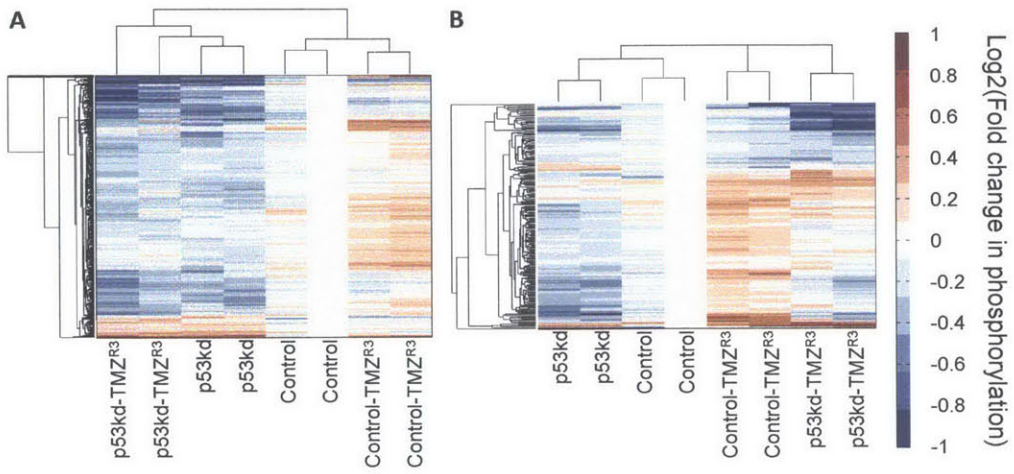

Figure 4.7 Hierarchical clustering of pS/T containing peptides identified as varying by p53 status or TMZ sensitivity.

(A) Hierarchical clustering of pS/T containing peptides identified as varying by p53 status.

(B) Hierarchical clustering of pS/T containing peptides identified as varying by TMZ sensitivity.

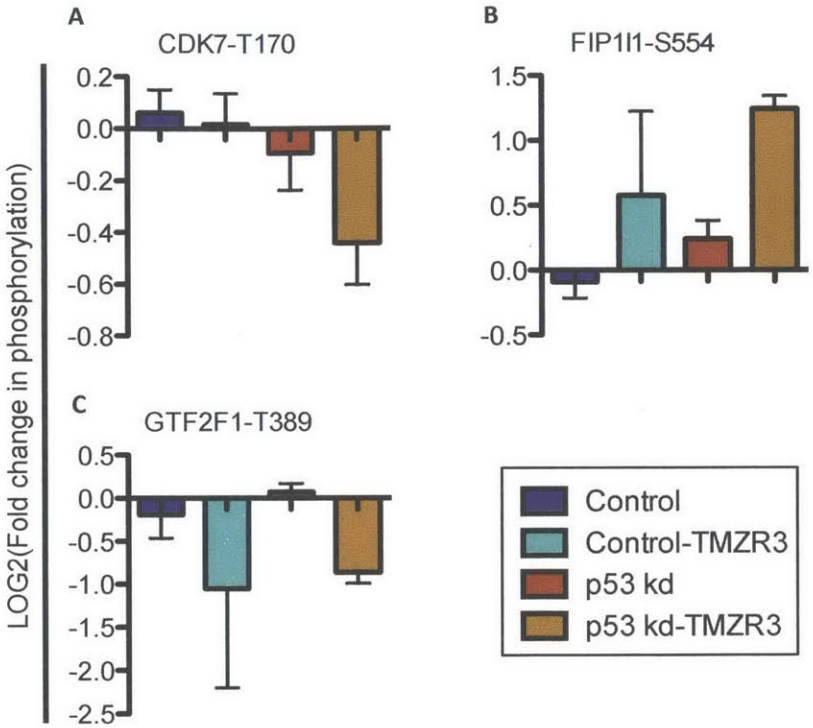

Figure 4.8 Select pS/T containing sites that vary due to p53 status or TMZ sensitivity.

(A) Phosphorylated CDK7-T170 levels in parental and TMZ^{R3} GBM cells.

(B) Phosphorylated FIP1L1-S554 levels in parental and TMZ^{R3} GBM cells.

(C) Phosphorylated GTF2F1-T389 levels in parental and TMZ^{R3} GBM cells.

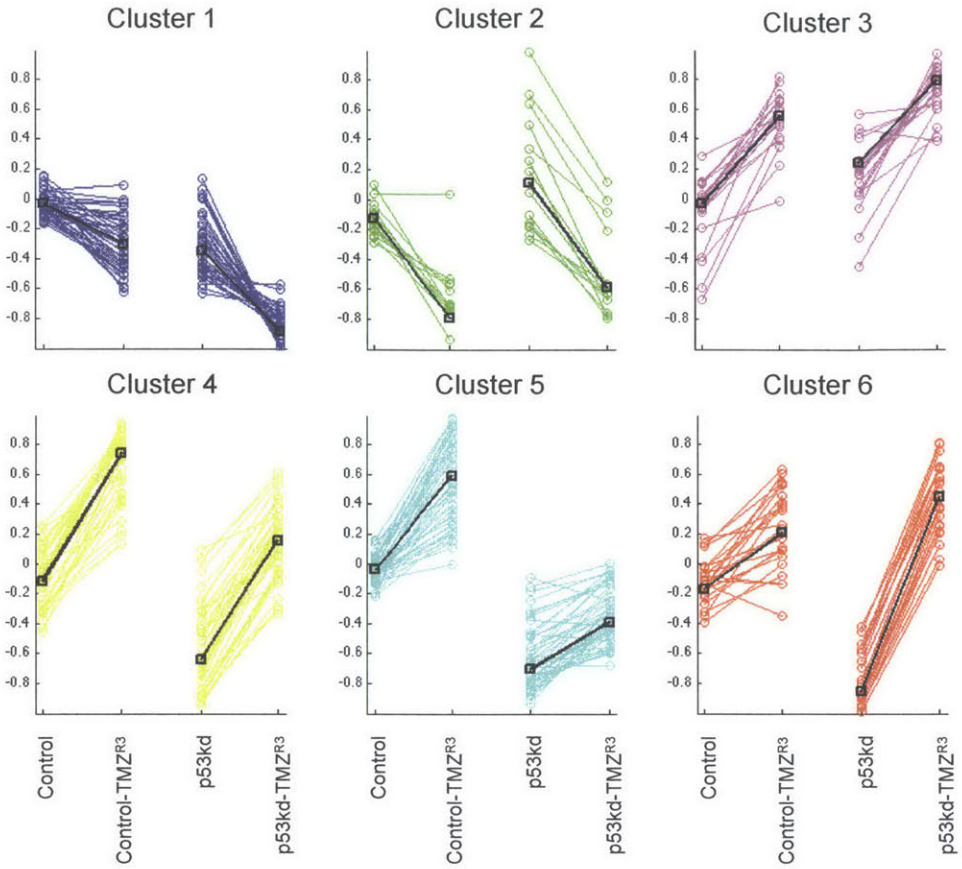

Figure 4.9 K-means clustering of pS/T sites that vary due to TMZ sensitivity.

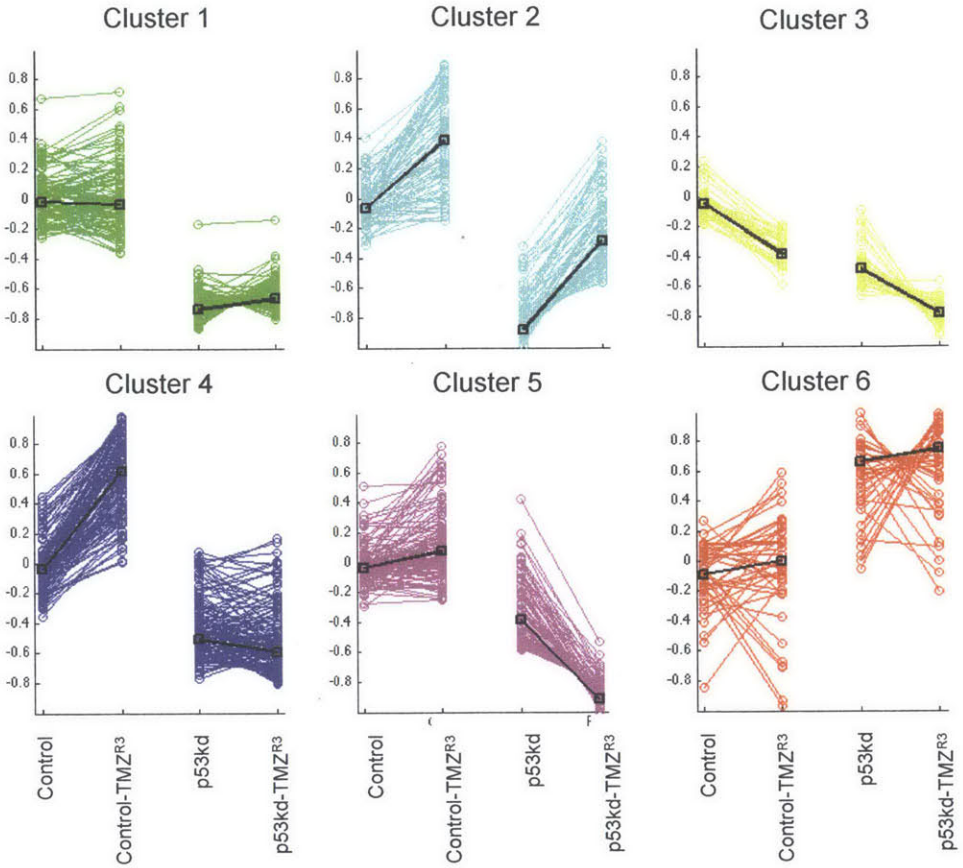

Figure 4.10 K-means clustering of pS/T sites that vary due to p53 status.

Kinase	Substrates/ Input	Substrates/ Database	Fraction/ Input	Fraction/ Database	p-Value
CDK2	21	398	0.368421053	0.100176189	8.49E-08
GSK3B	23	501	0.403508772	0.126101183	1.90E-07
RPS6KA3	13	330	0.228070175	0.083060659	7.58E-04
CDC2	15	421	0.263157895	0.105965266	7.69E-04
MAPK14	14	377	0.245614035	0.094890511	8.09E-04
PRKCB1	11	254	0.192982456	0.063931538	9.84E-04
MAPK10	7	109	0.122807018	0.027435188	0.001096496
SGK	5	65	0.087719298	0.016360433	0.002845423
CSNK1E	7	134	0.122807018	0.033727662	0.003379267
AKT1	7	176	0.122807018	0.044299018	0.01371171
GSK3A	3	33	0.052631579	0.008306066	0.013766846
MAPK8	8	234	0.140350877	0.058897559	0.019252704
SGK3	2	14	0.035087719	0.003523786	0.020772814
FER	2	15	0.035087719	0.003775485	0.023331164
AURKC	1	1	0.01754386	2.52E-04	0.028091252
MAPK13	2	17	0.035087719	0.004278882	0.028811939
NTRK3	2	18	0.035087719	0.004530581	0.03172674
SNRK	1	2	0.01754386	5.03E-04	0.041844677
TRIM33	1	2	0.01754386	5.03E-04	0.041844677

Table 4.1 Results of Kinase Enrichment analysis of proteins containing phosphorylation sites that vary due to TMZ sensitivity.

Motif	Motif Score	Foreground Matches	Foreground Size	Background Matches	Background Size	Fold Increase
....P.sP.....	20.41	26	193	10017	1094911	14.73
...R..s....T.	19.96	10	97	3078	1010576	33.85
.....sP.....	16	70	167	74318	1084894	6.12
.....Rs.S....	14.17	11	87	7105	1007498	17.93
...R..s.....	6.03	17	76	56558	1000393	3.96
.....Rt.....	4.9	10	35	37629	687043	5.22
.....Rs.....	4.52	10	46	39648	884303	4.85
.....s....E.	4.19	13	59	59532	943835	3.49

Table 4.2 Sequence motifs enriched in phosphorylation sites that vary significantly due to TMZ sensitivity.

Motif	Motif Score	Foreground Matches	Foreground Size	Background Matches	Background Size	Fold Increase
.....sDEE...	39.43	23	719	575	1000433	55.66
.....Rs.S....	32	64	696	6710	999858	13.7
.....Rt.S....	32	46	304	3781	682830	27.33
...RR.s.....	29.81	61	830	5073	1010576	14.64
....P.sP.....	28.85	173	1659	10017	1094911	11.4
.R.R..s.....	27.54	50	769	5070	1005503	12.89
.....s..E.E.	26.7	40	632	6212	993148	10.12
...R..sP.....	26.63	90	1486	4813	1084894	13.65
.....tPP....	26.2	34	338	4213	687043	16.4
.....sP.K...	24.55	52	1324	2762	1075788	15.3
.....sP...R.	24.13	72	1396	4293	1080081	12.98
...R..s.D....	22.58	20	592	2161	986936	15.43
.....sSP....	19.12	27	275	8168	802018	9.64
.....s.SP...	16.01	20	205	7075	747795	10.31
.....sP.....	16	442	1272	62450	1073026	5.97
...R..s.....	16	100	572	47434	984775	3.63
.....Rs.....	16	77	472	41988	937341	3.64
.....tP.....	16	76	258	44073	679049	4.54
.....s..E...	14.27	62	337	51519	853537	3.05
.....Ks.....	13.72	58	395	41816	895353	3.14
.....Rt.....	13.46	38	182	31125	634976	4.26
.....Kt.....	12.84	36	144	35962	603851	4.2
.....s.E....	9.84	43	248	46055	793850	2.99
.....t.P....	9.54	28	108	37532	567889	3.92
.....s.D....	7.37	29	185	36637	740720	3.17
....S.s.....	6.77	40	156	76331	704083	2.37
.....s..S...	5.84	32	116	71557	627752	2.42
.....t.S....	5.28	22	80	51556	530357	2.83

Table 4.3 Sequence motifs enriched in all pS/T containing phosphopeptides sites identified in this study prior to ANOVA filtering.

	Motif	Motif Score	Foreground Matches	Foreground Size	Background Matches	Background Size	Fold Increase
Cluster 1	....P.sP.....	14.96	10	49	10017	1094911	22.31
	.....sP.....	4.37	11	39	74318	1084894	4.12
	...R..s.....	4.6	9	28	60857	1010576	5.34
Cluster 2	.....sP.....	5.95	8	13	84335	1094911	7.99
Cluster 3	...R..s.....	5.76	7	12	60857	1010576	9.69
	.....sP.....	5.7	10	22	84335	1094911	5.9
Cluster 4	.....sP.....	16	25	39	84335	1094911	8.32
Cluster 5	.....sP.....	13.81	25	53	84335	1094911	6.12
	...R..s.....	4.6	9	28	60857	1010576	5.34
Cluster 6	.....sP.....	4.92	9	21	84335	1094911	5.56

Table 4.4 Sequence motifs enriched in k-means clusters of phosphorylation sites that vary significantly due to TMZ sensitivity.

	Motif	Motif Score	Foreground Matches	Foreground Size	Background Matches	Background Size	Fold Increase
Cluster 1	.....sP.....	16	47	102	84335	1094911	5.98
	...R..s.....	7.03	16	55	60857	1010576	4.83
	.....tP.....	4.63	8	19	48630	687043	5.95
Cluster 2	.....sP.....	16	43	89	84335	1094911	6.27
	...R..s.....	4.89	12	46	60857	1010576	4.33
	.....Rs.....	4.44	9	34	48159	949719	5.22
Cluster 3	.....sP.....	7.44	16	42	84335	1094911	4.95
	.....s.S....	4.4	11	26	109584	1010576	3.9
Cluster 4	.....sP..K..	20.42	12	138	3652	1094911	26.07
	.....sP.....	16	57	126	80683	1091259	6.12
	.....Rs.....	11.37	22	69	53447	1010576	6.03
	.....Rt.....	7.14	9	17	37629	687043	9.67
	...R..s.....	5.74	13	47	55569	957129	4.76
	.....Ks.....	5.64	10	34	42112	901560	6.3
Cluster 5	.....sP.....	16	49	97	84335	1094911	6.56
	.....Rt.S....	12.17	6	12	3437	638413	92.87
	...R..s.....	7.98	16	48	60857	1010576	5.54
	.....tP.....	6.87	11	23	48630	687043	6.76
Cluster 6	.....sP.....	8.88	18	44	84335	1094911	5.31
	...R..s.....	8.01	12	26	60857	1010576	7.66
	.....s..E...	4.84	7	14	64124	949719	7.41

Table 4.5 Sequence motifs enriched in k-means clusters of phosphorylation sites that vary significantly due to p53 status.

References

Alessi, D. R., Caudwell, F. B., Andjelkovic, M., Hemmings, B. A., and Cohen, P. (1996). Molecular basis for the substrate specificity of protein kinase B; comparison with MAPKAP kinase-1 and p70 S6 kinase. FEBS letters *399*, 333-338.

Bhaduri, S., and Pryciak, P. M. (2011). Cyclin-specific docking motifs promote phosphorylation of yeast signaling proteins by G1/S Cdk complexes. Current biology : CB *21*, 1615-1623.

Chou, M. F., and Schwartz, D. (2011). Biological sequence motif discovery using motif-x. Current protocols in bioinformatics / editoral board, Andreas D Baxevanis [et al] *Chapter 13*, Unit 13 15-24.

Ciccia, A., and Elledge, S. J. (2010). The DNA damage response: making it safe to play with knives. Molecular cell *40*, 179-204.

Dunn, G. P., Rinne, M. L., Wykosky, J., Genovese, G., Quayle, S. N., Dunn, I. F., Agarwalla, P. K., Chheda, M. G., Campos, B., Wang, A., *et al.* (2012). Emerging insights into the molecular and cellular basis of glioblastoma. Genes & development *26*, 756-784.

Ficarro, S. B., Adelmant, G., Tomar, M. N., Zhang, Y., Cheng, V. J., and Marto, J. A. (2009). Magnetic bead processor for rapid evaluation and optimization of parameters for phosphopeptide enrichment. Analytical chemistry *81*, 4566-4575.

Gan, H. K., Cvrljevic, A. N., and Johns, T. G. (2013). The epidermal growth factor receptor variant III (EGFRvIII): where wild things are altered. The FEBS journal *280*, 5350-5370.

Garrett, S., Barton, W. A., Knights, R., Jin, P., Morgan, D. O., and Fisher, R. P. (2001). Reciprocal activation by cyclin-dependent kinases 2 and 7 is directed by substrate specificity determinants outside the T loop. Molecular and cellular biology *21*, 88-99.

Giancotti, F. G., and Ruoslahti, E. (1999). Integrin signaling. Science *285*, 1028-1032.

Giannakouros, T., Nikolakaki, E., Mylonis, I., and Georgatsou, E. (2011). Serine-arginine protein kinases: a small protein kinase family with a large cellular presence. The FEBS journal *278*, 570-586.

Guo, F., Li, J., Du, W., Zhang, S., O'Connor, M., Thomas, G., Kozma, S., Zingarelli, B., Pang, Q., and Zheng, Y. (2013). mTOR regulates DNA damage response through NF-kappaB-mediated FANCD2 pathway in hematopoietic cells. Leukemia *27*, 2040-2046.

Hirose, Y., Berger, M. S., and Pieper, R. O. (2001). Abrogation of the Chk1-mediated G(2) checkpoint pathway potentiates temozolomide-induced toxicity in a p53-independent manner in human glioblastoma cells. Cancer research *61*, 5843-5849.

Hirose, Y., Katayama, M., Mirzoeva, O. K., Berger, M. S., and Pieper, R. O. (2005). Akt activation suppresses Chk2-mediated, methylating agent-induced G2 arrest and protects from temozolomide-induced mitotic catastrophe and cellular senescence. Cancer research *65*, 4861-4869.

Hirose, Y., Katayama, M., Stokoe, D., Haas-Kogan, D. A., Berger, M. S., and Pieper, R. O. (2003). The p38 mitogen-activated protein kinase pathway links the DNA mismatch repair system to the G2 checkpoint and to resistance to chemotherapeutic DNA-methylating agents. Molecular and cellular biology *23*, 8306-8315.

Hochegger, H., Takeda, S., and Hunt, T. (2008). Cyclin-dependent kinases and cell-cycle transitions: does one fit all? Nature reviews Molecular cell biology *9*, 910-916.

Huang, P. H., Mukasa, A., Bonavia, R., Flynn, R. A., Brewer, Z. E., Cavenee, W. K., Furnari, F. B., and White, F. M. (2007). Quantitative analysis of EGFRvIII cellular signaling networks reveals a combinatorial therapeutic strategy for glioblastoma.

Proceedings of the National Academy of Sciences of the United States of America *104*, 12867-12872.

Janouskova, H., Maglott, A., Leger, D. Y., Bossert, C., Noulet, F., Guerin, E., Guenot, D., Pinel, S., Chastagner, P., Plenat, F., *et al.* (2012). Integrin alpha5beta1 plays a critical role in resistance to temozolomide by interfering with the p53 pathway in high-grade glioma. Cancer research *72*, 3463-3470.

Johnson, H., Del Rosario, A. M., Bryson, B. D., Schroeder, M. A., Sarkaria, J. N., and White, F. M. (2012). Molecular characterization of EGFR and EGFRvIII signaling networks in human glioblastoma tumor xenografts. Molecular & cellular proteomics : MCP *11*, 1724-1740.

Kashishian, A., Kazlauskas, A., and Cooper, J. A. (1992). Phosphorylation sites in the PDGF receptor with different specificities for binding GAP and PI3 kinase in vivo. The EMBO journal *11*, 1373-1382.

Kazlauskas, A., and Cooper, J. A. (1989). Autophosphorylation of the PDGF receptor in the kinase insert region regulates interactions with cell proteins. Cell *58*, 1121-1133.

Koul, D. (2008). PTEN signaling pathways in glioblastoma. Cancer biology & therapy *7*, 1321-1325.

Lachmann, A., and Ma'ayan, A. (2009). KEA: kinase enrichment analysis. Bioinformatics *25*, 684-686.

Lee, E. R., Kim, J. Y., Kang, Y. J., Ahn, J. Y., Kim, J. H., Kim, B. W., Choi, H. Y., Jeong, M. Y., and Cho, S. G. (2006). Interplay between PI3K/Akt and MAPK signaling pathways in DNA-damaging drug-induced apoptosis. Biochimica et biophysica acta *1763*, 958-968.

Manning, B. D., and Cantley, L. C. (2007). AKT/PKB signaling: navigating downstream. Cell *129*, 1261-1274.

McEllin, B., Camacho, C. V., Mukherjee, B., Hahm, B., Tomimatsu, N., Bachoo, R. M., and Burma, S. (2010). PTEN loss compromises homologous recombination repair in astrocytes: implications for glioblastoma therapy with temozolomide or poly(ADP-ribose) polymerase inhibitors. Cancer research *70*, 5457-5464.

Mukherjee, B., McEllin, B., Camacho, C. V., Tomimatsu, N., Sirasanagandala, S., Nannepaga, S., Hatanpaa, K. J., Mickey, B., Madden, C., Maher, E., *et al.* (2009). EGFRvIII and DNA double-strand break repair: a molecular mechanism for radioresistance in glioblastoma. Cancer research *69*, 4252-4259.

Nakada, M., Nambu, E., Furuyama, N., Yoshida, Y., Takino, T., Hayashi, Y., Sato, H., Sai, Y., Tsuji, T., Miyamoto, K. I., *et al.* (2013). Integrin alpha3 is overexpressed in glioma stem-like cells and promotes invasion. British journal of cancer *108*, 2516-2524.

Nazarenko, I., Hede, S. M., He, X., Hedren, A., Thompson, J., Lindstrom, M. S., and Nister, M. (2012). PDGF and PDGF receptors in glioma. Upsala journal of medical sciences *117*, 99-112.

Nikitin, P. A., Price, A. M., McFadden, K., Yan, C. M., and Luftig, M. A. (2014). Mitogen-induced B-cell proliferation activates chk2-dependent g1/s cell cycle arrest. PloS one *9*, e87299.

Ohba, S., Hirose, Y., Kawase, T., and Sano, H. (2009). Inhibition of c-Jun N-terminal kinase enhances temozolomide-induced cytotoxicity in human glioma cells. Journal of neuro-oncology *95*, 307-316.

Pardanani, A., Ketterling, R. P., Brockman, S. R., Flynn, H. C., Paternoster, S. F., Shearer, B. M., Reeder, T. L., Li, C. Y., Cross, N. C., Cools, J., *et al.* (2003). CHIC2 deletion, a surrogate for FIP1L1-PDGFRA fusion, occurs in systemic mastocytosis associated with eosinophilia and predicts response to imatinib mesylate therapy. Blood *102*, 3093-3096.

Pearson, R. B., and Kemp, B. E. (1991). Protein kinase phosphorylation site sequences and consensus specificity motifs: tabulations. Methods in enzymology *200*, 62-81.

Phillips, H. S., Kharbanda, S., Chen, R., Forrest, W. F., Soriano, R. H., Wu, T. D., Misra, A., Nigro, J. M., Colman, H., Soroceanu, L., *et al.* (2006). Molecular subclasses of high-grade glioma predict prognosis, delineate a pattern of disease progression, and resemble stages in neurogenesis. Cancer cell *9*, 157-173.

Prasad, J., Colwill, K., Pawson, T., and Manley, J. L. (1999). The protein kinase Clk/Sty directly modulates SR protein activity: both hyper- and hypophosphorylation inhibit splicing. Molecular and cellular biology *19*, 6991-7000.

Roskoski, R., Jr. (2012). ERK1/2 MAP kinases: structure, function, and regulation. Pharmacological research : the official journal of the Italian Pharmacological Society *66*, 105-143.

Rossignol, M., Keriel, A., Staub, A., and Egly, J. M. (1999). Kinase activity and phosphorylation of the largest subunit of TFIIF transcription factor. The Journal of biological chemistry *274*, 22387-22392.

Roux, P. P., and Blenis, J. (2004). ERK and p38 MAPK-activated protein kinases: a family of protein kinases with diverse biological functions. Microbiology and molecular biology reviews : MMBR *68*, 320-344.

Schulman, B. A., Lindstrom, D. L., and Harlow, E. (1998). Substrate recruitment to cyclin-dependent kinase 2 by a multipurpose docking site on cyclin A. Proceedings of the National Academy of Sciences of the United States of America *95*, 10453-10458.

Schwartz, D., and Gygi, S. P. (2005). An iterative statistical approach to the identification of protein phosphorylation motifs from large-scale data sets. Nature biotechnology *23*, 1391-1398.

Sheridan, D. L., Kong, Y., Parker, S. A., Dalby, K. N., and Turk, B. E. (2008). Substrate discrimination among mitogen-activated protein kinases through distinct docking sequence motifs. The Journal of biological chemistry *283*, 19511-19520.

Sirbu, B. M., and Cortez, D. (2013). DNA damage response: three levels of DNA repair regulation. Cold Spring Harbor perspectives in biology *5*, a012724.

Songyang, Z., Lu, K. P., Kwon, Y. T., Tsai, L. H., Filhol, O., Cochet, C., Brickey, D. A., Soderling, T. R., Bartleson, C., Graves, D. J., *et al.* (1996). A structural basis for substrate specificities of protein Ser/Thr kinases: primary sequence preference of casein kinases I and II, NIMA, phosphorylase kinase, calmodulin-dependent kinase II, CDK5, and Erk1. Molecular and cellular biology *16*, 6486-6493.

Veevers-Lowe, J., Ball, S. G., Shuttleworth, A., and Kielty, C. M. (2011). Mesenchymal stem cell migration is regulated by fibronectin through alpha5beta1-integrin-mediated activation of PDGFR-beta and potentiation of growth factor signals. Journal of cell science *124*, 1288-1300.

Verhaak, R. G., Hoadley, K. A., Purdom, E., Wang, V., Qi, Y., Wilkerson, M. D., Miller, C. R., Ding, L., Golub, T., Mesirov, J. P., *et al.* (2010). Integrated genomic analysis identifies clinically relevant subtypes of glioblastoma characterized by abnormalities in PDGFRA, IDH1, EGFR, and NF1. Cancer cell *17*, 98-110.

Walz, C., Score, J., Mix, J., Cilloni, D., Roche-Lestienne, C., Yeh, R. F., Wiemels, J. L., Ottaviani, E., Erben, P., Hochhaus, A., *et al.* (2009). The molecular anatomy of the FIP1L1-PDGFRA fusion gene. Leukemia *23*, 271-278.

Wrighton, K. H., Lin, X., and Feng, X. H. (2009). Phospho-control of TGF-beta superfamily signaling. Cell research *19*, 8-20.

Chapter V: Discussion

Chapter V: Discussion

Key concepts and conclusions

In the presented study, we begin by investigating changes that accompany acquired TMZ resistance of GBM cells *in vitro*. Resistant cells were generated by periodic exposure of GBM cells to increased doses of TMZ in a manner that emulates patient treatment. Candidate based screening of factors involved in the processing of TMZ-induced O^6-meG lesions demonstrated that minor decreases in the MMR components, MSH6 and MSH2 protein levels, correlate with moderate decreases in MMR activity and large increases in TMZ resistance in our *in vitro* model. Functional analysis of the effects of decreased MSH6 and MSH2 protein levels confirmed minor decreases in MSH2 as a potent inducer of TMZ resistance both *in vitro* and in a GBM mouse model *in vivo*. Moreover, we demonstrate that low *MSH2* transcript levels correlate with decreased overall survival in a population of TMZ treated GBM patients, an outcome that would be expected if tumors were less responsive to TMZ therapy. In addition, phosphoproteomic profiling of TMZ sensitive and resistant GBM cells was employed to identify alterations in the cellular signaling network that accompany TMZ resistance. Mathematical and computational approaches identified numerous phosphorylation sites that differ based on TMZ sensitivity. We identified changes in phosphorylation at sites that suggest increased PDGFR and/or integrin signaling in TMZ resistant GBM cells. Further, motif analysis of pS and pT containing peptides showed that a majority of the changes contain signatures for possible deregulation of kinases from the CDK/MAPK family.

Increased MGMT activity is not selected for in TMZ^{R3} GBM cells

The MGMT protein is able to efficiently repair O^6-meG lesions by transferring the methyl group from the O^6 position of guanine to a cysteine residue in its active site. Methylation of MGMT subsequently leads to its ubiquitination and proteosomal-mediated degradation (Kaina et al., 2007). *MGMT* promoter methylation remains the most widely used prognostic indicator for the response of GBM patients to TMZ. Robust methylation of the *MGMT* promoter correlates strongly with increased survival of GBM patients following standard therapy with concurrent radiation and TMZ exposure (Hegi et al., 2005). Interestingly, methylation of the *MGMT* promoter was also correlated with increased survival of GBM patients treated with radiotherapy alone (Hegi et al., 2005). As methylation of *MGMT* is likely reflective of the global epigenetic profile of a tumor it is possible that methylation of the *MGMT* promoter also correlates with an epigenetic state more susceptible to therapy-induced regression. U87MG GBM cells do not express MGMT due to promoter methylation of the *MGMT* locus (Lorente et al., 2008). In our *in vitro* model of acquired resistance, repeated TMZ exposure did not lead to increased expression of MGMT or MGMT activity in TMZ^{R3} GBM cells. Therefore, increased MGMT activity is not a factor in the TMZ resistant phenotype of these cells. This result is consistent with a recent study, the largest to date, comparing changes in *MGMT* methylation status in matched primary and recurrent GBM tumors, which found that methylation status rarely changed at tumor recurrence (Felsberg et al., 2011). Taken together, these results indicate that while MGMT is a potent predictor of response of GBM tumors to initial TMZ treatment there does not appear to be a strong selective pressure to increase MGMT levels in response to repeated TMZ exposure.

Minor decreases in MMR components alter the sensitivity of GBM to TMZ

Compared to their parental counterparts, TMZ^{R3} GBM cells display minor decreases in the protein levels of the MMR MutSα recognition complex components, MSH6 (50% decreased) and MSH2 (25% decreased). This decrease correlates to decreased MMR activity against a single base pair mismatch, a MutSα substrate. TMZ^{R3} GBM cells display tremendous resistance to TMZ exposure compared to their parental counterparts, therefore it seemed unlikely that these moderate MMR decreases could result in a large shift in the sensitivity of GBM cells to TMZ. However, these results were consistent with recent analysis of MMR protein levels between matched primary and recurrent GBM tumors where decreases in at least one MMR component was a frequent event at tumor recurrence (Felsberg et al., 2011). To investigate the dependence between MSH6, MSH2 levels and TMZ sensitivity we generated a library of GBM cell lines with a gradation of MSH6 and MSH2 knockdown. The sensitivity of MSH6 knockdown cells revealed a bimodal response with GBM cells transitioning from a sensitive to resistant phenotype when MSH6 levels dropped below 50%. In contrast, as little as 20% MSH2 knockdown led to a decrease in the sensitivity of GBM cells to TMZ. Further, decreased MMR activity was observed in MSH6 and MSH2 knockdowns that display resistance to TMZ, suggesting that moderate decreases in MMR components have an immediate effect on MMR activity and, presumably, the ability of GBM cells to process O^6-meG:T mismatches into toxic strand breaks. MMR deficiency has classically been defined by identifying microsatellite instability or a somatic hypermutator phenotype, markers that report on complete MMR deficiency (Li, 2008). Recent work has demonstrated that MSH2 and MLH1 knockdown did not lead to instability of microsatellites in human colorectal cancer cells suggesting that even a marginal level of functional MMR is able to maintain genomic integrity (Barber, 2012). However, in this study, knockdown was able to induce resistance to 5-fluorouracil suggesting there are

different thresholds for maintaining genomic stability and MMR dependent drug toxicity (Barber, 2012). MMR is though to travel with the replication fork, possibly by its association with proliferating cell nuclear antigen (PCNA), to increase fidelity during replication by repairing mismatches produced by the replicative DNA polymerases (Edelbrock et al., 2013; Jiricny, 2006). Recent studies have shown that noncanonical MMR, MMR activity that is not strand directed or replication coupled, can occur outside of S phase in response to MNNG, an O^6-meG producing alkylating agent (Pena-Diaz et al., 2012). Therefore, the MMR thresholds for replication coupled repair versus MMR-mediated toxicity to specific agents may be different for replication dependent and independent MMR.

In our MSH6 and MSH2 knockdowns, TMZ resistance is only seen at MSH6 knockdown levels where MSH2 protein levels are also decreased, whereas any level of MSH2 knockdown leads to decreases in MSH6 protein levels. Therefore, it appears that the different behaviors observed between MSH6 and MSH2 levels and sensitivity to TMZ are due to knockdown levels at which stabilization of the MutSα dimerization partner is affected. It is unlikely that these differences are due to the stoichiometry of MSH proteins in the U87MG GBM cells, from which the knockdown cells are generated, as *MSH2* transcript levels correlate more strongly than *MSH6* transcript levels to the overall survival in TMZ treated GBM patients. The MutSα and MutSβ recognition complexes are heterodimers, both of which contain MSH2 in complex with MSH6 and MSH3, respectively. The MutSα heterodimer is solely responsible for recognizing single base pair mismatches such as those produced due to the presence of O^6-meG lesions in DNA (Jiricny, 2006; Li, 2008). As previously stated, the strength of the association between MSH2 and MSH6 as well as between MSH2 and MSH3 has not been explored. One could imagine that conditions that favor MutSβ formation would lead to a depletion of MutSα upon even minor losses of MSH2. In the future, a simple kinetic model may be

used to describe how the stoichiometry of MSH2, MSH3 and MSH6 determines the proportion of MutSα and MutSβ. In combination with the sensitivity measurements of cells with various MSH levels, the relative amounts of these proteins can be used to predict the sensitivity of cells to TMZ. Further, the finding that *MSH2* transcript levels are predictive for patient survival in TMZ treated GBM patients demonstrates that MMR activity can be used as a prognostic indicator for patient response to TMZ treatment. To build a model for clinical application, an approach could take into account the relative *MSH2*, *MSH3* and *MSH6* transcript levels obtained from tumor biopsies/resection to predict whether a patient is likely or unlikely to benefit from TMZ treatment.

Exploring the role of additional DNA repair and damage tolerance pathways on the resistant phenotype of TMZ^{R3} GBM cells

Base and nucleotide excision repair pathways. There are other DNA repair pathways capable of responding to the damage induced by alkylating agents. As mentioned previously, the base excision repair (BER) pathway is capable of repairing the cytotoxic and mutagenic N3-meA adducts induced by TMZ treatment (Fu et al., 2012). Previous studies have demonstrated a correlation between AAG (also known as MPG), the glycosylase that initiates repair of N3-meA, and response to TMZ. GBM cells have been shown to be equally resistant to TMZ when expressing either high AAG or MGMT suggesting both O^6-meG and N3-meA lesions are highly toxic when unrepaired. Further, it was shown that AAG levels predictive for overall survival in GBM patients (Agnihotri et al., 2012). To the best of our knowledge, no studies have investigated changes in AAG expression or activity between primary and recurrent GBM. Our *in vitro* system of acquired TMZ resistance allows us to begin to address whether a selective pressure exits for increased AAG activity after repeated TMZ exposure. Additionally, *in vitro* and *in*

vivo experiments have shown that O^6-meG lesions can be substrates for the nucleotide excision repair pathway (Huang et al., 1994; Samson et al., 1988). However, the efficiency of repair is likely low in *in vivo*, as O^6-meG lesions appear mostly unrepaired in the absence of MGMT (Huang et al., 1994). Quantification of O^6-meG levels in parental and TMZ^{R3} GBM cells revealed that O^6-meG adduct levels were equivalent after TMZ treatment therefore it appears unlikely that NER activity is altered specifically to cope with O^6-meG lesions yet may have a role in repairing N7-meG induced abasic sites or other NER substrates that may arise from TMZ treatment.

Double strand break repair. In MGMT deficient cells, where O^6-meG lesions persist, TMZ induces double strand break formation due to replication fork collapse mediated by MMR induced single strand gaps formed at O^6-meG:T mispairs (Mojas et al., 2007). The repair of these double strand breaks can occur through error free or error prone pathways, namely homologous recombination (HR) and non-homologous end-joining (NHEJ), respectively (Jackson, 2002). Studies investigating the effects of aberrant double strand break damage signaling on TMZ sensitivity have had conflicting results. Deficiencies in meiotic recombination 11 (MRE11) and Nijmegen breakage syndrome 1 protein (NBS1), both components of the Mre11-Rad50-Nbs1 (MRN) DSB signaling complex, have been found to lead to resistance and sensitization, respectively, of cells following TMZ exposure (Eich et al., 2010; Mirzoeva et al., 2006). The MRN complex is shared by HR and NHEJ to sense and direct repair of DSB ends (Lamarche et al., 2010). Therefore these results may reflect the preferred pathway downstream of MRN complex activation. In our *in vitro* model of acquired TMZ resistance, TMZ^{R3} did not display a significant difference in sensitivity to double strand break induction by ionizing radiation. However, a shift in HR to NHEJ or vice versa for DSB processing may alter the response to alkylating agent induced DSBs but not those induced by IR. Using flow cytometry HCR approaches developed in our laboratory, we are in a position to investigate whether

changes in AAG, NER, HR and NHEJ activity are altered in GBM cells in response after repeated TMZ exposure.

Translesion bypass of O^6-meG lesions. The absence of both MMR and MGMT activity leads to the accumulation of O^6-meG lesions in the genome. Upon replication, these lesions are highly mutagenic giving rise to G:C to A:T transversions (Fu et al., 2012). Loss of the translesion synthesis (TLS) pathway polymerases pol ζ and pol κ has been demonstrated to increase the sensitivity of cells to O^6-meG producing S_N1 alkylating agents (Roos et al., 2009; Takenaka et al., 2006). *In vitro*, TLS polymerase η and κ have been shown to be as likely to incorporate C or T opposite O^6-meG while polymerase ι has a strong preference for T incorporation (Choi et al., 2006). Therefore, TLS polymerases do not decrease the rate of transitions *in vivo* but are a tolerance mechanism as a response to stalling of replicative polymerases at O^6-meG lesions. Targeting of TLS polymerases may be a way to sensitize MMR and MGMT deficient GBM cells to TMZ by inhibiting the efficiency of O^6-meG lesion bypass.

Systems level profiling of TMZ sensitive and resistant GBM cells

Through candidate-based approaches, we identified minor decreases in MMR components as a factor in the acquired resistance of GBM cells to TMZ. However, the selection process undergone by TMZ^{R3} cells was likely to alter a wide variety of cellular processes to help cells cope with repeated injury and/or help maintain genomic integrity as well as to mitigate the effect of changes that alter response to drug exposure. In addition to the possible changes at the DNA repair level described earlier, alterations likely took place to increase the ability of cells to arrest, allowing time for damage repair, to allow them to ignore damage induced death signals, and ultimately to resume proliferation after repeated genomic insult. To investigate the effects of repeated TMZ

exposure on the global cellular signaling network we performed phosphoproteomic profiling of parental and TMZ^{R3} GBM cells. ANOVA analysis of the phosphoproteomic network revealed numerous changes upon acquisition of TMZ resistance. Of note was the observation that p53 deficiency leads to wide scale changes in the phosphoproteome even before going through TMZ selection. In the absence of DNA damage, p53 protein levels are low due to a negative feedback loop mediated by the E3-ubiquitin ligase mouse double minute 2 homolog (MDM2), a p53 transcriptional target that ubiquitinates p53 making it a substrate for proteosomal degradation (Chene, 2003). Upon damage induction, phosphorylation of p53 by the DNA damage sensing kinases (ATM, ATR or DNA-PK) or effectors of the DNA damage response (CHK1 or CHK2) disrupts association with MDM2 leading to a robust increase in p53 protein levels and activation of its transcriptional program (Sengupta and Harris, 2005; Shieh et al., 1997). The importance of p53 as a central node is evident by the observation that p53 loss leads to numerous changes in the phosphoproteome even in the absence of p53 activating stimuli. However, these changes do not appear to alter the sensitivity of cells to acute TMZ exposure or their ability to acquire TMZ resistance after repeated TMZ exposure.

Analysis of pY sites altered upon the acquisition of TMZ resistance revealed phosphorylation sites that are consistently increased or decreased in both TMZ resistant cell lines (+/- p53) compared to parental. These sites could therefore constitute signatures for molecular alterations that display strong selective pressure upon repeated TMZ exposure. Of particular interest is the identification of increased phosphorylation of PDGFRα on Y742. As previously described, increased PDGFR activity is a hallmark of proneural GBM, a GBM tumor subtype that does not display significant therapy induced tumor regression. The analogous residue on PDGFRβ, Y751, has been shown to be autophosphorylated in response to ligand binding (Kashishian et al., 1992; Kazlauskas

and Cooper, 1989). Moreover, phosphorylation at this site has been shown to reveal a docking motif for the p85 regulatory subunit of PI-3K, the activator of the AKT pathway (Kashishian et al., 1992; Kazlauskas and Cooper, 1990), therefore this site may be informative for increased PDGFR and AKT activity in response to chronic TMZ treatment. Phosphorylation at the C-terminal residue (Y1051) of integrin α3 was also increased in TMZ^{R3} GBM cells. Although this site is not characterized, integrins specifically are of interest as increased integrin signaling has been demonstrated to increase survival of TMZ exposed GBM cells (Janouskova et al., 2012). Interestingly, increased FAK1 activity, a tyrosine kinase activated by integrin ligand binding, has been shown to result in PDGF independent phosphorylation of Y751 on PDGFRβ suggesting a link between integrin signaling and PDGFR activation (Veevers-Lowe et al., 2011). Currently, we are exploring the effects of PDGFR activation and inhibition on the sensitivity of GBM cells to TMZ. Further, we will extend this study to investigate the effects of integrin/FAK1 signaling on TMZ sensitivity as well as the effects from targeting these pathways simultaneously.

For analysis of pS/T phosphorylation, we employed k-means clustering and motif analysis with the aim of identifying kinases responsible for the changes in phosphorylation after acquired TMZ resistance. This approach identified clusters with various behaviors with sites increased or decreased consistently in both TMZ resistant lines (cluster 1-4) and clusters where differences were prominent in one of the two TMZ^{R3} GBM cells (cluster 5 and 6) (Figure 4.11). The abundance of PX(S)P and (S)P motifs, associated with CDK/MAPK substrates (Songyang et al., 1996), in all clusters, regardless of dynamics, highlights the central role of the CDK/MAPK kinase family in cell growth, proliferation and response to stimuli. Both control-TMZ^{R3} and p53kd-TMZ^{R3} GBM cells display decreased proliferation in comparison to their parental counterparts. p53kd-TMZ^{R3}, which display the largest decrease in proliferation rate, displayed decreased

phosphorylation of the pro-growth and survival kinases ERK1 and ERK2 on residues that, when phosphorylated, lead to increased kinase activity (Roskoski, 2012). Further, we identified decreased phosphorylation of T170 on CDK7, a subunit of the CDK activation complex (CAK), in p53kd-TMZ^{R3} cells. As with the ERK sites identified, phosphorylation at T170 increases CAK kinase activity (Garrett et al., 2001). Taken together, it appears that CDK/MAPK signals that alter cell cycle progression are decreased in p53kd-TMZ^{R3} GBM cells and opens the possibility that similar mechanisms are at play in control-TMZ^{R3} cells. This decreased proliferation rate may be necessary for cells to repair damage induced by TMZ as well as increased damage from loss of factors that ensure genomic integrity, such as decreased MMR activity. By increasing ERK and CDK activity, we can explore whether this decreased proliferation is necessary for stability of TMZ^{R3} GBM cells. Similarly, inhibition of ERK and CDK activity during repeated TMZ exposure of TMZ sensitive cells can assess whether decreased cell cycle progression increases survival of GBM cells after repeated TMZ injury. It should be noted, however, that studies looking at the effect of ERK activation and inhibition on the survival of GBM cells expressing a constitutive version of EGFR found that both treatments can lead to decreased viability of GBM cells (Huang et al., 2010). Therefore, it may be possible that GBM cells undergo selective pressure to obtain the correct balance of pro-growth signals necessary for optimal cellular survival.

The goal of this study is to identify treatments options for GBM patients with recurrent tumors whose options as of now remain bleak and largely untested for efficacy. Based on chapter 2 and 3 of the presented work, we propose that BCNU treatment is a viable alternative for a subset of recurrent GBM patients after failed TMZ therapy. Recent work has shown that a portion of patients with recurrent disease do benefit from this treatment and we propose that this therapy will be specially beneficial for MGMT deficient TMZ resistant tumors where decreased MMR is the most likely mechanism of

chemoresistance. With our unbiased screening outlined in chapter 4, we aim to identify molecular changes that accompany TMZ resistance to target nodes necessary for cellular maintenance and viability in resistant cells. Moreover, we aim to identify cellular components that, when targeted, increase the efficacy of TMZ treatment and decrease the rate of tumor recurrence.

References

Agnihotri, S., Gajadhar, A. S., Ternamian, C., Gorlia, T., Diefes, K. L., Mischel, P. S., Kelly, J., McGown, G., Thorncroft, M., Carlson, B. L., *et al.* (2012). Alkylpurine-DNA-N-glycosylase confers resistance to temozolomide in xenograft models of glioblastoma multiforme and is associated with poor survival in patients. J Clin Invest *122*, 253-266.

Barber, A. (2012) The roles of MLH1 and MSH2 in growth and drug resistance in human colorectal cancer cells, University of Guelph, Ontario, Canada.

Chene, P. (2003). Inhibiting the p53-MDM2 interaction: an important target for cancer therapy. Nature reviews Cancer *3*, 102-109.

Choi, J. Y., Chowdhury, G., Zang, H., Angel, K. C., Vu, C. C., Peterson, L. A., and Guengerich, F. P. (2006). Translesion synthesis across O6-alkylguanine DNA adducts by recombinant human DNA polymerases. The Journal of biological chemistry *281*, 38244-38256.

Edelbrock, M. A., Kaliyaperumal, S., and Williams, K. J. (2013). Structural, molecular and cellular functions of MSH2 and MSH6 during DNA mismatch repair, damage signaling and other noncanonical activities. Mutation research *743-744*, 53-66.

Eich, M., Roos, W. P., Dianov, G. L., Digweed, M., and Kaina, B. (2010). Nijmegen breakage syndrome protein (NBN) causes resistance to methylating anticancer drugs such as temozolomide. Molecular pharmacology *78*, 943-951.

Felsberg, J., Thon, N., Eigenbrod, S., Hentschel, B., Sabel, M. C., Westphal, M., Schackert, G., Kreth, F. W., Pietsch, T., Loffler, M., *et al.* (2011). Promoter methylation and expression of MGMT and the DNA mismatch repair genes MLH1, MSH2, MSH6 and PMS2 in paired primary and recurrent glioblastomas. Int J Cancer *129*, 659-670.

Fu, D., Calvo, J. A., and Samson, L. D. (2012). Balancing repair and tolerance of DNA damage caused by alkylating agents. Nature reviews Cancer *12*, 104-120.

Garrett, S., Barton, W. A., Knights, R., Jin, P., Morgan, D. O., and Fisher, R. P. (2001). Reciprocal activation by cyclin-dependent kinases 2 and 7 is directed by substrate specificity determinants outside the T loop. Molecular and cellular biology *21*, 88-99.

Hegi, M. E., Diserens, A. C., Gorlia, T., Hamou, M. F., de Tribolet, N., Weller, M., Kros, J. M., Hainfellner, J. A., Mason, W., Mariani, L., *et al.* (2005). MGMT gene silencing and benefit from temozolomide in glioblastoma. The New England journal of medicine *352*, 997-1003.

Huang, J. C., Hsu, D. S., Kazantsev, A., and Sancar, A. (1994). Substrate spectrum of human excinuclease: repair of abasic sites, methylated bases, mismatches, and bulky adducts. Proceedings of the National Academy of Sciences of the United States of America *91*, 12213-12217.

Huang, P. H., Miraldi, E. R., Xu, A. M., Kundukulam, V. A., Del Rosario, A. M., Flynn, R. A., Cavenee, W. K., Furnari, F. B., and White, F. M. (2010). Phosphotyrosine signaling analysis of site-specific mutations on EGFRvIII identifies determinants governing glioblastoma cell growth. Molecular bioSystems *6*, 1227-1237.

Jackson, S. P. (2002). Sensing and repairing DNA double-strand breaks. Carcinogenesis *23*, 687-696.

Janouskova, H., Maglott, A., Leger, D. Y., Bossert, C., Noulet, F., Guerin, E., Guenot, D., Pinel, S., Chastagner, P., Plenat, F., *et al.* (2012). Integrin alpha5beta1 plays a critical role in resistance to temozolomide by interfering with the p53 pathway in high-grade glioma. Cancer research *72*, 3463-3470.

Jiricny, J. (2006). The multifaceted mismatch-repair system. Nature reviews Molecular cell biology *7*, 335-346.

Kaina, B., Christmann, M., Naumann, S., and Roos, W. P. (2007). MGMT: key node in the battle against genotoxicity, carcinogenicity and apoptosis induced by alkylating agents. DNA repair *6*, 1079-1099.

Kashishian, A., Kazlauskas, A., and Cooper, J. A. (1992). Phosphorylation sites in the PDGF receptor with different specificities for binding GAP and PI3 kinase in vivo. The EMBO journal *11*, 1373-1382.

Kazlauskas, A., and Cooper, J. A. (1989). Autophosphorylation of the PDGF receptor in the kinase insert region regulates interactions with cell proteins. Cell *58*, 1121-1133.

Kazlauskas, A., and Cooper, J. A. (1990). Phosphorylation of the PDGF receptor beta subunit creates a tight binding site for phosphatidylinositol 3 kinase. The EMBO journal *9*, 3279-3286.

Lamarche, B. J., Orazio, N. I., and Weitzman, M. D. (2010). The MRN complex in double-strand break repair and telomere maintenance. FEBS letters *584*, 3682-3695.

Li, G. M. (2008). Mechanisms and functions of DNA mismatch repair. Cell research *18*, 85-98.

Lorente, A., Mueller, W., Urdangarin, E., Lazcoz, P., von Deimling, A., and Castresana, J. S. (2008). Detection of methylation in promoter sequences by melting curve analysis-based semiquantitative real time PCR. Bmc Cancer *8*.

Mirzoeva, O. K., Kawaguchi, T., and Pieper, R. O. (2006). The Mre11/Rad50/Nbs1 complex interacts with the mismatch repair system and contributes to temozolomide-induced G2 arrest and cytotoxicity. Molecular cancer therapeutics *5*, 2757-2766.

Mojas, N., Lopes, M., and Jiricny, J. (2007). Mismatch repair-dependent processing of methylation damage gives rise to persistent single-stranded gaps in newly replicated DNA. Genes & development *21*, 3342-3355.

Pena-Diaz, J., Bregenhorn, S., Ghodgaonkar, M., Follonier, C., Artola-Boran, M., Castor, D., Lopes, M., Sartori, A. A., and Jiricny, J. (2012). Noncanonical mismatch repair as a source of genomic instability in human cells. Molecular cell *47*, 669-680.

Roos, W. P., Tsaalbi-Shtylik, A., Tsaryk, R., Guvercin, F., de Wind, N., and Kaina, B. (2009). The translesion polymerase Rev3L in the tolerance of alkylating anticancer drugs. Molecular pharmacology *76*, 927-934.

Roskoski, R., Jr. (2012). ERK1/2 MAP kinases: structure, function, and regulation. Pharmacological research : the official journal of the Italian Pharmacological Society *66*, 105-143.

Samson, L., Thomale, J., and Rajewsky, M. F. (1988). Alternative pathways for the in vivo repair of O6-alkylguanine and O4-alkylthymine in Escherichia coli: the adaptive response and nucleotide excision repair. The EMBO journal *7*, 2261-2267.

Sengupta, S., and Harris, C. C. (2005). p53: traffic cop at the crossroads of DNA repair and recombination. Nature reviews Molecular cell biology *6*, 44-55.

Shieh, S. Y., Ikeda, M., Taya, Y., and Prives, C. (1997). DNA damage-induced phosphorylation of p53 alleviates inhibition by MDM2. Cell *91*, 325-334.

Songyang, Z., Lu, K. P., Kwon, Y. T., Tsai, L. H., Filhol, O., Cochet, C., Brickey, D. A., Soderling, T. R., Bartleson, C., Graves, D. J., *et al.* (1996). A structural basis for substrate specificities of protein Ser/Thr kinases: primary sequence preference of casein kinases I and II, NIMA, phosphorylase kinase, calmodulin-dependent kinase II, CDK5, and Erk1. Molecular and cellular biology *16*, 6486-6493.

Takenaka, K., Ogi, T., Okada, T., Sonoda, E., Guo, C., Friedberg, E. C., and Takeda, S. (2006). Involvement of vertebrate Polkappa in translesion DNA synthesis across DNA monoalkylation damage. The Journal of biological chemistry *281*, 2000-2004.

Veevers-Lowe, J., Ball, S. G., Shuttleworth, A., and Kielty, C. M. (2011). Mesenchymal stem cell migration is regulated by fibronectin through alpha5beta1-integrin-mediated activation of PDGFR-beta and potentiation of growth factor signals. Journal of cell science *124*, 1288-1300.